

https://dspace.org/

Permutation coded multiple access and MIMO techniques for hybrid powerline and visible light communication

Shimaponda-Nawa, Mulundumina

2022
https://hdl.handle.net/10539/34396

Downloaded from a DSpace repository. https://dspace.org/



UNIVERSITY OF THE
WITWATERSRAND,
JOHANNESBURG

Permutation Coded Multiple Access and MIMO Techniques for Hybrid Powerline and Visible Light Communication

Mulundumina Shimaponda-Nawa
(ORCID: 0000 0000 0002 1963 1318)

A thesis submitted to the Faculty of Engineering and the Built Environment, University of the Witwatersrand, Johannesburg, South Africa, in fulfilment of the requirements for the degree of Doctor of Philosophy

in the

Optical Communication Lab
School of Electrical and Information Engineering

May 2022

Declaration

I declare that, except where due acknowledgment has been made, this thesis being submitted for the Degree of Doctor of Philosophy to the University of the Witwatersrand in Johannesburg, is my own unaided work. I confirm that it has not been submitted before for any degree or examination to any other University.

MULUNDUMINA SHIMAPONDA-NAWA

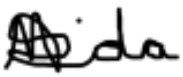

May 2022

Abstract

Smart homes, smart cities, smart mines, wearables and connected cars are just but a few areas where the internet of things (IoT) has developed and will continue to grow. This growth, demands increasingly wide coverage areas, high capacities and data rates to maintain reliable and ubiquitous connectivity of several smart devices and machines, regardless of their environment and geographical locations. These connectivity demands present a challenge on the current commonly used standalone radio frequency (RF) networks. This challenge on the RF networks presents an opportunity for hybrid networks where various communication technologies complement each other to achieve the device-to-device and device-to-infrastructure connectivity. A hybrid of powerline communication (PLC) and visible light communication (VLC) technologies, is one of the cost-effective schemes recently proposed to achieve high-speed communication in both indoor and outdoor environments, since both constituent technologies seem ubiquitous. However, being an emerging and developing integrated scheme, various areas of the hybrid PLC and VLC (HPV) system still require optimisation. As such, this work investigates indoor coded multiple access (MA) and multiple-input multiple-output (MIMO) techniques for hybrid power-line and visible light communication (HPV) systems, with practical channel considerations. A specific focus is placed on the system error rate performance enhancement and complexity reduction.

First, an MA optical wireless communication system using permutation codes (PCs), is investigated. It is proposed and shown that a soft-decision (SD) decoder based on the Hungarian and Murty's algorithms for solving linear programming problems, precisely referred to as the HM decoder, can simultaneously decode multiple permutation codewords (PCWs). Additionally, the work shows that the SD HM decoder enhances the reliability of the MA optical wireless communication system and reduces the system complexity when compared to the hard-decision decoders based on exhaustive search methods. Furthermore, the properties of the different combinations of (PCWs) and their decodability by the HM decoder are studied. Then, a generalised space-time coded MIMO (GSTC-MIMO) scheme, whose encoder is adapted to the HM decoder for reliability enhancement of the system, is proposed. These results provide the motivation to apply and extend the encoder adaptation principle to the design of MA permutation codebooks, where the assignment of user disjoint codebooks is based on the judicial criteria of the combination properties of the PCWs from the different user codebooks.

The power-line communication (PLC) channel is inherently susceptible to impulse noise because of electrical devices randomly connecting to the power grid. This adversely affects the error performance of the HPV system. To mitigate the effect of the impulse noise, two schemes are proposed. The first scheme is a combination of orthogonal frequency division multiplex (OFDM) and M-ary frequency shift keying (MFSK), aided with permutation codes (PC OFDM-MFSK). This scheme well mitigates the impulse noise in PLC systems, however, with a reduced data rate when compared to a system employing classical OFDM. Hence, a generalisation of the permutation coded scheme is introduced to enhance the data-rate of the HPV system. The second, is a novel scheme based on a time-diversity concept that uses the Hermitian symmetry structure to introduce data repetition to produce some redundancy of the transmitted data. This strengthens the resistance to occasional high-peak impulse noise in the PLC channel. It is shown in this work that by using the time-diversity Hermitian symmetry (TDHS) scheme, the probability of the effect of impulse noise on data symbols through a PLC channel, is drastically reduced by 75%. As a result, the overall system's bit error rate (BER) and goodput performance, is enhanced.

To Puluso Curtis, Tumelo Carson, Watupa Tapelo and in loving memory of a dear inspirational father, Hon Dr Lluminzu John Shimaponda.

Acknowledgements

I would like to unreservedly thank my supervisors, Prof. Ling Cheng and Dr. Oluwafemi Kolade, without whom this work would not have been successfully completed. I am grateful to Prof. Ling for his wide knowledge and insights, as well as for the honest and sometimes uncomfortable brainstorming sessions (a.k.a: whiteboard boxing), positive criticism of my work , that led me to work harder and smarter into conceiving not so obvious ideas to drive this work. I thank him for the very excellent mentorship and dedication to his work like its the only thing on earth. Furthermore, I am sincerely grateful to Dr. Kolade for his ever thorough way of handling research work, his great ideas and patience through this PhD journey. I thank him for his positive criticism and honesty, for his continuous encouragement and advice that created resilience in me to complete this work.

I would like to express my profound appreciation to my husband, Muku-Kupo, for ever caring and supporting me through this journey, in all aspects. His love, patience and encouragement have been a great source of motivation. I am also deeply grateful to my three sons, for always mentioning me in their prayers and encouraging me to get to the finishing line. I wish them success in life. Special appreciation goes to my amazing mum, Mutinta, sisters, brothers and their families for always checking up on me and understanding my absence at some so very important family meetings. I am also grateful for the support and love I received from my husband's family and allowing me to have been an absent wife.

Research work is never easy without friends who will constantly check up on you, encourage and motivate you during low moments. I am so grateful to my friends, Shalom, Vivian, Lucet, Daniel, Osedum, Tawanda, Justice and the "ladies". They made the work manageable. Special thanks too, go to all of Prof. Ling's students in the Optical Communications Lab, as well as all postgrad students and stuff in the School of Electrical and Information Engineering (EIE), for creating a conducive environment for work and healthy interaction.

I am grateful to SITA Aero and the African Union through the Mwalimu Nyerere Scholarship for women on Science, Technology, Engineering and Mathematics (STEM) and all funding opportunities from the School of EIE.

Finally and most importantly, I am forever in awe of the mercies and grace of God through out this program. For providing all the resources including the right human resource that I needed. I am deeply so grateful to God for taking me through, till the end.



Contents

Acknowledgements **vii**

Contents **ix**

List of Figures **xv**

List of Tables **xix**

1 Introduction **1**
1.1 Introduction 1
1.2 Research Objective and Contributions 4
1.3 Thesis Outline 8

2 Background and Preliminaries **11**
2.1 Introduction 11
2.2 Hybrid Powerline and Visible Light Communication . 13
2.2.1 Powerline Communication (PLC) 13
2.2.1.1 PLC Channel Model 14
2.2.2 Visible Light Communication (VLC) 17
2.2.2.1 VLC Channel Model 22
2.3 Multiple-Input Multiple-Output (MIMO) Techniques for Optical Wireless Communication 25
2.4 Orthogonal Frequency Division Multiplex (OFDM) and M-ary Frequency Shift Keying (M-FSK) 28
2.4.1 Orthogonal Frequency Division Multiplex (OFDM) in Optical Wireless Communication 29
2.4.2 M-ary Frequency Shift Keying (MFSK) . . . 32
2.5 Multiple Access and Multiple Access Decoding . . . 33
2.5.1 Multiple Access 33
2.5.2 Multiple Access Techniques in PLC Systems . 36
2.5.3 Multiple Access Techniques in VLC 37

2.5.4 Multiple Access Techniques in HPV Systems . 38
2.5.5 Codes for the MA HPV System 39
2.5.5.1 Optical Orthogonal Codes (OOCs) . 41
2.5.5.2 OOC Encoding and Decoding . . . 42
2.5.6 Binary Superimposed Codes 44
2.6 Summary 45

3 Space-Time Coding for VLC System Employing Imaging Receivers 47
3.1 Introduction 47
3.2 Alamouti Space-Time Coded MIMO 48
3.3 System Model 49
3.3.1 Two-Hop Transmission Process 52
3.3.2 Imaging Receiver 54
3.4 Simulation Results and Discussion 56
3.4.1 BER Performance Comparison for Non-Imaging (NImR) and ImRs 57
3.4.2 Performance Evaluation for Different Number of Receiver Pixels 58
3.4.3 Performance Impact due to Receiver Location 60
3.5 Summary 61

4 Soft-Decision Decoding of Permutation-based Optical Codes for a Multiple Access System 63
4.1 Introduction 63
4.2 Multiple Access Encoding 65
4.2.1 Channel Model 68
4.3 Decoding POCs 69
4.3.1 Decoding by Exhaustive Search (ES) Methods 69
4.3.1.1 Minimum Distance (MD) Decoder . 70
4.3.1.2 Exhaustive Search-Correlation (ES-C) Decoder 70
4.3.2 Soft-Decision Hungarian-Murty (HM) Decoding 71
4.4 Simulation Results and Analysis 74
4.4.1 Decoding Computational Complexity Analysis 74
4.4.2 BLER Performance in the Presence of Asymmetric Errors 75

4.4.2.1 Comparison based on Code Length . 75
4.4.2.2 Code Distance Properties and Decoder Capability 77
4.4.3 Probability of Error Analysis in the Presence of Binary Asymmetric Errors and AWGN . . 79
4.5 Summary 81

5 Encoder Adaptation for Generalised Space-Time Coded MIMO Systems using a Hungarian-Murty Soft-Decision Decoder 83
5.1 Introduction 83
5.2 GSTC-MIMO System Model 88
5.2.1 MIMO Channel Model for VLC 89
5.2.2 Space-Time Coded MIMO (STC-MIMO) . . . 90
5.2.2.1 Permutation Codewords for STC-MIMO 90
5.2.2.2 STC-MIMO System 90
5.2.3 Generalized STC-MIMO System 92
5.3 Adapting the GSTC-MIMO Encoder to the HM Decoder Capability 94
5.3.1 Soft-Decision Hungarian-Murty (HM) Decoder 94
5.3.2 Permutation-Codeword Combination Properties 97
5.3.3 GSTC-MIMO Encoder based on Partitioned Codebooks 101
5.4 Simulation Results and Analysis 102
5.4.1 Bit Error Rate (BER) Performance in MIMO Systems 103
5.4.2 Energy Efficiency Evaluation and Comparison 107
5.4.3 Multiple Access STC-MIMO (MA STC-MIMO) System 108
5.5 Summary 112

6 Generalised Permutation Coded OFDM-MFSK in Hybrid Powerline and Visible Light Communication 115
6.1 Introduction 115
6.2 OFDM-MFSK based HPV System 120
6.2.1 An Overview of the OFDM-MFSK 120

6.2.2 System Model 122
6.2.2.1 PLC Section and the Integration Unit 123
6.2.2.2 VLC Section 124
6.3 Generalised Permutation-Coded OFDM-MFSK based HPV System 127
6.3.1 Permutation-Coded OFDM-MFSK based HPV System 127
6.3.1.1 System Model for the Permutation-Coded OFDM-MFSK based HPV System 128
6.3.1.2 Soft-Decision Decoding for PC OFDM-MFSK HPV System 129
6.3.2 Generalisation of the PC OFDM-MFSK based HPV System 131
6.4 Simulation and Results Analysis 133
6.4.1 BER Performance Comparison of OFDM HPV and OFDM-MFSK HPV Systems 133
6.4.2 DC Biasing and Clipping Effects on BER Performance of the OFDM HPV and OFDM-MFSK HPV Systems 135
6.4.3 Coded and Uncoded OFDM-MFSK based HPV System 135
6.4.4 Impulse Noise Effects 137
6.4.5 GPC OFDM-MFSK HPV System Performance 138
6.4.5.1 Bit Error Rate Performance 138
6.4.5.2 Data Rate Comparison 138
6.5 Summary 139

7 Impulse Noise Mitigation by Time-Diversity Hermitian Symmetry scheme in HPV Systems 141
7.1 Introduction 141
7.2 Problem statement and Motivation 146
7.3 Time Diversity Hermitian Symmetry based HPV System Models 151
7.3.1 TDHS based HPV System 152
7.3.1.1 System Model Overview 152

7.3.1.2 Impulse Noise Detection 156
7.3.2 Permutation Coded Time-Diversity Hermitian Symmetry (PC-TDHS) based HPV System . . 158
7.3.2.1 Permutation Codes and Soft-Decision Decoding 160
7.3.3 Multiple Access for PC-TDHS based HPV System 162
7.4 Simulation Results and Analysis 165
7.4.1 Impact of the A-Value on System Performance 166
7.4.2 BER Performance Comparison Between Uncoded TDHS and PC-TDHS Single User HPV Systems using HD and SD Decoders 168
7.4.3 Performance Comparison Between HPV Systems Employing Amplify-And-Forward (AF) and Decode-And-Forward (DF) Relaying Protocols 169
7.4.4 BER Performance PC-TDHS based MA HPV Systems 172
7.5 Summary 172

8 Conclusion and Future Work 175
8.1 Conclusion 175
8.2 Future Work 178

List of Figures

2.1 Hybrid PLC and VLC schematic diagram 13
2.2 Physical link configurations [53] 18
2.3 VLC propagation model for LOS and reflections . . 24
2.4 A channel model representation of an $N_t \times N_r$ antenna MIMO system 26
2.5 Optical OFDM system diagram 30
2.6 Illustration of orthogonal multiple access schemes [149] 35
2.7 Indoor environment scenario of multiple access HPV system 38

3.1 Representation of the Alamouti space-time coded scheme 49
3.2 SISO and ASTC ($N_t \times N_r = 2 \times 1$) BER plots. . . . 49
3.3 VLC system room setup: upright transmitter, relays and imaging receiver 50
3.4 System block diagram of an upright VLC transmitter connected to a PLC channel with Alamouti coded relay nodes and imaging receiver. 51
3.5 Imaging receiver structure [59] 55
3.6 Performance comparison for non-imaging and imaging receivers 58
3.7 Performance comparison: Imaging receivers with different number of pixels 59
3.8 Performance variation due to receiver location 60

4.1 Multiple access communication system model 66
4.2 Asymmetric error probability representation 69
4.3 BLER performance of POC of varying lengths in the presence of asymmetric errors 76
4.4 Code and decoder capability performance for PCs with varying distance properties, $M = 5, m = 4$. 78

4.5 BLER performance when binary asymmetric errors and AWGN are considered. $e_0 = 0.02$, $M = 4, m = 2$. 80

5.1 System model of the permutation-based STC-MIMO communication system 92
5.2 Examples of codeword pairs in four periods 96
5.3 Adapted GSTC-MIMO Encoder 102
5.4 BER performance, STC and GSTC-MIMO systems. 105
5.5 Bit error rate (BER) performance of the MA STC-MIMO system with varying user TE separation . . . 108
5.6 Representation of power distribution from the TEs for varying Δd. (a) $\Delta d = 0.1$ m (b) $\Delta d = 0.2$ m 109
5.7 Representation of power distribution from the TEs for varying Δd. (a) $\Delta d = 0.4$ m. (b) $\Delta d = 1$ m. 110

6.1 System block diagram of OFDM-MFSK based HPV system 122
6.2 Representation of encoded bits mapped to PCs in a GPC OFDM-MFSK. $N = 32$, $k = 2$, $M = 4$. The encoded bits 0100 and 0110 are mapped to 2143 and 2431, respectively. 132
6.3 BER performance comparison of OFDM and OFDM-MFSK for varying sub-carrier window sizes, N 134
6.4 Hard-decision versus soft-decision decoding. $A = 0.1$. 136
6.5 Effect of varying A values on BER performance for the OFDM, coded and uncoded OFDM-MFSK based HPV systems, including the GPC based system . . . 137
6.6 Data rate comparison for OFDM-MFSK, PC OFDM-MFSK and GPC OFDM-MFSK scheme for $\mathcal{PC}(M = 4, d_{\min} = 3)$ and varying N. 139

7.1 A depiction of hybrid networks of RF, PLC and VLC technologies for infrastructure and device interconnection. 143
7.2 Block diagram for TDHS based HPV system 153
7.3 Block diagram showing the signal output from the S/P, OFDM mapping & Hermitian symmetry alignment and the IFFT blocks of Figure 7.2. 155

7.4 Block diagram for TDHS MA HPV Communication System 163
7.5 Time-slot activation representation in a multiple access PC-TDHS HPV system. User information symbols for two users mapped to user PCWs 2134 and 3142 for the two users. 164
7.6 BER performance for TDHS and non-TDHS system for varying A-values. 167
7.7 BER performance comparison between TDHS and Non-TDHS based HPV systems for coded and uncoded schemes. $A = 0.05$, $M = 4$ for coded systems. 168
7.8 Goodput performance comparison for coded TDHS and non-TDHS systems employing AF and DF relaying protocols. SD decoding was used for all the systems. 170
7.9 Comparison of major signal processes between TDHS system using the AF relaying protocol and non-TDHS system using the DF relaying protocol. Grey portions depict common processes, while white portions indicate processes not applicable to a particular system. Blue and orange portions depict processes applicable only to either the TDHS or the non-TDHS system, respectively. 171
7.10 BER performance of the multiple access HPV system using the permutation coded TDHS. $A = 0.05$, $L = 4$, $m = 2$. 173

List of Tables

2.1 Characteristics of optical wireless communication link configuration [66] 21

3.1 Simulation Parameters Used 56

4.1 Permutation-based optical code (POC) generated from $\mathcal{PC}$ $(M = 3, d_{\min} = 2)$ 67

5.1 $\mathcal{PC}(M = 4, d_{\min} = 3)$ 95
5.2 Simulation Parameters 103

7.1 Impulse Noise Error Probabilities on the received signal components from PLC 157

List of Abbreviations

ACO-OFDM **A**symmetrically **C**lipped **O**ptical **OFDM**

ADRs **A**ngle **D**iversity **R**eceivers

ADRs **A**ngle **D**iversity **R**eceivers

AE-GSTC **A**dapted **E**ncoder-**G**eneralised **S**pace-**T**ime **C**oded

AF **A**mplify-and-**F**orward

AP **A**ccess **P**oint

ASTC **A**lamouti **S**pace-**T**ime **C**oded

AWGN **A**dditive **W**hite **G**aussian **N**oise

BER **B**it **E**rror **R**ate

BLER **Bl**ock **E**rror **R**ate

BPSK **B**inary **P**hase **S**hift **K**eying

CDMA **C**ode **D**ivision **M**ultiple **A**ccess

DC **D**irect **C**urrent

DCO-OFDM **DC** biased **O**ptical **O**FDM

DD **D**irect **D**etection

DF **D**ecode-and-**F**orward

EE **E**nergy **E**fficiency

ES **E**xhaustive **S**earch

ES-C **E**xhaustive **S**earch-**C**orrelation

EW **E**qual **W**eight

FDMA **F**requency **D**ivision **M**ultiple **A**ccess

FFT **F**ast **F**ourier **T**ransform

FOV **F**ield **o**f **V**iew

FSO **F**ree-**S**pace **O**ptical

GSTC **G**eneralised **S**pace-**T**ime **C**oded

HD **H**ard-**D**ecision

HM **H**ungarian-**M**urty

HPV **H**ybrid **P**owerline and **V**isible Light Communication

HS **H**ermitian **S**ymmetry

ICI **I**nter-**C**hannel **I**nterference

IFFT **I**nverse **F**ast **F**ourier **T**ransform

IM/DD **I**ntensity **M**odulated **D**irect **D**etection

ImR **I**maging **R**eceiver

IoT **I**nternet **o**f **T**hings

IR **I**nfra-**R**ed

ISI **I**nter-**S**ymbol **I**nterference

LED **L**ight **E**mitting **D**iode

LOS **L**ine **o**f **S**ight

LP **L**inear **P**rogramming

LUT **L**ook **U**p **T**able

MA **M**ultiple Access

MAI **M**ultiple **A**ccess **I**nterference

MD **M**inimum **D**istance

***M*-FSK** *M*-ary **F**requency **S**hift **K**eying

MIMO **M**ultiple-**I**nput-**M**ultiple-**O**utput

ML **M**aximum **L**ikelihood

MOLR **M**utually **O**rthogonal **L**atin **R**ectangle

MOLS **M**utually **O**rthogonal **L**atin **S**quare

MRC **M**aximum **R**atio **C**ombining

NImR **N**on-**I**maging **R**eceiver

NLOS **N**on-direct **L**ine **O**f **S**ight

NOMA **N**on **O**rthoogonal **M**ultiple **A**ccess

OCDMA **O**ptical **C**DMA

OFDM **O**rthogonal **F**requency **D**ivision **M**ultiplex

OFDMA **O**rthogonal **FDMA**

OMA **O**ptical **M**ultiple **A**ccess

O-MIMO **O**ptical-**MIMO**

OOC **O**ptical **O**rthogonal **C**ode

OOK **O**n-**O**ff **K**eying

PAPR **P**eak-to-**A**verage **P**ower **R**atio

PC **P**ermutation **C**ode

PCW **P**ermutations **C**odeword

PD **P**hoto**D**iode

PLC **P**owerline **C**ommunication

POC **P**ermutation-based **O**ptical **C**ode

PSK **P**hase-**S**hift **K**eying

QAM **Q**uadrature **A**mplitude **M**odulation

RC **R**epetition **C**oding

RE **R**eceive **E**lement

RF **R**adio **F**requency

Rx **R**eceiver

SCM **S**ingle **C**arrier **M**odulation

SD **S**oft-**D**ecision

SDMA **S**patial **D**ivision **M**ultiple **A**ccess

SHMM **S**emi-**H**idden **M**arkov-**M**odel

SIMO **S**ingle-**I**nput **M**ultiple-**O**utput

SISO **S**ingle-**I**nput **S**ingle-**O**utput

SM **S**patial **M**odulation

SMP **S**patial **M**ultiplexing

SNM **S**ub-carrier **N**umber **M**odulation

SNR **S**ignal to **N**oise **R**atio

ST **S**pace-**T**ime

STBC **S**pace-**T**ime **B**lock **C**oding

STC **S**pace-**T**ime **C**oded

STSK **S**pace-**T**ime **S**hift **K**eying

TD **T**ime **D**iversity

TDHS **T**ime-**D**iversity **H**ermitian **S**ymmetry

TDMA **T**ime **D**ivision **M**ultiple **A**ccess

TE **T**ransmit **E**lement

THz **T**era**H**ertz

Tx **T**ransmitter

VLC **V**isible **L**ight **C**ommunication

V2X **V**ehicle-**2**-**I**nfrastructure

V2V **V**ehicle-**2**-**V**ehicle

VW **V**ariable **W**eight

WiFi **W**ireless **F**idelity

WOMA **W**ireless **O**ptical **M**ultiple **A**ccess

Publications

Published

1. *Mulundumina Shimaponda-Nawa, Shamin Achari, Dushantha Nalin K Jayakody, and Ling Cheng*, "Visible Light Communication System Employing Space Time Coded Relay Nodes and Imaging Receivers". *SAIEE Africa Research Journal, 111(2): 56–64, 2020.*

2. *Mulundumina Shimaponda-Nawa, Oluwafemi Kolade, Wenbo Ding, Dushantha Nalin K Jayakody, and Ling Cheng*, "Soft-Decision Decoding of Permutation-based Optical Codes for a Multiple Access System". *IEEE Communications Letters, 25(9): 2824–2828, 2021.*

3. *Mulundumina Shimaponda-Nawa, Oluwafemi Kolade, and Ling Cheng*, "Generalised Permutation Coded OFDM-MFSK in Hybrid Power Line and Visible Light Communication". *IEEE Access Journal, 10:20783-20792, 2022.*

Under Review

1. *Mulundumina Shimaponda-Nawa, Oluwafemi Kolade, Jianhua He, Wenbo Ding and Ling Cheng*, "Impulse Noise Mitigation by Time-Diversity Hermitian Symmetry scheme in HPV Systems". *Under review with The IEEE Internet of Things Journal.*

CHAPTER 1

Introduction

1.1 Introduction

Outdoor and indoor environments such as play parks, roads, homes, industrial areas, offices and conference rooms normally have multiple smart devices that require simultaneous connections to the network and to one another via the internet communication network [136, 160]. This has recently been crowned as the internet of things (IoT), where smart devices connect to share and exchange information, regardless of their environment and geographical locations. The challenge posed on the network is the ability to provide simultaneous ubiquitous and reliable connection for all these smart devices without or with minimum interference or collisions. Conventionally, this is achieved by wireless fidelity (WiFi) networks. However, WiFi is based on the radio frequency (RF) technology whose spectrum resource is scare and already congested. Hence, the inevitability of the research hype into alternative communication technologies like powerline communication (PLC) and visible light communication (VLC). These alternative communication technologies need to also be able to achieve the multiple and simultaneous connectivity trend demands.

The simultaneous connectivity of multiple users to a network is achieved by the use of multiple access (MA) techniques which allow multiple users to share the network resources. The orthogonality characteristic in different domains such as time, space, frequency as well as codes is widely used to distinguish users or information transmitted from different users. This avoids potential multiple access interference (MAI) among users. While VLC is able to serve multiple users as an access point, it, however, requires an information back-haul network to provide data to its optical transmitters, thus forming a hybrid communication system. The commonly used VLC back-haul networks are based on RF, optical fiber or PLC technologies [59, 83, 95, 120].

VLC is a type of optical wireless communication technology that transmits information signals by visible light electromagnetic waves. It is thus capable of providing illumination and data communication simultaneously. The concept of VLC stems from the introduction of power efficient solid state lighting [127, 150] in conjunction with the concept of electronic wireless communication using visible light established by Alexander Graham Bell in 1880 [21]. Solid state lighting was introduced with advantages of efficient power consumption, brighter and long-life [150]. Thus, since the first demonstration of VLC [84, 139], light emitting diodes (LEDs) became the source of light widely used as transmitters. This is due to their advantages of low cost yet with an increased energy efficiency (EE), durability and their ability to be modulated at high speed. Apart from the

much desired wide unlicensed spectrum in the order of several hundred terahertz (THz), some notable advantages attributed to VLC technology are its non-subjection to interference by electromagnetic sources and congestion as well as high level of security as it does not penetrate through walls. Some of the potential application areas of VLC are hospitals where WiFi could be undesirable due to electromagnetic interference, smart transport systems, smart lighting of smart buildings and underwater communication [20, 63, 94].

Meanwhile, the powerline provides power to the VLC transmitters and is capable of transmitting information [23, 32, 63, 84, 88, 139], commonly referred to as powerline communication (PLC). Like VLC, PLC has an advantage of having ubiquitous presence in indoor environments which is a desirable communication network feature for coverage enhancement. Some of the applications of PLC include providing remote meter reading services, voice communication and data acquisition, intra-vehicle communication, [23, 32, 63, 88]. Taking advantage of the fact that powerlines provide power to the lighting infrastructure used for VLC, authors in [83] established a cost effective hybrid communication system consisting of PLC and VLC. It is commonly referred to as the hybrid powerline and visible light communication (HPV) system.

The fact that both powerline and solid state lighting upon which VLC is built, were not initially designed for communication applications, the HPV system is usually prone to performance issues due to

the effects that each channel suffers when the communication application is exploited. However, because of the potential that the HPV system has demonstrated, especially in terms of the application to smart cities, aircraft networking, vehicle technology, hospitals and other electromagnetic radiation restricted areas, open research areas aimed at improving this hybrid system are still numerous.

In view of the above, this work investigates multiple techniques including MA, multiple-input-multiple-output (MIMO), time-diversity, permutation coding, and soft decision decoding (SD) of permutation code (PC) over a VLC channel, PLC channel and an HPV system. Specific research objectives and contributions are provided in the next section.

1.2 Research Objective and Contributions

The objective of this work is to enhance the error performance and reduce the complexity of the HPV system. This is achieved by the following contributions:

1. ***Bit error rate performance improvement by the use of space-time coding and imaging receiver***

   In multiple-in multiple-output (MIMO) systems, it is desirable to have spatially uncorrelated channels in order to avoid inter-channel interference. However, optical MIMO (O-MIMO) systems, especially those employed for indoor applications, are highly correlated, which could enable only minor diversity gains.

Thus, to improve the performance of an HPV system having a MIMO configuration at the VLC section, In this work the use of Alamouti space-time coded (STC) optical relays with an imaging receiver (ImR), is proposed. The Alamouti STC MIMO technique improves the BER performance of the system by the transmit diversity feature, while the ImR further improves the error performance by its ability to de-correlate optical MIMO links. A signal-to-noise ratio (SNR) gain exceeding 7 dB at a BER performance of 10^{-4}, is achieved when the system employing an ImR is compared to that using a non-imaging receiver (NImR). Additionally, the performance of ImRs with varying number of pixels, is also compared, where it is established that the system's BER is proportional to the number of pixels of the ImR. The details of this contribution are provided in Chapter 3 of this thesis.

2. ***Decoding complexity reduction in a permutation coded optical MA system by a soft-decision (SD) decoder based on optimization algorithms***

   An MA soft-decision (SD) decoder based on the cost rankings of the channel output matrix, is proposed, demonstrted and applied in an optical wireless communication system, in which permutation-based optical codes (POCs) are used. The proposed decoder determines the possible transmitted MA codewords by implementing the optimization Hungarian and Murty's

algorithms to solve and rank the costs of all the possible codewords of the received signal. The performance of the proposed Hungarian-Murty (HM) decoder is evaluated in comparison with two decoders based on the exhaustive search (ES) technique, in terms of computational complexity and block error rate (BLER). It is found that when POCs are employed, the proposed HM decoder achieves better BER performance with a low decoding complexity in comparison to the exhaustive search (ES) based decoders. The proposed HM decoder is found to have a tremendously low computational complexity of $O(M^4)$ compared to $O(M! \cdot M^2)$ of the two ES-based decoders, where M denotes the length of the PC. Thus, This contribution is detailed in Chapter 4 of this thesis. The SD HM decoder is then applied to systems in subsequent chapters of this work.

3. ***Optimisation of the SD decoder performance***

A study on the optimisation of the SD HM decoder investigated in Chapter 4, is conducted. Firstly, a generalised STC-MIMO (GSTC-MIMO) system based on PCs, is proposed and designed. It is shown in this study that when permutation codes (PCs) are used in conjunction with the SD HM decoder in a generalised STC-MIMO (GSTC-MIMO) system, the decoder performance can be optimised by judiciously selecting the codewords to be used at each transmit period. Precisely, based on the weight properties of the simultaneously selected codewords, a theorem defining the capability of the HM decoder, is provided. As such,

an adaptation of the space-time (ST) encoder to improve the HM decoder capability, is proposed. It is shown that the GSTC-MIMO system using the decoder-adapted ST encoder outperforms the GSTC-MIMO system using the conventional ST encoder by an SNR exceeding 5 dB. This is detailed in Chapter 5 of this thesis.

4. ***PLC impulse noise mitigation and data-rate enhancement for the HPV system.***

   Orthogonal frequency division multiplexing (OFDM) with M-ary frequency shift keying (MFSK), referred to as the OFDM-MFSK scheme, and its permutation coded variant, have in literature been shown to well mitigate impulse noise in PLC channels. It is conceived in this work that the gains from these schemes would positively impact the error performance of the HPV system. Furthermore, based on the results obtained from Chapters 4 and 5 regarding the performance and optimisation of the SD HM decoder, an HPV system employing PC OFDM-MFSK, is proposed. Additionally, the data-rate of the PC OFDM-MFSK is enhanced by the proposed generalisation scheme based on permutation codes. It is shown in this study that the use of OFDM-MFSK improves the performance of an HPV system compared to that using only the classical OFDM modulation scheme by an SNR gain of 6 dB at a BER of 10^{-4}. A further SNR gain of approximately 3 dB is achieved for the PC OFDM-MFSK HPV system using SD HM decoder. Moreover,

the generalisation of the PC OFDM-MFSK HPV system, does not increase the decoding complexity when the SD HM decoder is used. This contribution is detailed in Chapter 6 of this thesis.

5. ***Impulse noise mitigation for HPV systems by the Time-Diversity Hermitian Symmetry (TDHS) scheme***. The PLC channel is inherently susceptible to impulse noise due to electrical appliances randomly connected to the powerline. This, as established in Chapter 6, adversely affects the HPV system BER performance. To address this issue, a time-diversity Hermitian symmetry (TDHS) scheme, which mitigates the effects of impulse noise in a PLC channel, is proposed. The scheme employs the Hermitian symmetry structure to recover information symbols likely to have been affected by the impulse noise. By using the TDHS scheme, the probability of the effect of impulse noise on data symbols through a PLC channel, is drastically reduced by 75%. As a result, the overall BER and goodput performance, is enhanced. This contribution is detailed in Chapter 7 of this thesis document.

1.3 Thesis Outline

The thesis has been presented as an eight-chapter document, covering the motivation and contributions in the study of the HPV system. Various subjects relating to channel characteristics, MIMO, MA and

decoding techniques applied to the different sections of the HPV system, have also been covered. The rest of the document is structured as follows:

Chapter 2, provides the background knowledge and some preliminary information on the channel models and techniques that are studied in the different chapters of this document. Techniques such as MIMO, MA, OFDM, MFSK, including some hard and soft-decision decoding algorithms, are discussed.

In Chapter 3, a practical indoor HPV system is investigated. The powerline is assumed to be the information back-haul structure and also coordinate the VLC relays installed in the ceiling. Precisely, the performance of a VLC system, with relay nodes equipped with a MIMO technique called space-time block coding (STBC), is investigated. The BER performance of the Alamouti coding scheme, which is a type of STBC, is specifically considered. In order to enhance the overall system reliability, an ImR, in conjunction with the relay-MIMO setup, is proposed. Since, an MA HPV system is subsequently investigated in the seventh chapter, a study on the decoding complexity of an MA system using PCs is undertaken and presented in Chapter 4. An investigation on the performance of an SD decoder based on optimisation algorithms, is conducted. Simulations are carried out and its performance in terms of the computational decoding complexity and BER, is compared to those of hard-decision decoders based on ES methods. Furthermore, a study on the optimisation of the SD decoder employed in Chapter 4, is carried out in

Chapter 5, from which an encoder adapted to the SD HM decoder is proposed based on a theorem developed from the weight properties of the codeword combinations.

In Chapter 6, the performance of the OFDM-MFSK scheme and its permutation coded variant is investigated for impulse noise mitigation in an HPV system. In addition, a generalisation of the PC OFDM-MFSK system to enhance the data-rate, is proposed. A novel TDHS scheme for impulse noise mitigation is proposed and its performance is investigated in Chapter 7. PCs are then applied to the TDHS HPV system in order to exploit the low decoding computational complexity of the SD HM decoder studied in Chapters 4 and 5. Furthermore, an MA system employing the proposed novel TDHS scheme is investigated, where multiple users access the HPV system distinguished by PCs. Finally, in Chapter 8, conclusions are drawn and pointers of probable future work, is summarised and presented.

CHAPTER 2

Background and Preliminaries

2.1 Introduction

Indoor tele-traffic accounts for approximately 80 percent of the total tele-traffic [28]. This trend of indoor tele-traffic growth is expected to continue due to more smart devices being introduced requiring simultaneous connectivity, as well as device-to-device connectivity for entertainment and e-commerce. As the need for more channel capacity at higher bit rates increases, the RF carrier frequencies and spectrum band equally need to be increased. However, higher radio frequencies are severely attenuated and wider spectrum bands may not be feasible due to current scarcity of the RF spectrum resource. Hence the introduction of visible light communication, which uses the visible electromagnetic spectrum section, presents an opportunity to use a range of unlicensed spectrum in the order of several hundred THz. As earlier mentioned, VLC transmitters would require a backbone network structure as they are normally deployed as network access points (APs), with PLC identified as one of the potential cost-effective networks for a backbone system. As emerging communication technologies are meant to complement, and in

some cases replace, the mature RF technology, it is necessary that some basic application features achieved by RF systems, equally be achieved by these alternative communication technologies.

PLC and VLC technologies have each attracted a lot of research attention [12, 14, 48, 54, 57, 59, 70, 72, 96, 113, 115, 117, 126, 143, 147, 148, 159, 162, 163], due to their common advantage of their ability to leverage on existing infrastructure. Furthermore, the integration of the two communication technologies has also been broadly studied. For instance, after the first proposal of an HPV system in [83], more research work focusing on areas ranging from channel modelling, integration of the two technology, to complex modulation techniques. For example, [78, 83, 92, 104] address the issue of integration of the two technologies, while in [5, 34, 38, 93], the channel modeling aspect is addressed. Further, modulation and multi-carrier aspects of the hybrid system are addressed in [34, 38, 82, 104].

The purpose of this chapter is to present some fundamental components building up to the integrated system of PLC and VLC. Background and basic channel details of the PLC, VLC and their integrated system, relevant to the focus of this thesis are given. Others include discussions on the OFDM and MFSK modulation, MIMO techniques in VLC, as this is one of the state-of-the-art schemes applied to the APs that directly interacts with the end users. Further, coded MA techniques, are presented.

2.2 Hybrid Powerline and Visible Light Communication

A simple schematic diagram of the HPV system showing the sections that the work in this thesis focuses on, is shown in Figure 2.1. In the following sections, we will discuss the channel models of the constituent technologies, i.e, PLC and VLC.

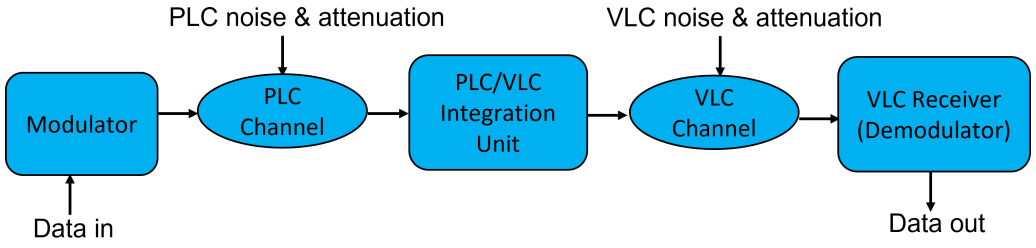

FIGURE 2.1: Hybrid PLC and VLC schematic diagram

2.2.1 Powerline Communication (PLC)

PLC, a communication technology that uses the power grid to transmit data signals has been in existence for several decades now [29, 113, 142]. Due to its ubiquitous nature, PLC finds applications in a wide range of areas such as home automation, control and monitoring [29, 34, 92, 121, 142, 145]. Other application areas include MA, sensors and vehicular communication [41, 118, 144]. In the early years when PLC systems were introduced, their use was restricted to narrow-band systems because powerlines highly suffer severe bandwidth constraints, power limits and high levels of noise, hence was not favourable for reliable data transmission. This was expected because powerlines were not initially designed to carry information signals. Furthermore, the PLC channel is a bus system where several

electrical equipment are randomly plugged in, causing varying levels of impedance and attenuation due to switching of electrical equipment. Additionally, PLC is also affected by various noise types, namely, coloured background, narrow-band, periodic and aperiodic impulse noise [33, 113, 132, 164]. Hence, channel modelling plays a critical role in developing noise mitigation schemes for PLC channels.

2.2.1.1 PLC Channel Model

The PLC channel modeling has been the basis of some of the proposed modulation and coding techniques to mitigate the most common noise types in the PLC channel. Several models proposed in literature [14, 143, 148, 165] can be widely classified into two approaches, namely the the top-down approach and the bottom-up approach [163], depending on whether the model development is based on measurements or just transmission line theory. As such, by means of data fitting, a top-down approach attempts to find the most fitted model from either impulse response or frequency response measurements, while in a bottom-up approach the channel model is derived from transmission line theory without relying on any measurement [163].

The model in [165] that describes the PLC channel based on the multipath phenomenon has widely been applied in data transmission investigation studies. In this model, the signal propagation in a PLC channel does not only take place along a direct path between the transmitter and receiver, but additional paths, also referred to

as echoes, are present. Furthermore, the signal has a frequency and length-dependent attenuation. As such, the channel transfer function where the weighting factor of the reflection and transmission factors of the multipaths along a propagation path are assumed to be almost equal, is expressed as [165]:

$$H_p(f) = \sum_{i=1}^{L_\mathrm{p}} \mathrm{g}_i e^{-(\alpha_0+\alpha_1 f^\mathrm{k})\tau_i v} e^{-j2\pi f\tau_i}, \tag{2.1}$$

where L_p is the number of effective echoes or dominant paths in the PLC channel, g_i is a weighting factor of the ith path and presents both the effect of transmission and reflection coefficients. The frequency-dependent attenuation coefficients, denoted by α_0 and α_1 are the attenuation parameters of the cable and k is the exponent of the attenuation factor (usual values are between 0.2 and 1) [34], v and τ_i are the group velocity and delay of the ith path, respectively.

In addition to being characterised by multipath propagation, the PLC channel is prone to noise disturbances due to devices plugged into the powerline or voltage variations from switching transients. In literature, two main noise types, namely background noise and impulse noise, have been considered. Background noise experiences small deviations with time, thus is usually modelled by the Gaussian distribution, whereas impulse noise is characterised by rapidly modified amplitudes. Several impulse noise models with and without memory, have been proposed [33, 58, 100, 101, 132]. Some of the impulse noise memoryless models include the Middleton Class A,

Bernoulli-Gaussian and Symmetric alpha-stable, while those with memory include Markov-Middleton and Markov-Gaussian [132].

In this thesis, the widely used Middleton Class A based on the Poisson-Gaussian model is adopted as it has been demonstrated to accurately model the impulse noise in indoor environments for data transmission applications. Using the analysis in [6, 132], the probability density function of a noise sample, is given by:

$$P_{\mathrm{d}}(n_{\mathrm{p}}) = \sum_{\mathfrak{m}=0}^{\infty} P_{\mathfrak{m}} \mathcal{N}(n_{\mathrm{p}}; 0, \sigma_{\mathfrak{m}}^2), \tag{2.2}$$

where n_{p} is the noise sample whose Gaussian probability density function has zero-mean and variance $\sigma_{\mathfrak{m}}^2$ and the parameter $\mathfrak{m} = 0, 1, 2, \ldots, \infty$ represents the random noise state that describes each sample. It has a Poisson-distribution given by:

$$P_{\mathfrak{m}} = \frac{A^{\mathfrak{m}} e^{-A}}{\mathfrak{m}!}, \tag{2.3}$$

and

$$\sigma_{\mathfrak{m}}^2 = \sigma_I^2 \frac{\mathfrak{m}}{A} + \sigma_G^2 = \sigma_G^2 \Big(\frac{\mathfrak{m}}{A\Gamma} + 1 \Big). \tag{2.4}$$

In (2.3), A is the Impulsive index which represents the frequency of occurrence of the zero-mean Gaussian sequence, in an observation period. The variance of the background noise modelled as additive white Gaussian noise (AWGN) is denoted by σ_G^2, while σ_I^2 denotes the variance of the impulse noise and their ratio (σ_G^2/σ_I^2) is denoted

by Γ. Impulse noise occurs in bursts and follows a Poisson distribution, contributes to the overall noise sample according to a Poisson-distributed random sequence [101], therefore, in an HPV system, it is necessary to account for such occurrences in the channel.

2.2.2 Visible Light Communication (VLC)

VLC emerged from the quest to find a solution to power efficient lighting. It is one of the emerging communication technologies that has been identified for easy integration with the smart powerline, especially on the last mile of the indoor communication network environments. VLC non-subject to interference by electromagnetic sources and congestion. Other notable advantages attributed to VLC technology are its license-free spectrum, high level of security as it does not penetrate through walls, as well as potential high data rate [72, 84, 117]. As mentioned before, some of the potential application areas of VLC are hospitals where WiFi could be undesirable, smart transport systems and smart lighting of smart buildings [34].

In VLC systems, LEDs are commonly used in illumination sources and simultaneously as transmit elements. This is as a result of low-cost, yet, increased energy efficiency, durability and ability to be modulated at high speed. However, LEDs suffer from modulation bandwidth limitation [44, 59, 159], therefore, hindering the full utilisation of the inherent wide frequency spectrum resource of VLC, resulting in limited achievable data rate and capacity. In light of this, several solutions, including multiple parallel communication,

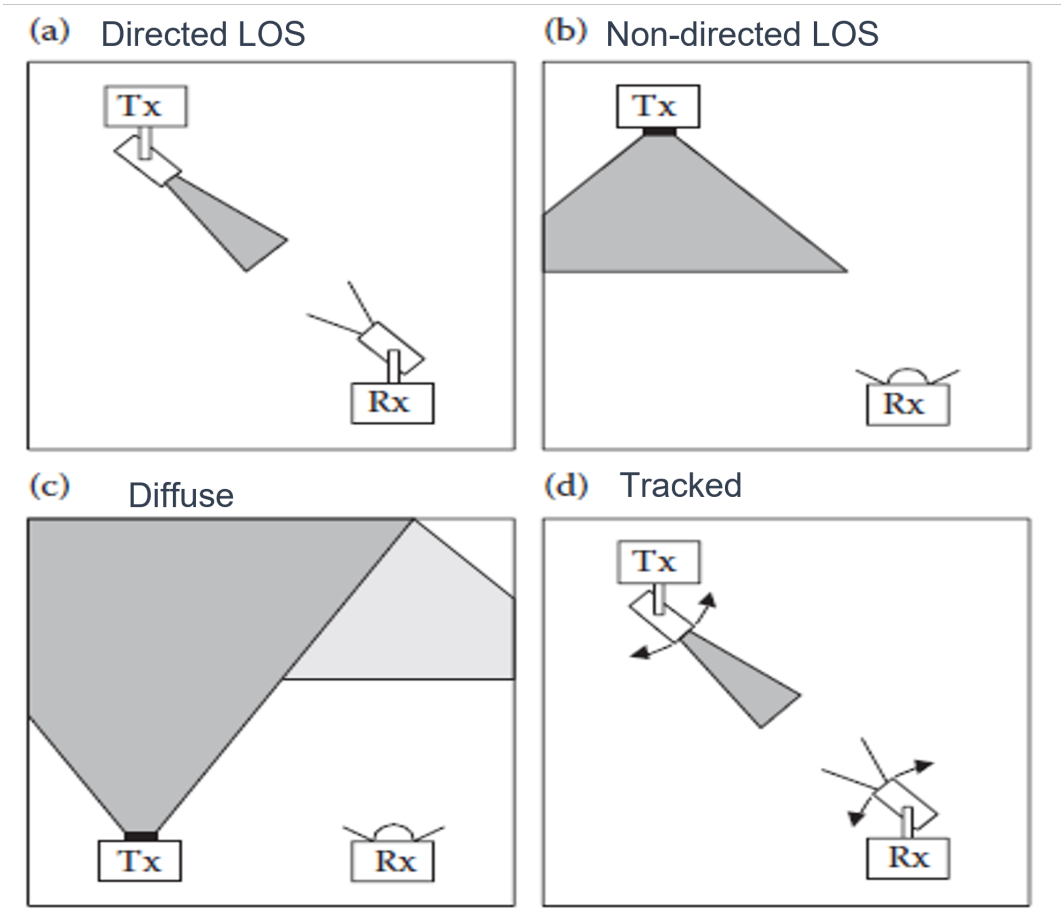

FIGURE 2.2: Physical link configurations [53]

.

advanced modulation schemes and alternative light sources, have been proposed to mitigate this drawback by LEDs [44, 59, 159].

Link configurations in VLC can be widely classified according to the degree of directionality between the transmitter and receiver. The four general physical optical wireless communication link configurations shown in Figure. 2.2 are directed line of sight (LOS), non-directed LOS (NLOS), diffuse and tracked [52, 66, 85, 89, 91, 108]. A table of their characteristics as presented in [66], is provided in Table 2.1.

1. Directed line of sight (LOS): The link configuration requires a

direct alignment of the transmitter and receive providing clear LOS, hence they can be used in both outdoor and indoor point-to-point communications, where narrow beam applications may be required. Because of the excellent alignment, the optical beam is usually narrow and only requires low power levels and the offer high data rates. It is however, highly prone to link blockage, not allowing flexibility to receiver station mobility, nor can it serve multiple receiver stations placed outside the LOS coverage. Hence, in applications where the transmitter needs to serve multiple receiver stations, the narrow optical beam source has to be replaced with a source of a wide optical footprint.

2. Non-directed LOS (NLOS): This is the most considered link configuration for indoor applications. Unlike the direct LOS, this configuration makes use of transmitters with wide beams and receivers with a wide field of view (FOV) [108]. In NLOS, reflections from the surfaces such as walls and ceilings are also considered as part of the transmitted signal, hence the receiver detects light from all directions. The major drawbacks of this configuration are inter-symbol interference (ISI) induced by multipath dispersion and the requirement for high power levels.

3. Diffuse: In the diffuse link configuration, the transmitter with a wide beam is placed pointing direct at the ceiling and the signal is reflected off to the receiver station. This configuration supports user mobility as it can still function without LOS

between the transmitter and the receiver. Severe multipath dispersion, pathloss and attenuation on the signal received by the photodetector (PD) are the main drawbacks of this configuration. Another way to combat these drawbacks and reduce the amount of ambient light noise, the conventionally used NImR can be replaced by an ImR having an array of photodetectors (PDs).

4. Tracked: This configuration offers improved mobility because its transceiver base stations are installed with beam steering mechanisms in the ceiling of a indoor environment, whereas the mobile stations would be placed at some location below the transceiver base station. The main draw of this configuration is the complexity of the tracking system. However, it has a lower power requirement, less ambient light interference, and reduced multipath-induced inter-symbol interference. The tracked link configuration can also offer high data rate similar to the direct LOS configuration [66].

At the receiver, highly sensitive PDs are usually employed to detect the light intensity from the transmitter. The PD has a response which is the integration of tens of thousands of very short wavelengths of the incident optical signal. Due to the fact that light signals are real and positive, intensity modulation and direct detection (IM/DD), is preferred for VLC.

TABLE 2.1: Characteristics of optical wireless communication link configuration [66]

Characteristic	**Direct LOS**	**Non-direct LOS**	**Diffuse**	**Tracked**
Link	Point-to-point	Point-to-multipoint	LAN Ad-hoc	Point-to-point
Flexibility	No	Yes	Yes	No
Transmitters	No	Yes	Yes	No
Receivers	Narrow FOV	Wide FOV	Wide FOV	Narrow FOV (Beam steering)
Power requirement	Low	High	High	Low
Data rate	High (100 Gbps	Few Mbps	16 Mbps	High
Advantages	Higher data rate Up to 5km link No multipath distortion No ambient light noise	Robust to blocking No alignment/tracking Robust to shadowing	Simple alignment Wider coverage Immune to blockage	Lower power usage Reduced multipath ISI Less ambient light noise
Disadvantages	Area coverage and mobility Blocking Alignment is required	High path loss Multipath induce ISI Ambient light noise	High path loss Shadowing Multipath dispersion High power usage	Complex tracking

The VLC technology has many potential applications areas. As such, a lot of research is being done to improve the technology further and demonstrate many applications. To achieve this, many techniques and schemes that have been applied to RF, like OFDM, MIMO and MA have been introduced in VLC with appropriate modifications [4, 34, 37, 138].

2.2.2.1 VLC Channel Model

The optical signal received from the PLC/VLC integration module can be expressed as [34]

$$y(t) = x(t) * h_{\mathrm{v}}(t) + n(t), \tag{2.5}$$

where $y(t)$, $x(t)$, $h_{\mathrm{v}}(t)$ and $n(t)$ denote the received signal, the transmitted intensity signal, the VLC channel impulse response, and the channel noise which is signal-independent and Gaussian, respectively. If only the LOS component is considered, then the VLC transfer function can be written as [34]:

$$H_{\mathrm{v}}(f) = H_{los} = S\eta_{los}e^{(-j2\pi f\tau_{los})}, \tag{2.6}$$

where $H_{\mathrm{v}}(f)$ is the discrete Fourier transform of the $h_{\mathrm{v}}(t)$, S is the photo sensitivity, η_{los} and τ_{los} are the gain and the delay of the LOS signal, respectively.

Considering that LEDs are the transmitting devices, a Lambertian propagation model is considered, with an assumption that the LOS components are dominant over all multipath components from the wall and ceiling reflections [105]. The channel gains considering LOS propagation for a receiver located at a distance of d_{v} and angle of irradiance θ, see Figure 2.3, with respect to the transmitter, can be approximated as [68],

$$h_{\mathrm{los}} = \begin{cases} \frac{A_r(\ell+1)}{2\pi d_{\mathrm{v}}^2} cos^{\ell}(\theta) cos(\psi), & 0 \leq \psi \leq \Psi_c, \\ 0 \quad \text{elsewhere}, \end{cases} \tag{2.7}$$

where A_r the effective collection area of the detector, ψ is the angle of incidence with respect to the receiver axis and ℓ is the Lambertian emission order given by $\ell = -\frac{\ln 2}{\ln cos(\Phi_{1/2})}$, $\Phi_{1/2}$ is the transmitter semi-angle at half power.

Further, when the indoor reflections are considered, the resulting channel gain between the transmitters and the receiver is defined by the distance d_1 between the transmitter and the reflection point, and the distance between the reflection point and the receiver, d_2. As shown in Figure 2.3, respective angles of irradiance and incidence, θ_{ref}, α, β and ψ_{ref} also have an influence on the resulting channel gain values.

The channel gain due to first order reflections is given by

$$h_{ref1} = \frac{A_r(\ell+1)}{2(\pi d_1 d_2)^2} cos^{\ell}(\theta_{ref}) cos(\alpha) cos(\beta) cos(\psi_{ref}) d_{A1} \rho_1, \tag{2.8}$$

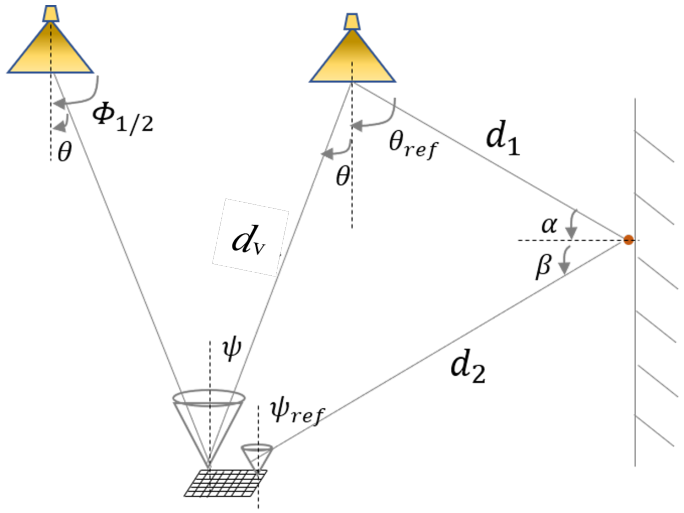

FIGURE 2.3: VLC propagation model for LOS and reflections

where d_{A1} and ρ_1 denote the area of the reflection element and the reflection coefficient of the reflector respectively. Similarly for the second order reflections, the resulting channel gain is given by

$$h_{ref2} = \frac{A_r(\ell+1)}{2(\pi d_1 d_2 d_3)^2} cos^{\ell}(\theta_{ref}) cos(\alpha) cos(\beta) cos(\gamma) \\ cos(\delta) cos(\psi_{ref}) d_{A1} \rho_1 d_{A2} \rho_2, \tag{2.9}$$

where d_3 is the distance between the second reflection point and the receiver, γ and δ denote the angles of irradiance and incidence with respect to the normal of the first reflection element and normal to the second reflection element, respectively. Similarly, d_{A2} and ρ_2 denote the area of the reflection element and the reflection coefficient of the second reflector. Assuming that the background noise affecting the optical receiver has the shot noise caused by background radiation as the dominant noise relative to thermal noise, and that the optical channel does not introduce any non-linearity, then the overall noise components are modelled as AWGN [108].

Thus considering both LOS and NLOS contributions to the received signal, equation (2.6) has an additional component accounting for the NLOS propagation.

$$H_{\mathrm{v}}(f) = H_{\mathrm{los}} + H_{\mathrm{nlos}}, \tag{2.10}$$

where H_{nlos} comprises all reflection orders considered.

2.3 Multiple-Input Multiple-Output (MIMO) Techniques for Optical Wireless Communication

MIMO, a transmission scheme that exploits spatial multiplexing and diversity to offer reliable communication and high data rate, has been widely studied and practically implemented in RF based networks [61, 103]. A MIMO channel model having N_t transmitting elements (TEs) and N_r receiving elements (REs), is represented by the diagram in Figure 2.4. A data symbol, x_t, where $t = 1, 2, \ldots, N_t$, transmitted by the tth transmitter experiences different channel coefficients to each of the N_r receiving elements. As such, the received signal $\boldsymbol{Y}$ from all the transmitting elements can be expressed as:

$$\boldsymbol{Y} = \boldsymbol{H}\boldsymbol{X} + \boldsymbol{N}_G, \tag{2.11}$$

where $\boldsymbol{H} \in \mathbb{R}^{N_t \times N_r}$ denotes the channel matrix of the channel coefficients between each transmitting and receiving elements. The signal

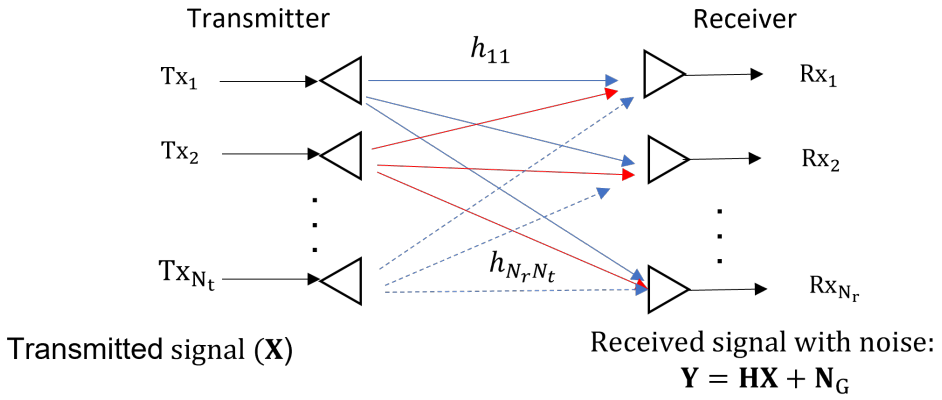

FIGURE 2.4: A channel model representation of an $N_t \times N_r$ antenna MIMO system

matrix comprising all transmitted data symbols from all transmitters is denoted by $\boldsymbol{X}$ and $\boldsymbol{N}_G$ is the noise affecting each data symbol independently.

Motivated by the successful implementation of RF MIMO [103], various research works aimed at achieving high capacity with enhanced reliability and spectral efficiencies, have been undertaken for optical systems [4, 7, 10, 44, 111, 133, 135, 154]. In MIMO systems, it is desirable to have spatially uncorrelated channels in order to avoid inter-channel interference. However, optical MIMO (O-MIMO) systems, especially those employed for indoor applications, are highly correlated, thus enabling only minor diversity gains [44]. Several MIMO techniques have been studied and proposed to reduce the correlation effect of O-MIMO systems. Some of these techniques include power imbalance between transmitters [43], as well as link blockage between some transmitter-receiver pairs [44]. Others are Repetition Coding (RC) to mitigate the correlation nature of indoor O-MIMO by increasing the transmit diversity gains where all

transmitters emit the same signal simultaneously, spatial modulation (SM) [44], [10], which was shown to be robust to high channel correlation since it completely avoids inter-channel interference (ICI) by activating only one transmitter at any transmit interval and the spatial multiplexing technique demonstrated to achieve higher data rates. Other techniques such as space-time coding techniques can be viewed as a combination of SM and space-time shift keying (STSK) schemes.

Another MIMO technique of interest is STBC where multiple copies of the message symbols are transmitted across a number of antennas to exploit the various received versions of the transmitted message and consequently improve the reliability of the communication system. Particularly, Alamouti coding is one of the types of STBC that is considered in the analysis of the work in Chapter 3 . However, because Alamouti coding was originally proposed for RF systems [2], it requires the use of complex signals and therefore, cannot be directly applied without modification to optical systems that deal with real and non-negative signals. Consequently, the authors in [133], describe a brilliant way of combining Alamouti coding with on-off keying (OOK) and adopted it for free-space optical (FSO) communication with direct detection (DD). They describe the modification of the Alamouti code and the associated decision metric such as to maintain all of the desirable properties of the original Alamouti scheme. Based on the modification of Alamouti coding by [133] and the general STBC techniques, some studies on the BER

performance analysis of Alamouti coding for optical wireless systems have been conducted with system performance improvements demonstrated [3, 4, 128, 135].

In [3], a performance comparison analysis of the STBC and RC techniques for VLC systems was conducted and it was shown that the performance of RC is better than the STBC when a single receiver is used, however, for the VLC O-MIMO, STBC outperforms the RC. Further, the performance of Alamouti coding in indoor optical wireless systems, using asymmetrically clipped optical OFDM (ACO-OFDM), was compared with a RC system [7]. These studies show that STBC is attractive for indoor VLC. Hence, space-time coded (STC-MIMO) techniques are studied for the VLC section, in this work. The STC-MIMO system based on the optical Alamouti coding is first investigated in Chapter 3 and then another based on permutation codes (PCs) is investigated and presented in Chapter 5.

2.4 Orthogonal Frequency Division Multiplex (OFDM) and M-ary Frequency Shift Keying (M-FSK)

In this section, an overview of OFDM in optical wireless communication, is presented. Additionally, an overview of M-FSK scheme, is also presented in the final part of the section.

2.4.1 Orthogonal Frequency Division Multiplex (OFDM) in Optical Wireless Communication

OFDM is a type of multi-carrier modulation that was first proposed in [25] to maximize the data rate and minimize the ICI and ISI, due to frequency-selective channels. In OFDM, information symbols are transmitted over multiple orthogonal sub-carriers within a single channel. A combination of fast Fourier transform (FFT) and its inverse, the inverse fast Fourier transform (IFFT) digital signal processing can be used to achieve the implementation of digital OFDM systems. In digital OFDM, input bits are grouped and mapped into N source symbols according to constellation points of a selected modulation scheme, such as phase shift keying (PSK) or quadrature amplitude modulation (QAM). Each of the N complex source information symbols which are mapped to N sub-carriers are input to the IFFT block. The N source symbols each have a symbol period of T_o seconds hence the output of the IFFT is N orthogonal sinusoids, representating the digital OFDM symbol in the time domain. The OFDM symbol is expressed as a summation of all the N orthogonal sinusoids as:

$$x(t) = \sum_{k=0}^{N-1} X(k) e^{(j2\pi f_k t)}, \tag{2.12}$$

where $X(k)$ denotes the kth orthogonal frequency component and $f_k = \frac{k}{T_o} \ \forall k = 0, 1, \ldots, N-1$. Consequently, the nth complex

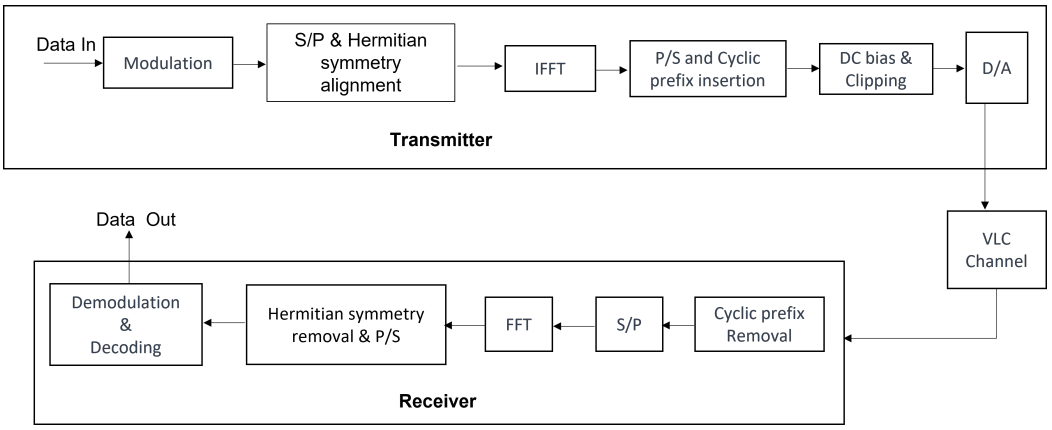

FIGURE 2.5: Optical OFDM system diagram

sample of $x(t)$ sampled at $\frac{T_o}{N}$ is expressed as:

$$x(n) = \sum_{k=0}^{N-1} X(k) e^{(j2\pi \frac{kn}{N}))}, \quad (2.13)$$

At the receiver side, FFT is used to demodulate the received OFDM signal $y(n)$, thus expressed as:

$$Y(k) = \sum_{k=0}^{N-1} y(n) e^{(-j2\pi f_k t)}, \quad (2.14)$$

In IM/DD optical systems, real and positive signals are required to modulate the light sources. To obtain the IM/DD compatible signals, the Hermitian symmetry (HS) property to generate real OFDM signals has widely been used [15, 93, 95]. As shown in Figure 2.5, before the N frequency symbols are sent to the IFFT block, they are made to satisfy the HS constraint. In an HS structure, a message symbol X_n is duplicated in the form of its complex conjugate X_n^*, for $n = 1, 2, \ldots, \frac{N}{2} - 1$. For N sub-carriers, the general expression relating the message symbols, their complex conjugate and their positions

due to the HS constraint is given as:

$$X_{(\xi+2)} = X^*_{(N-\xi)}, \;\; \xi = 0, 1, 2, \ldots, \frac{N}{2} - 2. \tag{2.15}$$

Thus, the HS structure is formed by concatenating the original vector of the message symbols with the vector of their complex conjugate symbols as,
$[0, X_2, X_3, \ldots, X_{(N/2)}, 0, X^*_{(N/2)}, \ldots, X^*_3, X^*_2]$. The $*$ superscript denotes the complex conjugate. The first and $(\frac{N}{2}+1)^{th}$ components in the HS structure are set to zero ($X_{(0)} = X_{(N/2+1)} = 0$), to avoid any DC shift or any residual complex component in the time domain signal.

To obtain positive unipolar signals, a technique referred to as hard clipping, where the negative amplitudes after the IFFT output are set to zero, can be used. However, this results in information loss hence affects the system reliability. As such, intensity-modulated optical OFDM schemes such as direct curect (DC) biased optical OFDM (DCO-OFDM) and asymmetrically clipped optical OFDM (ACO-OFDM) have been proposed [8]. In DCO-OFDM, a fixed bias is added to the time domain signal and the negative peaks are clipped, while in ACO-OFDM all the even indexed sub-carriers are set to zero. The HS is imposed on the data-carrying odd indexed sub-carriers as in DCO-OFDM. All the negative peaks are removed by clipping the resultant signal at zero. Because of its simplicity, DCO-OFDM is elected to be used in this work.

In this work, two simple methods of DC biasing, respectively referred to as DC1 and DC2, are considered. In the DC1 biasing method, the DC bias added to all the components at the output of the IFFT block is equal to the absolute value of the lowest negative amplitude of the real bipolar signal at the output of the IFFT block. On the other hand, DC2 biasing refers to a bias of $10\log_{10}(\zeta^2+1)$ [8], where ζ, refers to the clipping factor.

2.4.2 M-ary Frequency Shift Keying (MFSK)

In an MFSK modulation scheme, symbols are modulated as one of the M available frequencies, such that the modulated symbol $x_i(t)$ is expressed by [151],

$$x_i(t) = \sqrt{\frac{2E_s}{T_s}}\cos(2\pi f_i t) \quad 0 \leq t \leq T_s \tag{2.16}$$

where E_s is the signal energy per modulated symbol and $i = 1, 2, \ldots, M$ and T_s the symbol period. Each of the M available frequencies are specified as

$$f_i = f_0 + \frac{i-1}{T_s}\cos(2\pi f_i t) \quad 1 \leq i \leq M. \tag{2.17}$$

With M available frequencies, $\log_2 M$ bits are transmitted at each sampling time, translating into a bandwidth efficiency of:

$$\eta = \frac{\log_2 M}{M}, \tag{2.18}$$

When an AWGN channel is considered, the error probability, P_s of a symbol with energy E_s can be approximated as [151],

$$P_s = \frac{1}{2} e^{-\frac{E_s}{2N_0}}, \tag{2.19}$$

where $E_s = E_b \log_2(M)$ and E_b is the energy per information bit. The AWGN noise power spectral density is denoted by N_0. Equation (2.18) demonstrates one of the drawbacks of MFSK schemes, low spectral efficiency, especially for large values of M. However, this modulation scheme has been shown to be robust against permanent frequency disturbances and impulse noise in PLC channels.

2.5 Multiple Access and Multiple Access Decoding

In this section, some MA techniques applied for to PLC, VLC and HPV systems are presented. The latter part of the section then focuses on decoding methods applied in MA techniques.

2.5.1 Multiple Access

MA techniques and their variations have been a major research focus in studies of supporting massive ubiquitous connectivity, low latency and highly efficient utilization of spectrum resources [19, 149]. Basically, MA techniques allow multiple users to use and share the channel resources like frequency, time-slots and code sequences. MA can be classified as orthogonal or non-orthogonal depending on whether users interfere with each other or not, as they share the channel

medium. In orthogonal MA, users theoretically do not interfere with each other as they share the communication channel [149]. In literature, various MA techniques have been applied to different communication technologies, of course, most were initially applied to RF communication systems, and then modified versions applied to other technologies according to the nature of the respective channels.

Various orthogonal MA techniques are shown in Figure 2.6 as illustrated in [149]. In time division multiple access (TDMA), a user is allowed to use the full bandwidth spectrum of the communication channel. However, each user is allocated a unique time-slot in a cyclical fashion on the channel. This allows separating a number of users in time on a single channel [116]. Availing the full bandwidth spectrum enhances the spectral efficiency per user, however, transmission delays are of concern as users have to wait for the availability of their allotted time-slot to be able to transmit.

On the other hand, frequency division multiple access (FDMA) subdivides the available channel bandwidth into a number of frequency non-overlapping sub-channels [116, 149]. A sub-channel is then assigned to each user upon request. The sub-channels are separated by a guard band to avoid ISI. However, these guard bands reduce the system bandwidth, hence the data rate is affected.

Orthogonal FDMA (OFDMA) is an enhancement of FDMA where users are assigned to groups of sub-carriers at different time slots.

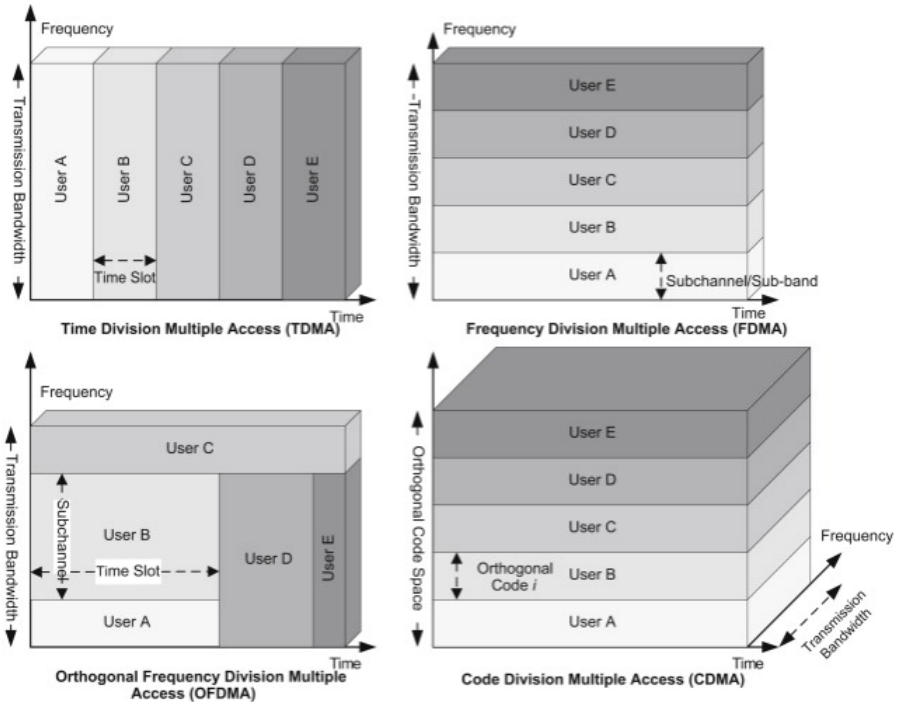

FIGURE 2.6: Illustration of orthogonal multiple access schemes [149]

In OFDMA, varying resource requirements is possible because sub-carrier spacing and time-slot duration are flexible as illustrated in Figure 2.6. As such OFMDA is said to enable better data rates and offer superior bandwidth efficiency.

In code division multiple access (CDMA), simultaneous access to the communication channel is basically achieved by assigning a unique code to every user [149]. Hence multiple users are able to access the channel at the same time while using the entire available frequency spectrum. The user's unique code is commonly referred to as a chipping sequence or signature sequence. Every message 'bit' to be transmitted is encoded by the user's respective chipping sequences. Various encoded messages from different channel users combine and the receiver must correctly identify the transmitting users and their corresponding messages. The receiver will also have a copy of the

transmitter's unique code to be used to decode the sent message. In CDMA, the signal transmissions among the multiple users completely overlap both in time and in frequency. However, because each signal is spread in frequency by a code sequence, the demodulation and separation of these signals at the receiver, is possible. Therefore, CDMA is highly spectral efficient and readily available for any user all the time. Due to simultaneous transmission of several users, there is a probability of decoding errors due to interference by other users. This is widely referred to as multiple access interference (MAI), the major cause of system degradation in CDMA enabled networks.

2.5.2 Multiple Access Techniques in PLC Systems

In literature, it is notable that, until recently when non-orthogonal multiple access (NOMA) was proposed to be used in PLC [118], the MA techniques employed in PLC have been TDMA, FDMA and CDMA, where the channel resource sharing is enabled by either assigning different time slots, frequency bands or unique code sequences to each user, respectively [13, 144, 146, 151]. However, the CDMA technique is more power and spectrum efficient compared to TDMA and FDMA. Moreover, because of the coded transmitted messages, it also offers security from unintended recipients. Thus, the work in this thesis focuses on the coded MA technique.

2.5.3 Multiple Access Techniques in VLC

In most VLC systems, IM/DD is used, as such, the system requires real and non-negative information signals to be transmitted. Therefore, applied modulation or MA techniques must take into account the modification to accommodate this major constraint in VLC systems. Various MA techniques that were originally applied in RF such as TDMA, spatial division multiple access (SDMA), FDMA, CDMA and NOMA, have been proposed for use in VLC [42, 56, 73, 98, 156, 158]. For example, in [73] TDMA was used to achieve beam forming to accommodate multiple target devices. In this scheme, it was proposed to focus the source light on different target device at each time slot, thus demonstrating an optical beam-forming ranging between 5 and 10 dB to each target device. However, the challenge of non-continuous transmission is undesirable. Furthermore, [156] used OFDMA to realize visible light positioning and communication simultaneously in the same band using OFDMA. They proposed a system where the whole bandwidth is divided to subcarrier blocks and the particular subcarrier blocks are exclusively assigned to the corresponding LEDs. The LEDs transmit different data sequences to the PD for VLC. The VLC's receiver measures the power of particular data sequences to estimate the channel gains and consequently the transmission distances. Based on the estimated transmission distances and the LEDs' locations, the positioning feature is realised without degrading the communication's throughput.

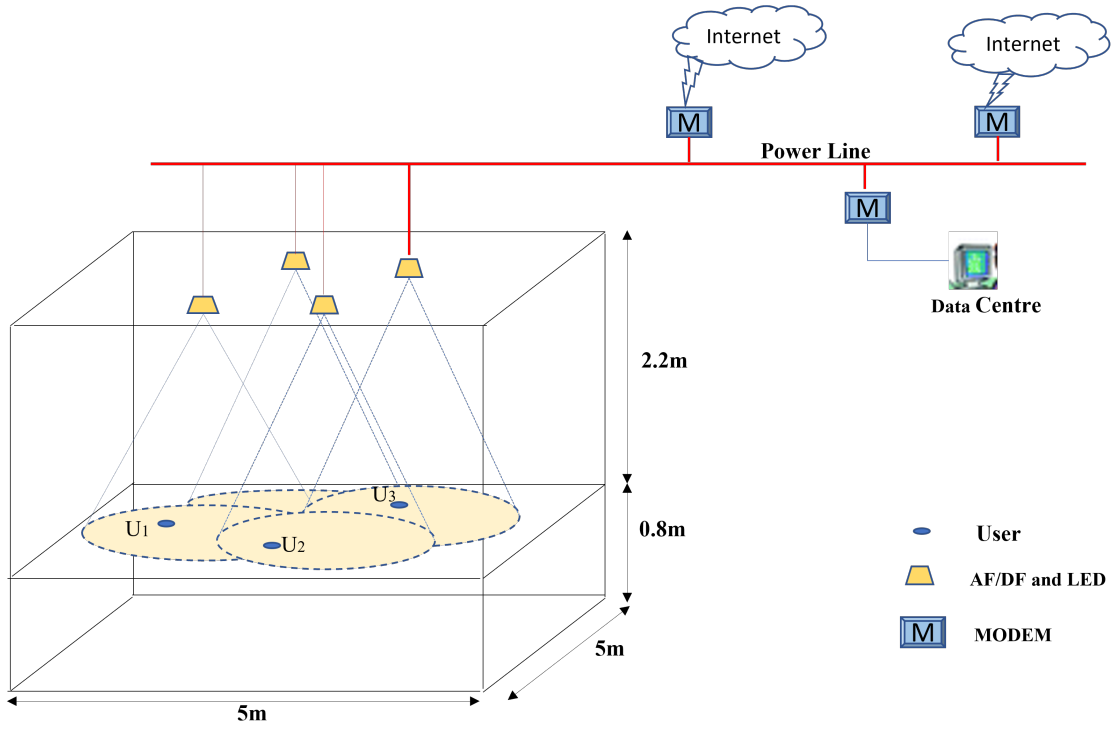

FIGURE 2.7: Indoor environment scenario of multiple access HPV system

CDMA is another MA technique that has been employed in VLC [42, 56]. However, it is equally observed that there is still a lot of work required to optimise the implementation of CDMA, in terms of the design of the optical code sequences to be used as well as the need for less complex decoding techniques that will complement its advantages of network security, power and spectral efficiency.

2.5.4 Multiple Access Techniques in HPV Systems

An indoor scenario of an MA system having several users accessing the network via a PLC channel is depicted in Figure 2.7. The powerline is the information backbone feeding the VLC transmitters which serve as access points (APs) for all users in the room. Significant research concerning MA techniques in different communication

technologies such as RF, PLC, fiber networks and VLC has been conducted. However, there has not been much work in the area of MA techniques for the HPV system. Meanwhile, the high demand for simultaneous connectivity to networks necessitates the investigation of MA techniques in HPV systems. The work in [93] is one of the few that considered multiuser scenario on the VLC section of an HPV system.

In [93], authors considered a multi-user integrated PLC and VLC system and mainly focused on the use of TDMA and FDMA jointly used with spatial optical OFDM (SO-OFDM), where, joint subcarrier allocation (SA) among multiple spatially distributed LED luminaries is considered. This implies that in a multi-user scenario, only some LEDs can serve specific users and user mobility could be restricted. Further, a subcarrier pairing (SP) scheme was introduced between the incoming signal from the PLC to the multiple LEDs luminaries. It was highlighted in [93] that the hybrid system employing OFDMA outperformed that using OFDM-TDMA in multi-user situations, however, at the expense of computational complexity. Thus, this gives an opportunity for further research in finding solutions that would reduce the computational complexity at different sections of the MA HPV systems.

2.5.5 Codes for the MA HPV System

The work in this thesis focuses on coded MA techniques because of their flexibility, in that, either time, frequency or both resources, can

be simultaneously shared by users. As mentioned earlier, MAI is a major drawback in CDMA systems, hence MA code selection is of the essence. In a coded MA HPV system, it would be efficient to use codes applicable to both the constituent channels of the system. In order to mitigate MAI and enhance decoding at the receiver, the chipping sequences (codewords) of the MA codebook have to satisfy the following two conditions [27, 124]:

1. Each chipping sequence should be distinguishable from a shifted version of itself.

2. Each chipping sequence should be distinguishable from every other sequence in the codebook, including their respective shifted versions.

From the above required conditions, it is clear that the magnitude of the auto-correlation for all non-zero shifts of any code sequence should be small. On the other hand, the cross-corrrelation of any two codewords should have a maximum value of zero. These conditions are easily achievable for channels transparent to signal polarity. However, optical channels require the use of real and positive codes mainly having a sequence of {0,1}, thus the minimum possible cross-correlation when a sequence of {0,1} is used, is 1. Codes based on these optical system requirements have been commonly known as optical orthogonal codes (OOCs) or unipolar orthogonal codes (UOCs). Optical-based codes are of interest to this study because of the VLC section in the investigated hybrid system.

2.5.5.1 Optical Orthogonal Codes (OOCs)

An optical orthogonal code (OOC), $\boldsymbol{C}$ is generally defined by its code length L, weight w and auto and cross correlation parameters, λ_a and λ_c, respectively. The code weight refers to the number of ones in each codeword, thus $(L - w)$ number of zeros in each codeword. Thus, a one dimensional OOC is expressed as $\mathcal{C}(L, w, \lambda_a, \lambda_c)$. The properties of the auto-correlation and cross correlation are given as (2.20) and (2.21), respectively [27, 124]

$$\sum_{t=0}^{L-1} x_t x_{t+\tau} \leq \lambda_a, \tag{2.20}$$

where τ, $0 < \tau < n$ denotes any integer shift and each codeword $\boldsymbol{x} = \{x_0, x_1, \ldots, x_{L-1}\} \in \boldsymbol{C}$. Similarly, the cross-correlation bound is:

$$\sum_{t=0}^{L-1} x_t y_{t+\tau} \leq \lambda_c, \tag{2.21}$$

for any $\boldsymbol{x} \neq \boldsymbol{y} \in \boldsymbol{C}$ and any integer shift τ_s. The cardinality $|\boldsymbol{C}|$ is the number of codewords in the OOC codebook. For any MA system, it is desirable to have a large cardinality so as to accommodate a large number of users, thus an OOC having the maximum size is said to be optimal. The largest possible $|\boldsymbol{C}|$ is denoted by $\Phi(L, w, \lambda_a, \lambda_c)$.

Using the positions of the non-zero elements, an OOC with $0, 1, \ldots, (L-1)$ positions can be represented in set notation. For example, the set notation of $\boldsymbol{x} = 1000100001000000100$, a codeword with $L = 19$ and $w = 4$, can be represented as $\{0, 4, 9, 16\}$. Each of the

L circular shifted versions of $\boldsymbol{x}$ represent the same codeword [47]. Hence, the first four set notation representations of $\boldsymbol{x}$ can be given as $\{3, 8, 15, 18\}$, $\{2, 7, 14, 17\}$, $\{1, 6, 13, 16\}$, $\{0, 5, 12, 15\}$.

The determination of the exact values of $\Phi(L, w, \lambda_a, \lambda_c)$ and the specific construction of optimal codes are of great interest as seen in literature, where the lower and upper bounds of the code's maximum cardinality and construction methods have been proposed [27, 47, 99, 124, 137]. The ideal OOC generating scheme would be one with maximum cardinality for given L, w, λ_a and λ_c. According to [27], an upper bound on the maximum code size of an ideal OOC, $\Phi(L, w, 1)$ where $\lambda_a = \lambda_c = 1$ is derived and given by

$$\Phi(L, w, 1) \leq \frac{L-1}{w(w-1)} \tag{2.22}$$

when L is even, the bound is said to be slightly stronger [27] and given as:

$$\Phi(L, w, 1) \leq \frac{L-2}{w(w-1)} \tag{2.23}$$

2.5.5.2 OOC Encoding and Decoding

In the coded MA system using OOCs, each user is assigned one of the codewords of length L such that, the user's information bit '$1'$ is mapped to the assigned codeword, while their information bit '$0'$, is equivalent to a sequence of zeros of the same length. All user encoded data is superposed and transmitted via a common channel. Let $b_u \in \{0, 1\}$ be the uth user's information bit and $\boldsymbol{x}_u$ its assigned

codeword. Hence, the received signal $r(t)$, the superposition of all the sequences from U active users is expressed as

$$\boldsymbol{r}(t) = \sum_{u=1}^{U} b_u \boldsymbol{x}_u (t - \tau_u) \tag{2.24}$$

where τ_u is the time delay for user u.

Although maximum likelihood (ML) detection can be used, the correlation decoding method has widely been used for optical systems. However, if the optical MA code used in the system is such that the combination of different codewords results in unique sequences, another exhaustive search decoding scheme based on the minimum distance of the received sequence and codewords in the look up table (LUT) at the receiver can be used.

To enhance the spectral efficiency, users are not only assigned single codewords but disjoint subsets having $|\boldsymbol{C}_u|$ codewords each, where $\boldsymbol{C}_u \subseteq \boldsymbol{C}$. As such, the user's code rate R_u is generally described as the ratio of b_u to L.

$$R_u = \frac{b_u}{L} = \frac{\log_2 |\boldsymbol{C}_u|}{L}. \tag{2.25}$$

However, the assignment of disjoint codes to each user in the MA system requires large code sizes which translate to very long code lengths, hence very low spectral efficiency gains are made.

Decoding by Correlation: At the receiver, the decoding process is aided by a correlator, which first compares $\boldsymbol{r}_t$ with a stored copy of the $\boldsymbol{x}_u$. If $u = 1$ signifying that the user of interest is user 1, then

the correlator output signal $\boldsymbol{y}_1$, assuming the transmission of bit '1' and ignoring the channel noise, can be expressed as [27, 125]

$$\boldsymbol{y}_1 = \int_0^T \boldsymbol{r}(t)\boldsymbol{x}_u(t)dt \tag{2.26}$$

If the interference effect of any u^{th} user on first user is denoted as $I_u^{(1)}$, then the magnitude of (2.26) is expressed as

$$\boldsymbol{y}_1 = b_u \cdot w + I_1 \tag{2.27}$$

where the total interference on the first user is represented by the second term in (2.27) given as $I_1 = \sum_{u=2}^{U} I_u^{(1)}$. If the incoming superposition signal contains the receiver's unique codewords, a peak is observed in the correlated signal. The key feature to ensure accurate data recovery is orthogonality of the codewords used.

2.5.6 Binary Superimposed Codes

Long code lengths for OOCs are one of the major parameters resulting in poor spectral efficiency. Hence, sub-optimal types of codes that may result in $\lambda_a > 1$ and $\lambda_c > 1$, can be applied in optical systems and consequently to the MA HPV systems, on condition of unique decodability. One such codes are binary superimposed codes [71] which consists of a set of codewords whose digit-by-digit Boolean sums result in uniquely distinguishable sequences. They have generally been constructed from different known code structures of linear

and non-linear block codes as demonstrated in [71]. Correlation decoding methods can be used as well as exhaustive decoding methods based on minimum distance. Superimposed codes are disjunctive meaning they satisfy the following properties:

1. For a given positive integer m also known as the order of the code, every Boolean sum of up to m different codewords is distinct from every other Boolean sum of m or fewer codewords.

2. The Boolean sum of m or fewer code words must logically not include a code word other than those used to form the sum.

To attain the above properties, four basic parameters are defined for superimposed codes; the codelength, L, the cardinality $|\boldsymbol{C}|$, the minimum Hamming distance $d_{\min}$ and the order of the code, m. In the coded MA systems investigated in this thesis, sub-optimal binary codes mainly constructed from PCs, have been used. Their construction will be presented in Chapter 4.

2.6 Summary

In this chapter, background details upon which the work in subsequent chapters is based, has been presented. Notably, channel models of the PLC and VLC have been presented. Others are MA and MIMO techniques, as will be applied in this work.

CHAPTER 3

Space-Time Coding for VLC System Employing Imaging Receivers

This chapter is based on the following publication: *Mulundumina Shimaponda-Nawa, Shamin Achari, Dushantha Nalin K Jayakody, and Ling Cheng*, "Visible Light Communication System Employing Space Time Coded Relay Nodes and Imaging Receivers". *SAIEE Africa Research Journal, 111(2):56–64, 2020.*

The author of this thesis conceptualized the work, performed the simulations, analyzed the results and wrote the paper.

3.1 Introduction

In this chapter, we specifically focus on the gains from STC-MIMO systems. A VLC system, whose source of information is assumed to be a powerline, and employs a combination of relaying and MIMO techniques, is proposed. Precisely, the performance of a VLC system, with relay nodes equipped with an STC-MIMO technique, is investigated. The BER performance of the Alamouti coding scheme, which is a type of space (STBC), is specifically considered. In order to enhance the overall system reliability, we propose to use an

imaging receiver (ImR), in conjunction with the relay-MIMO setup. In comparison to when a non-imaging receiver (NImR) is employed, an improved signal-to-noise ratio (SNR) of 7 dB is observed when an ImR with a specific number of pixels, is used, hence, improving the BER. We also investigate and show that the selected number of pixels and receiver location have an effect on the system BER. SNR values of 9 dB, 11 dB and 15 dB were required to maintain a BER of 10^{-4} for imaging receivers with 70, 50 and 20 pixels, respectively.

3.2 Alamouti Space-Time Coded MIMO

The Alamouti space-time coded (ASTC) scheme, initially proposed by [2] has been one of the basic STBC studied over the years. It is a simple MIMO technique that achieves spatial diversity by using two transmit antennas Tx_1 and Tx_2 as represented in Figure 3.1. In an ASTC scheme, the sequence of information symbols $\{x_1, x_2, x_3, \ldots, x_I\}$ is segmented into groups of two. The transmission of symbols is such that, in the first time slot, the first symbol x_1 in the group of two is transmitted from Tx_1, while the second symbol x_2 is transmitted from Tx_2. In the second time slot, the complex conjugate components $-x_2^*$ and x_1^* are transmitted from Tx_1 and Tx_2, respectively. The process is repeated for the rest of the symbols. Since two time slots are required to transmit two symbols, the spectral efficiency is equivalent to that of a single-input single-output (SISO) system. However, the ASTC scheme enhances the system reliability compared to a SISO system as seen in Figure 3.2.

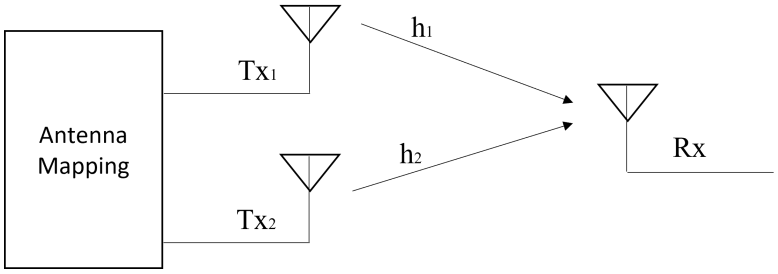

FIGURE 3.1: Representation of the Alamouti space-time coded scheme

With regards to the

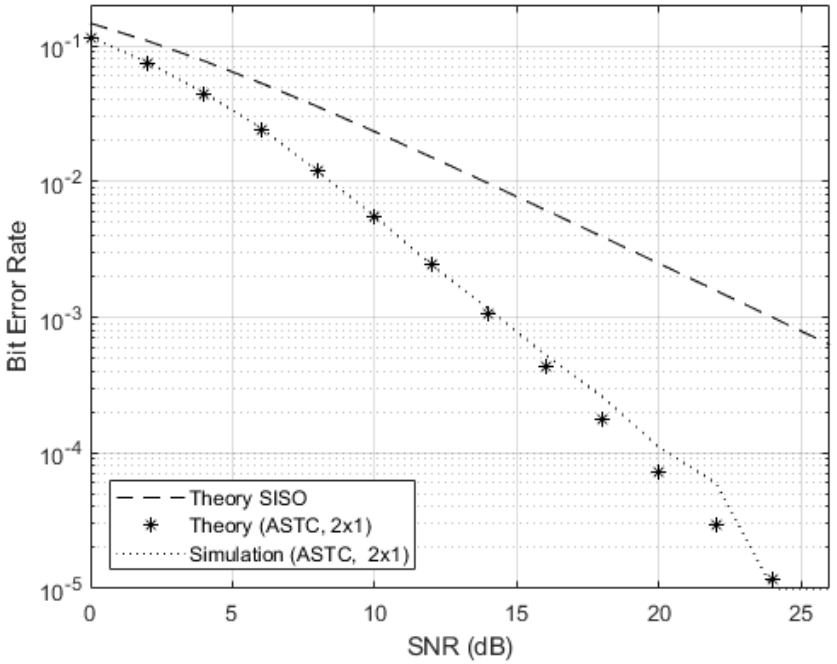

FIGURE 3.2: SISO and ASTC ($N_t \times N_r = 2 \times 1$) BER plots.

3.3 System Model

We consider a room scenario of dimensions 5 m × 5 m × 3 m (width × length × height) and focus on three main communication elements, i.e. the upright transmitter (UTx), the relay nodes and ImR, as depicted in Figure 3.3. Both the transmitter and ImR are located at a particular height above the floor, while the relay nodes are

installed in the ceiling of the room. The information source of the UTx is the power line connected via a power plug, in the considered room. The UTx transmits the information to the ImR only via the relay nodes and it is assumed that there is no direct communication between the UTx and the ImR. We further assume an interference free scenario between the lights of the transmitter and that of the relay nodes. The two primary roles of the relays installed in the ceiling are illumination and information transfer between the UTx the ImR.

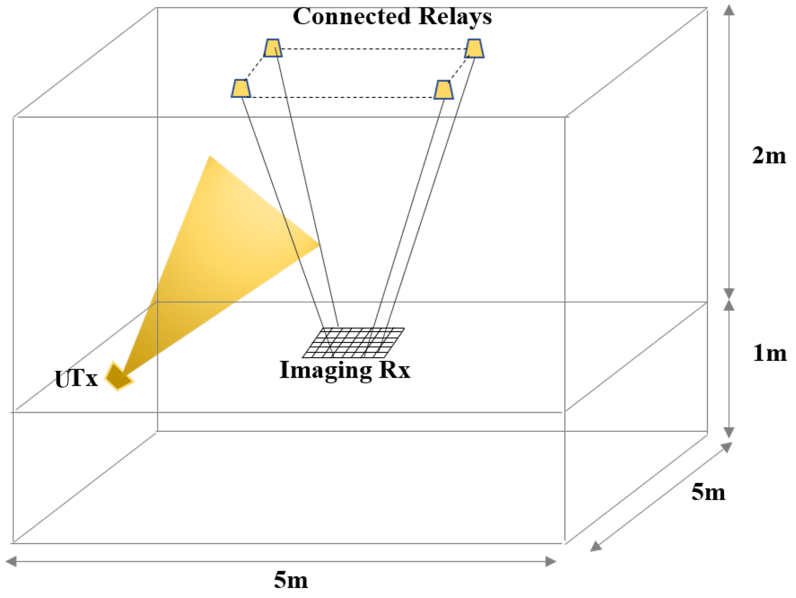

FIGURE 3.3: VLC system room setup: upright transmitter, relays and imaging receiver

The information flow of the system is presented by a block diagram of Figure 3.4. The UTx, receives the information to be sent, from the powerline. We adopted a PLC-VLC conversion structure proposed by [95], where the modulation schemes and carrier spectrum of PLC and VLC are the same. The UTx, then sends an amplified version of the received signal to the relay nodes via a VLC channel. The

relays are interconnected and controlled via a common controller that equally ensures synchronisation of the relays. The controller also coordinates all the relay operations to ensure the STBC configuration is achieved.

The Alamouti encoded data are transmitted to the destination, the ImR, via the VLC channel. At the receiver, the photo-currents received in each pixel of the ImR are amplified and decoded separately using the maximum likelihood decision metric. After the individual pixel decoding and estimation, the reconstruction processes of the message are done based on a majority voting decision technique using the estimated messages by individual pixels. Although the aspect of the control feedback from the ImR to the relay unit has not been discussed in this study, we suggest the use of a low data rate infra-red (IR) link to achieve this.

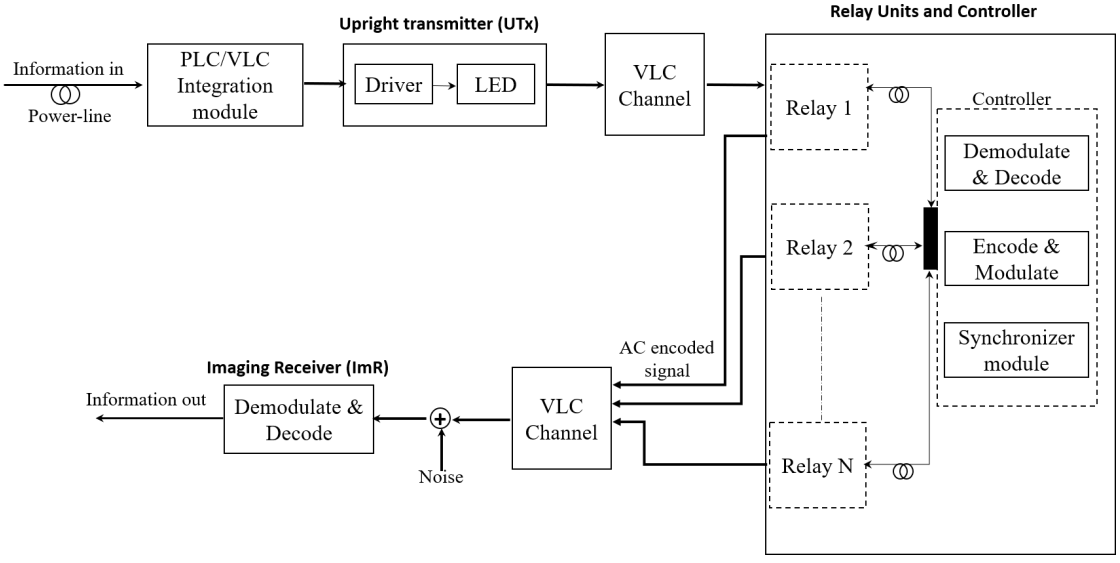

FIGURE 3.4: System block diagram of an upright VLC transmitter connected to a PLC channel with Alamouti coded relay nodes and imaging receiver.

3.3.1 Two-Hop Transmission Process

As represented in Figures 3.3 and 3.4, the VLC information source, the UTx, located on the communication plane, transmits the information to all the relays which are interconnected and cooperate in operation. The transmitter-relay scenario is a single-input multiple-output (SIMO). The received signals at the relay nodes are processed by maximum ratio combining (MRC) at the controller, after which they are re-encoded for re-transmission to the destination.

We consider relay nodes operated in an ASTC scheme. According to the conventional ASTC scheme of [2], that considers two transmitters and one receiver, the symbols to be transmitted, x_1 and x_2, coded in space (rows) and time (columns) are represented as

$$\mathbf{x} = \begin{bmatrix} x_1 & -x_2^* \\ x_2 & x_1^* \end{bmatrix}, \tag{3.1}$$

where x_1^* and x_2^* are complex conjugate components. If the channel parameters between transmit elements (TEs) 1 and 2 and the receiver, are denoted by h_1 and h_2 as depicted in Figure 3.1, then the received signals r_1 and r_2, at the two time intervals can be written as

$$\left\{ \begin{array}{l} r_1 = h_1 x_1 + h_2 x_2 + n_1 \\ r_2 = -h_1 x_2^* + h_2 x_1^* + n_2 \end{array} \right\}, \tag{3.2}$$

where n_1 and n_2, are random variables representing receiver noise modelled as AWGN.

In VLC however, there exists a signal constraint, that requires the transmitted signals to be real and positive, since light signals are neither complex nor negative. Therefore, we adopt the modified Alamouti coding scheme in [133], which considers this constraint. According to [133], the coded symbols to be transmitted at the first and second time intervals are represented as

$$\mathbf{x} = \begin{bmatrix} x_1 & \bar{x}_2 \\ x_2 & x_1 \end{bmatrix}, \tag{3.3}$$

where, a complement symbol $\bar{x}_i$ can be represented as $\bar{x}_i = -x_i + \mathcal{I}$ and $\mathcal{I}$ is a positive constant related to the intensity of the light source. The Alamouti coded symbols are then transmitted over an optical wireless channel with channel gains between any transmitter-receiver pair denoted as h_{ij}, i and j denote the receiver and transmit indices. Accordingly, adopting the mathematical model of [133], the received electrical signals for each transmit interval are denoted as y_1 and y_2 and given as

$$\left.\begin{aligned} y_1 &= h_{11}x_1 + h_{12}x_2 + n_1 \\ y_2 &= h_{11}\bar{x}_2 + h_{12}x_1 + n_2 \end{aligned}\right\}, \tag{3.4}$$

where n_1 and n_2 are noise components modelled as independent zero-mean Gaussian real random variables with variance σ^2. With the assumption that the receiver has perfect knowledge of the channel, the receiver can use y_1 and y_2 of (3.4) to statistically construct the

symbols transmitted at each interval [133] as 3.5:

$$\left.\begin{cases} \tilde{x}_1 = h_{11}y_1 + h_{12}y_2 - h_{11}h_{12} \\ \tilde{x}_2 = h_{12}y_1 + h_{11}y_2 - h_{11}^2 \end{cases}\right\}. \tag{3.5}$$

From the derivation of [133] and considering that the transmitted information symbols, x_1 and x_2, are independently chosen from the input symbol stream, a maximum likelihood decision is made separately on each of them by using,

$$m(\tilde{x}_i, x_i) = (\tilde{x}_i - x_i)^2 + (h_{11}^2 + h_{12}^2 - 1)x_i^2,\ i = 1, 2, \tag{3.6}$$

and finally a decision rule is made that $x_i = \hat{x}_i$, if

$$(\tilde{x}_i, \hat{x}_i)^2 + (h_{11}^2 + h_{12}^2 - 1)\ \hat{x}_i^2 \leq (\tilde{x}_i, x_i)^2\ + (h_{11}^2 + h_{12}^2 - 1)x_i^2, \text{ for } x_i \neq \hat{x}_i. \tag{3.7}$$

This is the decision metric that will be used in the simulations to demonstrate the enhanced performance of the system under consideration.

3.3.2 Imaging Receiver

In [59], two main receiver types for VLC systems were investigated, i.e. non-imaging angle diversity receivers (ADRs) and ImR. In their investigation and analysis, they demonstrated that the ImR outperforms the systems using ADR in terms of robustness against shadowing and the ability to maintain LOS even in the harsh environment

of shadowing. Therefore, in this chapter, we propose to use an ImR in order to use it's merit that enhances ISI avoidance. The avoidance of ISI is achieved by the fact that the ImR consists and uses a number of pixels that only detects a limited number of signals that could reach the receiver at different times due to different path lengths. Having a combination of Alamouti coded relays with the ImR, combines the advantages that the individual techniques possess. Thus, the proposed system is robust against shadowing and allows mobility due to a number of installed relays. The adopted structure of the

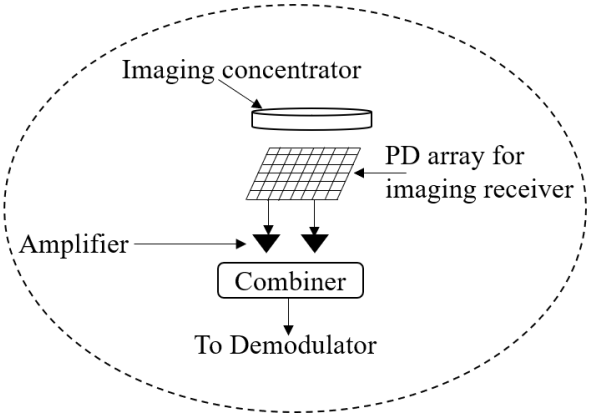

FIGURE 3.5: Imaging receiver structure [59]

ImR is shown in Figure 3.5 [59, 68]. Given the wide spread development of electro-optical system for telecommunication, the demand of customised opto-electronics devices has increased, thus, availability of the ImR for practical systems is no longer an issue. When the transmitted signal is received at each pixel, the metric specified in (3.6) is individually applied at each pixel and then a majority voting techniques is applied to finally construct the received message.

3.4 Simulation Results and Discussion

Firstly, the performance comparison of a non-imaging receiver and ImR, considering both the LOS and NLOS, are presented. Further, we considered ImRs with different number of pixels and varied the receiver location in the room. Referring to Figure 3.3 for the room setup and using the simulation parameters in Table 3.1, the obtained results are presented in subsequent subsections. It should be noted

TABLE 3.1: Simulation Parameters Used

Room Parameters	
Parameter	***value***
Room size (W × L × H)	5 m × 5 m × 3 m
Wall reflectivity (ρ)	0.8
Area of reflection elements, d_A	5 m × 5 m
Number of reflection elements	2500
Transmitter and Relay Parameters	
Parameter	***Value***
Number of Transmitters (UTx)	1
UTx height from floor	1 m
Locations (x,y,z)	(1,1,1)
Number of Relays	4 (2 for each ASTC configuration)
Relay Locations (x,y,z)	(1.25,1.25,3), (1.25,3.75,3)
	(3.75,1.25,3), (3.75,3.75,3)
Transmitted Optical Power	2 W
Receiver Parameters	
Parameter	***Value***
Receiver plane height from floor	1 m
Number of Receiver Pixels	20, 50, 70
Receiver locations (x,y,z)	(1.25,1.5,1), (2.5,1.5,1)
	(1.25,4.5,1), (2.5,4.5,1)
Single detector FOV	70

that due to the symmetry of the room under consideration, when relay position combinations, A and B or C and D are assumed, the

results of each relay pair are equal. A, B, C and D are ceiling positions with the following respective x and y coordinates: A(x = 1.25 m, y = 1.25 m), B(x = 3.75 m, y = 1.25 m), C(x = 1.25 m, y = 3.75 m) and D(x = 3.75 m, y = 3.75 m). Thus, we only considered one relay pair for our analysis.

3.4.1 BER Performance Comparison for Non-Imaging (NImR) and ImRs

The BER performance comparison was carried out for non-imaging and imaging receivers with relay nodes positioned at x = 1.25 m, y = 1.25 m and x = 3.75 m, y = 1.25 m, while the receiver location was x = 1.25 m, y = 1.5 m. We specifically considered two scenarios; firstly, for the LOS propagation and secondly, NLOS up to the second order reflections.

Figure 3.6 shows that the ASTC system using an ImR outperforms the Alamouti system using a NImR, by about 7 dB, when LOS is considered. This is due to the fact that the array of the receiver pixels is seen as multiple receivers, hence, the benefit of a high receive diversity. Additionally, the majority voting technique for imaging receivers increases the decoding accuracy. When compared to the performance of the NImR, the logarithmic decrease of the BER for the ImR at lower SNR, is very clear from Figure 3.6, demonstrating the combinational benefit of the ASTC MIMO technique with the ImR, in that both techniques have a capability of de-correlating the

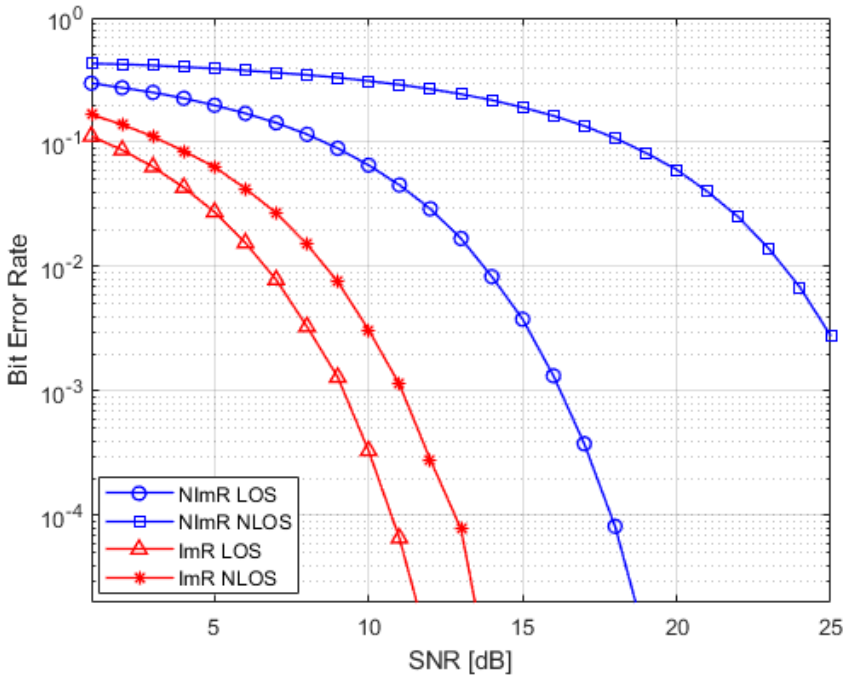

FIGURE 3.6: Performance comparison for non-imaging and imaging receivers

inherent highly correlated indoor MIMO links. Thus, this demonstrates the potential of the proposed scheme in achieving high link reliability. Furthermore, the combination of relays and ImR, enhances the robustness against shadowing as evidenced by the performance of the NLOS links in comparison to both LOS and NLOS links, when the NImR scheme is used. We observe an enhanced performance of over 5 dB and 10 dB respectively, at a BER of 10^{-3} .

3.4.2 Performance Evaluation for Different Number of Receiver Pixels

In Figure 3.7, we observe that the system BER performance is proportional to the number of pixels used for a particular receiver. When the number of pixels is reduced from 50 to 20, an additional 4 dB

SNR is required to achieve a BER of 10^{-4}, while an increment to 70 pixels improves the system SNR by approximately 2 dB. This enhancement is attributed to individual pixel decoding metric and the high probability accurate decoding by majority voting when a large sample size is considered. With increased number of pixels, one of the advantages of MIMO, which is, enhanced link diversity, resulting in system performance improvement, is evident. Thus, imaging receivers with hundreds of pixels would definitely enhance system performance. However, a very high number of pixels would require more processing resources. Therefore, a trade off between the system performance and the processing speed, needs to be well analysed.

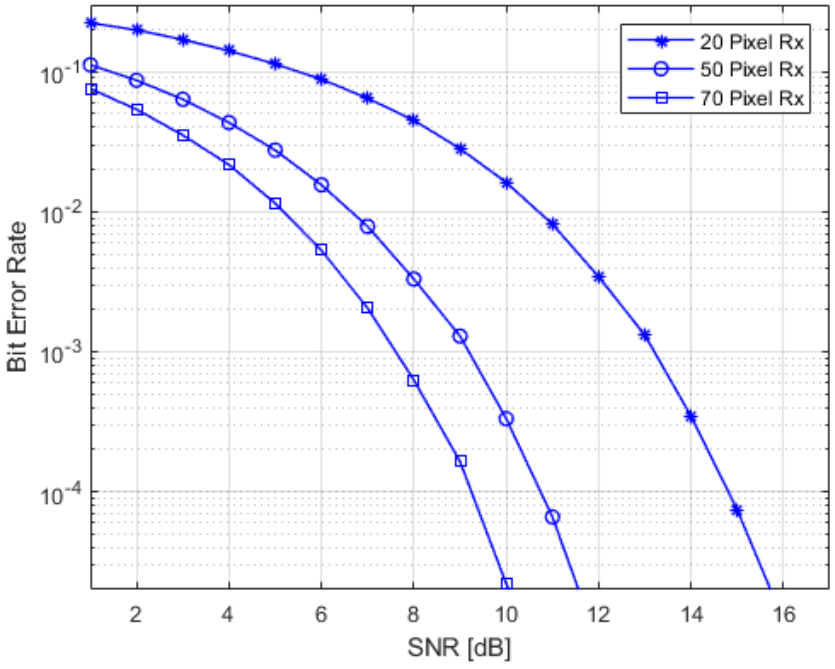

FIGURE 3.7: Performance comparison: Imaging receivers with different number of pixels

3.4.3 Performance Impact due to Receiver Location

Two x-coordinates, x = 1.25 m and x = 2.5 m, with varying y-coordinates were used to investigate the receiver location impact on system performance. From Figure 3.8, though the performance

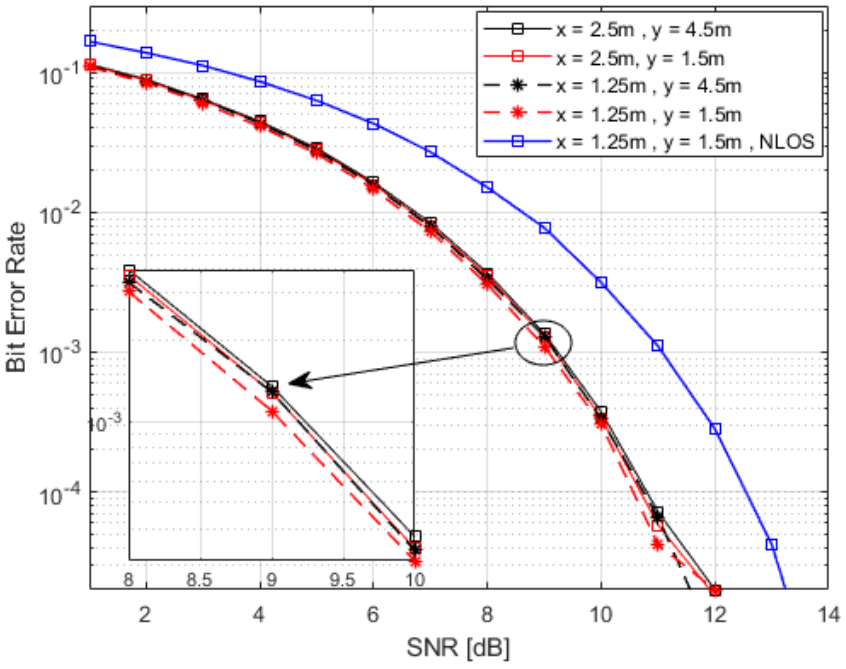

FIGURE 3.8: Performance variation due to receiver location

difference is not huge, it was observed that when the ImR was place along x = 1.25 m, the BER performance was better than when it was placed along x = 2.5 m. The difference in performance at different receiver locations, with better performance being at (x,y) = (1.25 m, 1.5 m), is due to the expected difference in channel gains, where higher gains are expected at locations closer to the relays. On the other hand, the minimal performance differences along the y-axis is a demonstration of the robustness of the combination of the ASTC relays and the ImR, where MIMO links are well de-correlated by the

ASTC scheme and LOS establishment due to multiple relays and multiple pixels. Further, when the LOS links were blocked and only NLOS propagation was available, the performance degradation in terms of BER of was evident, proving the high dependence of LOS propagation in VLC links.

3.5 Summary

In this chapter, we have proposed and investigated a combination operation of relays, applying the Alamouti MIMO coding technique and imaging receivers, of a VLC system. The system performance enhancement in terms of BER was demonstrated by comparing the results of our proposed scheme to that of an ASTC system using non-imaging receivers. The improved performance is attributed to the robustness of the relay and ImRs against shadowing, as well as the ability of the ASTC to de-correlate MIMO links. Further, the impact of the number of pixels on the imaging receiver was investigated and it is shown that the BER performance is proportional to the number of receiver pixels. This is attributed the probabilistic decision based on the majority voting technique that was applied in the scheme using an ImR. It has also been shown that the distance and orientation of the source-destination link has a great influence on link performance. The farther and out of the transmitters view the receiver is, the more the performance of the system degrades.

CHAPTER 4

Soft-Decision Decoding of Permutation-based Optical Codes for a Multiple Access System

---

This chapter is based on the following publication: *Mulundumina Shimaponda-Nawa, Oluwafemi Kolade, Wenbo Ding, Dushantha Nalin K Jayakody, and Ling Cheng*, "Soft-Decision Decoding of Permutation-based Optical Codes for a Multiple Access System". *IEEE Communications Letters, 25(9):2824–2828, 2021.*

The author of this thesis conceptualized the work, performed the simulations, analyzed the results and wrote the paper.

4.1 Introduction

In this chapter, an MA SD decoder based on the cost rankings of the channel output matrix, is proposed and applied in an optical wireless communication system in which permutation-based optical codes (POCs), are used. The proposed decoder determines the possible transmitted MA codewords by implementing the Hungarian and Murty's algorithms to solve and rank the costs of all the possible codewords of the received signal. The performance of the proposed Hungarian and Murty (HM) decoder is evaluated in comparison with

two decoders based on the ES technique, in terms of computational complexity and block error rate (BLER). It is found that when POCs are employed, the proposed HM decoder achieves better BLER performance with a low decoding complexity in comparison to the ES based decoders.

PCs proposed in [134] and investigated for use in PLC MA systems [11, 13, 131], can be used in wireless optical MA (WOMA) systems with an increased data rate and number of users, depending on the selected minimum Hamming distance. The use of PCs in WOMA can be ascertained by the work in [35], where a class of OOCs based on mutually orthogonal Latin squares (MOLSs) and mutually orthogonal Latin rectangles (MOLRs) (which use permutations) were employed for optical code-division multiple access (OCDMA). PCs have an advantage of allowing all users to send constant energy signals over the channel. Thus, no power of a single user overwhelms the others. Another advantage is the guaranteed decodability for a given number of active users even in the presence of channel noise [11, 13, 131].

In [131], the authors investigated the effect of the Hamming distance d, on PCs for multiuser communication in the powerline channel. They showed that a set of permutation sequences of certain cardinality $|\boldsymbol{P}|$ with minimum Hamming distance $d_{\min}$, can be partitioned to form uniquely decodable PCs with varying performances. In [11, 13, 131] and most of the work in WOMA systems, focus on the use of ES decoding techniques based on $d_{\min}$ and correlation [27, 35].

However, the decoding complexity of ES-based decoders increases by an exponential order. As such, studies to investigate alternative, less complex decoding methods are necessary. In [79], optimization algorithms for improving the performance of the permutation trellis code, were proposed. It was established that due to the structure of the encoder, the channel output could be interpreted as an assignment problem, hence, soft-decision detection based on the Hungarian algorithm, was proposed.

The decoding capabilities proposed in [79] are exploited for implementation of a low-complexity MA decoder based on the cost rankings of the channel output matrix, by the Hungarian [86] and Murty [106] algorithms. It is shown that based on the cost rankings of the best solutions to the assignment problem, multiple transmitted permutation codewords (PCWs) can be deduced. Therefore, we refer to the proposed decoder as the HM decoder. When the AWGN effect is considered, the HM decoder is applied as a soft-decision decoder. Consequently, the advantage over hard-decision decoders is expected in the BLER performance.

4.2 Multiple Access Encoding

We consider a WOMA communication system with multiple channel inputs and a single summed output channel, as shown in Figure 4.1. The data bits from each user are encoded by their respective MA codes before transmission over the MA channel. At the receiver, the

decoder maps the received signal to the respective user codewords, from which the likely transmitted data bits are estimated. For simplicity, we consider OOK modulation, denoting the presence and absence of light pulses during transmission. We also assume a bit and block synchronised system. T users can access the channel but only up to m users can be uniquely identified at each transmit interval and their transmitted messages correctly recovered. To achieve this, POCs are used.

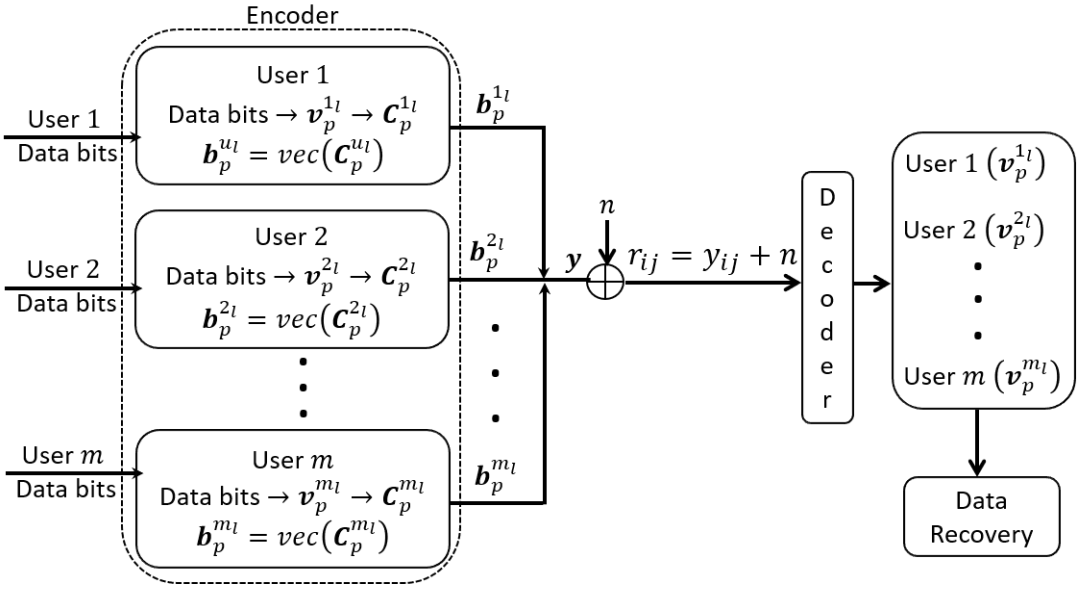

FIGURE 4.1: Multiple access communication system model

To ensure the unique decipherability of the transmitted codewords, a disjunctive restriction on the generated POCs is imposed. A disjunctive code is defined as a binary code, $\mathcal{D}(L, m, |\boldsymbol{B}|)$ of code length, L and cardinality, $|\boldsymbol{B}|$, if the Boolean sum of at most one codeword belonging to each m disjoint subsets of the code is uniquely decipherable [71]. As such, any Boolean sum of m or less codewords, results into a unique sequence and all participating users can be identified,

thus eliminating MAI [31, 71]. We employ disjunctive POCs of constant weight w, generated from PCs. This means all the generated codewords in the binary codebook have the same weight, w, which refers to the sum of binary bits '1' in each codeword.

To generate a POC codeword, a PCW $\boldsymbol{v}_p \in \boldsymbol{P}$, which is a permutation of integers $1, 2, \ldots, M$, is used. All the codewords in $\boldsymbol{P}$ can be arranged into a matrix such that each codeword $\boldsymbol{v}_p$ belongs to row p, in $\boldsymbol{P}$. We use the notation $\mathcal{PC}(M, d_{\min})$ to describe a codebook with minimum Hamming distance $d_{\min}$, with each codeword having a length of M. Then, $\boldsymbol{v}_p$ is converted to an equivalent $[0,1]^{M\times M}$ codeword matrix $\boldsymbol{C}_p$ such that in each column of $\boldsymbol{C}_p$, a '1' fills the position which corresponds to the codeword's integer, while other $M-1$ values in the column are set to '0'. A binary codeword, $\boldsymbol{b}_p = vec(\boldsymbol{C}_p)$, of length $N = M^2$, is then derived by performing a vectorial stacking operation $vec(\cdot)$. A codeword mapping example from non-binary permutation codes to POCs, using the method just described, is shown in Table 4.1.

TABLE 4.1: Permutation-based optical code (POC) generated from $\mathcal{PC}$ ($M = 3, d_{\min} = 2$)

Permutation code $\boldsymbol{v}_p$	**Code Index**	**POC ($\boldsymbol{b}_p$)**
3 2 1	1	0 0 1 0 1 0 1 0 0
3 1 2	2	0 0 1 1 0 0 0 1 0
2 3 1	3	0 1 0 0 0 1 1 0 0
2 1 3	4	0 1 0 1 0 0 0 0 1
1 3 2	5	1 0 0 0 0 1 0 1 0
1 2 3	6	1 0 0 0 1 0 0 0 1

In a T-user WOMA system, each user is assigned a unique binary codeword $\boldsymbol{b}_p \in \boldsymbol{B}$. Hence, up to m of T, $(m \leq T)$, users can be uniquely identified at each transmit interval. The codeword $\boldsymbol{b}_p$ is transmitted when the user transmits a '1', while an all-zero sequence of the same length, is transmitted when any user transmits a '0'. In this work, we consider a scenario proposed in [131], where a codebook $\boldsymbol{P}$ can be partitioned into sub-codebooks. Each sub-codebook $\boldsymbol{P}_u$ is assigned to a user and contains $|\boldsymbol{P}_u|$ codewords. As such, we have $\boldsymbol{v}_p^{u_l} \mapsto \boldsymbol{C}_p^{u_l}$ and $vec(\boldsymbol{C}_p^{u_l}) \mapsto \boldsymbol{b}_p^{u_l}$, where the matrix $\boldsymbol{C}_p^{u_l} = [c_{ij}] \in \{0, 1\}$, $u = 1, 2, \ldots, m$, $l = (1, 2, \ldots, |\boldsymbol{P}_u|)$. Consequently, the Boolean sum of the active users is expressed as, $\boldsymbol{y} = \bigvee_{u=1}^{m} \boldsymbol{b}_p^{u_l}$ and can be represented by an equivalent $M \times M$ matrix $Y = [y_{ij}] \in \{0, 1\}$.

4.2.1 Channel Model

An optical communication channel can be considered as an asymmetrical channel where the ratio between the probability of error in the data bits of type $1 \rightarrow 0$, e_1 or $0 \rightarrow 1$, e_0 can be large. Thus, one type can be assumed. In this work, we assume that a binary bit '1' is transmitted and received without error, whereas the binary bit '0' may be received as a '0' or '1'. This can be illustrated like the Z-channel shown in Figure 4.2.

Optical wireless systems often operate in the presence of ambient background lights which are a source of the shot noise component in the receiver. Coupled with the thermal noise which is always present due to the receiver electronics, the noise, n, is modelled as AWGN

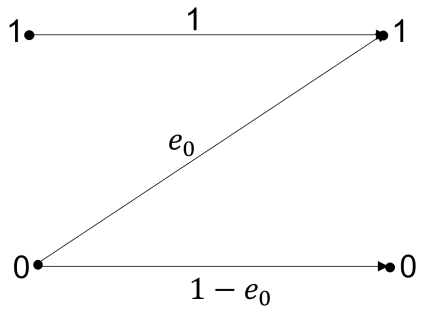

FIGURE 4.2: Asymmetric error probability representation

[159], with a zero-mean normal distribution and variance $\frac{N_0}{2}$ denoted by $\mathcal{N}\big(0, \frac{N_0}{2}\big)$. Thus, each received sample is given as

$$r_{ij} \ = y_{ij} \ + n. \tag{4.1}$$

4.3 Decoding POCs

Three decoding methods are discussed in this section namely: minimum distance (MD) decoding, exhaustive search-correlation (ES-C) decoding and HM decoding. The MD and ES-C methods are based on the hard-decision exhaustive search technique while the HM method is a soft-decision decoding technique.

4.3.1 Decoding by Exhaustive Search (ES) Methods

The channel output is represented by an $M \times M$ matrix $\boldsymbol{R} = [r_{ij}] \in \mathbb{R}$. For ES-based decoders, $\boldsymbol{R}$ is first demodulated to $\boldsymbol{R}_{\text{th}} = [r^{\text{th}}{}_{ij}] \in \{0, 1\}$.

4.3.1.1 Minimum Distance (MD) Decoder

In this method, the receiver has a look up table (LUT) of size $\mathcal{L}$, consisting of all possible Boolean summations of user codeword combinations. Each summation is denoted by an $M \times M$ matrix, $\boldsymbol{\mathcal{Y}} = [\mathrm{y}_{ij}] \in \{0, 1\}$. $\mathcal{L} = \sum_{\mu} \binom{|\boldsymbol{B}|}{\mu}$, where $\mu = (1, 2, \ldots, m)$, $|\boldsymbol{B}| = M!\ /\ (d_{\ \mathrm{min}} - 1)\ !$. Thus, LUT $\propto M!$. The MD decoder performs the following:

Algorithm 1 MD decoding of POCs

Input: Channel output matrix $\boldsymbol{R}$

Output: Array of decoded PCWs, $\boldsymbol{D}$

1: Convert $\boldsymbol{R}$ to $\boldsymbol{R}_{\mathrm{th}}$

2: **for all** $\boldsymbol{\mathcal{Y}}$ **do**

$d = \sum_{i=1}^{M} \sum_{j=1}^{M} (r_{ij}^{\mathrm{th}} \neq \mathrm{y}_{ij})$ {Complexity: $O(M^2)$}

3: **end for** {Complexity: $O(M!)$}

4: $\hat{\boldsymbol{R}} = \boldsymbol{\mathcal{Y}}$ corresponding to $\min(d)$

5: map $\hat{\boldsymbol{R}}$ to the respective array of PCWs

{Overall decoder complexity order is $O(M! \cdot M^2)$}

4.3.1.2 Exhaustive Search-Correlation (ES-C) Decoder

A matrix $\boldsymbol{C}_p^{u_l}$ is said to be included in the receive matrix $\boldsymbol{R}$ if and only if $\mathrm{corr}(\boldsymbol{R}, \boldsymbol{C}_p^{u_l}) = w$, where corr(.) denotes the correlation function. Decoding in ES-C decoder is achieved by the following:

Algorithm 2 ES-C decoding of POCs

Input: Channel output matrix $\boldsymbol{R}$

Output: Array of decoded PCWs, $\boldsymbol{D}$

1: Convert $\boldsymbol{R}$ to $\boldsymbol{R}_{\text{th}}$

2: **for** all $\boldsymbol{C}_p^{u_l} \in \boldsymbol{B}$ **do**

$\text{corr}(\boldsymbol{R}_{th}, \boldsymbol{C}_p^{u_l}) = \sum_{i=1}^{M} \sum_{j=1}^{M} r_{ij}^{\text{th}} c_{ij}$ {Complexity: $O(M^2)$}

3: **end for** {Complexity: $O(M!)$}

4: **if** $\text{corr}(\boldsymbol{R}_{\text{th}}, \boldsymbol{C}_p^{u_l}) = M$ **then**

5: $\boldsymbol{C}_p^{u_l}$ is one of the likely transmitted PCW

6: **end if**

{Overall decoder complexity order is $O(M! \cdot M^2)$}

4.3.2 Soft-Decision Hungarian-Murty (HM) Decoding

The proposed low-complexity MA decoder is based on the Hungarian and Murty's algorithms. The Hungarian algorithm solves an assignment problem, where the objective is to assign a number of resources to an equal number of activities [86]. Thus, minimising the total cost or maximising the total profit by such an allocation. The Hungarian algorithm assigns a job to each worker such that a worker can only be assigned one task [76, 86]. Thus, when the Hungarian algorithm is applied in the MA system using the POC, the aim will be to find the optimal solution that combines the costs of all the likely transmitted PCWs. The mathematical model of an assignment problem [80, 86], can be expressed as:

$$K = \sum_{i=1}^{M} \sum_{j=1}^{M} k_{ij} q_{ij}, \tag{4.2}$$

subject to the constraints

$$\sum_{i=1}^{M} q_{ij} = \sum_{j=1}^{M} q_{ij} = 1, \ \ (i, j = 1, 2, \ldots, M), \tag{4.3}$$

where K in (4.2) is the cost of the assignment, k_{ij} the cost of assignment of a resource to an activity. The Hungarian algorithm finds the $M \times M$ matrix, $\boldsymbol{\mathcal{H}} = [k_{ij}] \in \{0, 1\}$ that yields the highest cost K, for a given square cost matrix. Each row-column pair represents a cell in the cost matrix and the sum of the cell values of all the row-column pairs in $\boldsymbol{\mathcal{H}}$ produces the cost K [86].

For a communication system using PCs, $r_{ij} \stackrel{\Delta}{=} k_{ij}$ in (4.2) and $\boldsymbol{R}'$ is the minimised matrix that yields the optimal cost K. However, in the MA system, r_{ij} contains a combination of costs corresponding to all the likely transmitted codewords. Thus, (4.2) can be modified as

$$K = \sum_{i=1}^{M} \sum_{j=1}^{M} r_{ij} c_{ij}, \tag{4.4}$$

subject to the constraints

$$\sum_{i=1}^{M} c_{ij} = \sum_{j=1}^{M} c_{ij} = 1, \ \ (i, j = 1, 2, \ldots, M). \tag{4.5}$$

The Hungarian algorithm of the HM decoder finds the matrix $\boldsymbol{R}'$ that produces the maximum cost K_1 corresponding to a permutation sequence $\boldsymbol{v}_p^{u_l}$, belonging to one of the m users. Then from $\boldsymbol{R}'$, using Murty's algorithm, the decoder finds the next highest $\mathcal{K}$ costs and ranks them in order of decreasing costs. From Murty's ranking, the

decoder then selects $m-1$ highest costs corresponding to the other $m-1$ users, to form an array of decoded PCWs, $\boldsymbol{D}$. This can be presented as follows:

Algorithm 3 HM decoding of POCs

Input: Channel output matrix $\boldsymbol{R}$

Output: Array of decoded PCWs, $\boldsymbol{D}$

1: By Hungarian method, find matrix $\boldsymbol{R}' = [r'_{ij}] \in \mathbb{R}$ {Complexity order of $O(M^3)$ [90]}

2: By Murty's algorithm, find the best $\mathcal{K}$ PCWs and ranks them in order of decreasing cost. {Complexity order of $O(M^4)$ [30]}

3: Select the m codewords corresponding to m highest costs to form $\boldsymbol{D}$ {Overall decoder complexity order is $O(M^4)$}

An example of HM decoding is as follows: Suppose $\mathcal{PC}(M=3, d_{\min}=2)$ as shown in Table 4.1. Assume $T=6$ and that for each user, $|\boldsymbol{P}_u|=1$. Further, suppose that $m=2$ users, u_1 and u_2, are allowed to transmit at any interval and that both users transmitted binary bits 1 at the same interval. Precisely, suppose that 213 and 132 of Table 4.1, have been assigned to u_1 and u_2, respectively. The signal $\boldsymbol{R}$ was received as:

$$\boldsymbol{R} = \begin{bmatrix} \boxed{0.8598} & 0.9495 & 0.1101 \\ 1.0132 & -0.0076 & \boxed{0.9998} \\ -0.1179 & \boxed{1.0889} & 0.9837 \end{bmatrix} \tag{4.6}$$

Using Algorithm 3, the Hungarian method finds $\boldsymbol{R}'$ and $K_1 = 2.9485$, corresponding to row-column values of {(1,1), (3,2), (2,3)}. Using the row values to form the corresponding codeword yields $\boldsymbol{v}_p^2 = 132$.

By Murty's algorithm, the costs from the second-highest cost to the $\mathcal{K}^{th}$ highest are found and ranked. In this example, $\mathcal{K} = 3$. Consequently, a list comprising $\{2.9485, 2.9464, 2.2122, -0.0154\}$ corresponding to $\{132, 213, 231, 321\}$, respectively, is obtained. Therefore, $m = 2$ codewords corresponding to the 2 highest costs are selected as the likely transmitted, resulting in $\boldsymbol{D} = \{\boldsymbol{v}_p^1 = 213, \boldsymbol{v}_p^2 = 132\}$.

4.4 Simulation Results and Analysis

A comparison of the computational complexity of the three discussed decoding methods is considered. Additionally, the BLER comparison of the systems employing the three decoding methods in the presence of binary asymmetric errors and a combination of binary asymmetric errors and AWGN.

4.4.1 Decoding Computational Complexity Analysis

For all the three decoders used in this study, the circuitry required for the decoding process, has not been considered. As presented in Section 4.3.1, MD and ES-C decoders exhaustively search for the most likely transmitted codewords from the lookup tables that are functions of the code cardinality which grows as $M!$. The length of the received sequence and vectors in the respective LUTs is $L = M^2$. As such the computational complexity of decoders based on the ES technique can be approximated to $O(M! \cdot M^2)$. On the other hand, the computational complexity of the HM decoder is based on the

size of the decoder input $M \times M$ matrix. The order of complexity combines the complexities of the Hungarian and Murty's algorithms of $O(M^3)$ [90] and $O(M^4)$ [30], respectively. Thus, considering the worst case order, the HM decoder has a computational complexity of $O(M^4)$. This is a much reduced complexity for the proposed MA decoder when compared to the MD and ES-C decoders.

Unlike in [80] which considers a single user scenario where the decoder can stop at the Hungarian algorithm with a complexity of $O(M^3)$, when it finds $\boldsymbol{v}_p \in \boldsymbol{P}$, the current work which considers an MA system always requires the use of the Murty's algorithm in order to find all the transmitted codewords. As such, the complexity of the MA system in this work is $O(M^4)$.

4.4.2 BLER Performance in the Presence of Asymmetric Errors

Permutation codes of $M = 3$, $M = 5$ and $M = 7$ were used and for the sake of manageable computational processes for the simulations, we used subsets instead of full codebook size of $M!$ codewords. We further considered different distance properties of the code subsets.

4.4.2.1 Comparison based on Code Length

POCs generated from PCs of $d_{\min} = M$ and lengths, $M = 3$, 5 and 7, translating to POCs of lengths $L = 9$, 25 and 49, are simulated. The three codes are of cardinality $|\boldsymbol{P}| \leq M!/(d_{\min} - 1)!$ [151]. From

Figure 4.3, the POC with $N = 49$ outperforms the shorter codes of $L = 9$ and 25. This can be attributed to the fact that longer POCs have more binary bit zeros, hence are more robust to asymmetric errors. The performance of the proposed HM decoder matches that of the ES-C decoder and both outperform the MD decoder. Thus, the proposed HM decoder becomes attractive and a more preferred candidate for use in WOMA systems. For applications where more users need to access the channel, $d_{\min}$ can be relaxed to values $d_{\min} < M$, but with a BLER degradation. Despite the degradation in BLER, the computational complexity for the HM decoder, remains the same for the same M, while complexities of ES-based decoders would have hugely increased as established in Section 4.4.1.

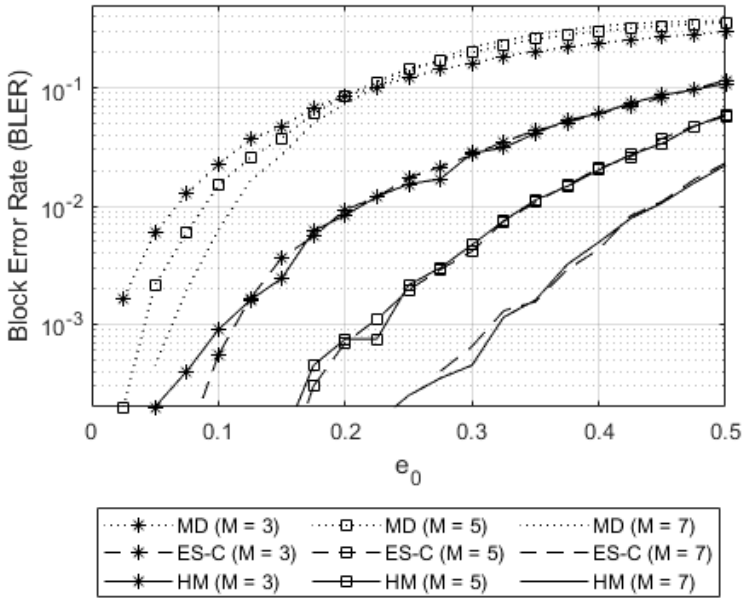

FIGURE 4.3: BLER performance of POC of varying lengths in the presence of asymmetric errors

4.4.2.2 Code Distance Properties and Decoder Capability

To analyse the effect that the variation of $d_{\min}$ has on the performance of the system, we consider two permutation codes, Code 1 and Code 2, both of cardinality $|\boldsymbol{P}|$, having $d_{\min} = 5$ and $d_{\min} = 4$, respectively. $M = 5$ for both codes. From Figure 4.4, Code 1 outperforms Code 2, in terms of BLER. This can be attributed to the $d_{\min}$ of Code 1 being maximum, that is, $d_{\min} = M$. Additionally, a degradation is noticed in all the three decoders when Code 2, with a lower $d_{\min}$, is used. However, for both codes, the BLER performance of the MD decoder is the worst. The poor performance of the MD decoder could be because, an increase in e_0 causes the identification of many likely transmitted codewords, where a wrong codeword is most likely to be selected as one that was transmitted. As such, this decoder requires decoding enhancement to enable correct selection among all the likely transmitted codeword. Unfortunately, this will add to the already high decoding complexity associated with the MD decoder. Again we observe that the performance of the HM decoder matches the performance of the ES-C decoder, but with a reduced decoding complexity.

Furthermore, despite the degraded BLER performance generally observed when Code 2 is used, its higher cardinality enables higher information rate than Code 1. This is because more than one codeword is assigned to each user. If $|\boldsymbol{P}_u|$ codewords are assigned to each user, then up to $m \log_2(|\boldsymbol{P}_u|)$ bits of information can be transmitted

for m users. Hence, there is a trade-off between the system BLER performance and the data rate, when a code of lower $d_{\min}$ is used.

Moreover, as seen from Figure 4.3, codes with larger M resulting in larger codebooks and longer codewords can be used for performance enhancement. Larger codebooks enable an increase in both the simultaneously supported users and $|\boldsymbol{P}_u|$ codewords assigned to users. While the MA systems based on the ES technique will suffer high decoding complexity when codes with larger M are employed, the system using the proposed HM decoder will not only have a higher data rate but will have a lower decoding complexity as well.

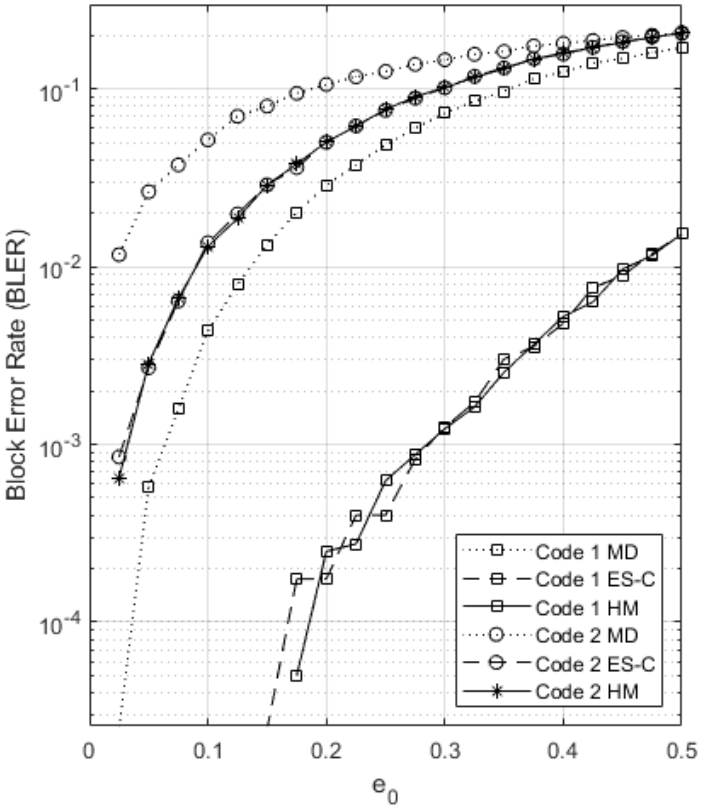

FIGURE 4.4: Code and decoder capability performance for PCs with varying distance properties, $M = 5, m = 4$.

4.4.3 Probability of Error Analysis in the Presence of Binary Asymmetric Errors and AWGN

The effect of both binary asymmetric errors and AWGN on the transmitted signal, is considered. As such the system probability of error, P_e^s must be calculated accordingly in terms of the probability of error due to binary asymmetric errors, P_a and the probability of error due to AWGN on an OOK modulated signal, P_e. The two error probabilities are respectively expressed as:

$$P_a = e_0, \tag{4.7}$$

while

$$P_e = \frac{1}{2}\text{erfc}\left(\sqrt{\frac{E_b}{4N_0}}\right), \tag{4.8}$$

where erfc(x) is the complementary error function of x, E_b and N_0 denote the signal and noise power, respectively. Note that despite the assumption that binary bit '1' is not affected by asymmetric errors, it will nevertheless, be affected by AWGN in the receiver. Thus, we consider a simplified derivation of P_e^s as:

$$P_e^s = \frac{1}{2}P_e + \frac{1}{2}(1 - P_a)P_e + \frac{1}{2}P_a(1 - P_e). \tag{4.9}$$

In (4.9), the first and second terms denote the error probabilities on '1' (ones) and '0' (zeros) that are not affected by asymmetric errors, respectively. The third term denotes the probability of '0' bits that are affected by both binary asymmetric errors and AWGN.

Consequently, (4.9) can be simplified as:

$$P_e^s = P_e - P_a \cdot P_e + \frac{1}{2} P_a, \tag{4.10}$$

and plotted as the analytical plot in Figure 4.5.

Figure 4.5 shows the BLER performance of the MD, ES-C and HM decoders when only AWGN is considered and when the effects of both the binary asymmetric errors and AWGN are considered. Precisely, $e_0 = 0.02$ has been assumed for the asymmetric effects. Any two users can transmit at each interval using POCs generated from $\mathcal{PC}(M = 4, d_{\min} = 3)$.

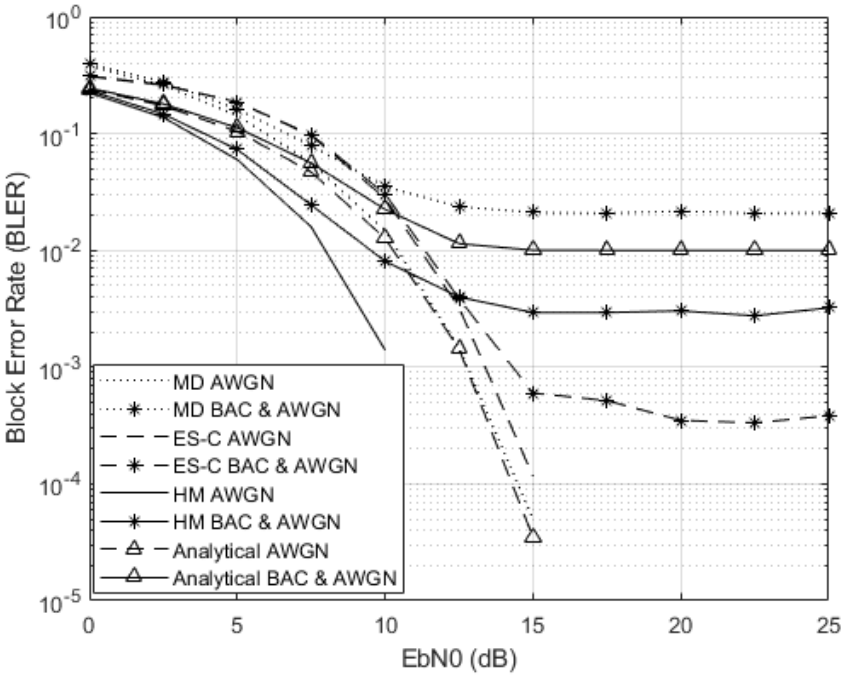

FIGURE 4.5: BLER performance when binary asymmetric errors and AWGN are considered. $e_0 = 0.02$, $M = 4, m = 2$.

In the presence of AWGN, the HM decoder is considered as a soft-decision (SD) decoder, avoiding errors that could be introduced by

the threshold detector before decoding, thus enhancing its performance. Furthermore, the cost ranking of all the possible solutions of the channel output matrix and the selection of the m highest costs corresponding to PCWs, enhances the performance of the HM decoder.

The effect of the binary asymmetric errors on the WOMA system is observed by comparing the performance graphs of the system with and without them. A performance degradation is noticed on graphs with asymmetric errors. Consequently, the effects of asymmetric errors cannot be neglected when designing different components of the system, such as the decoder.

The properties of the MA codes, such as the $d_{\min}$ within the sub-codebooks assigned to each user and the $d_{\min}$ between the sub-codebooks, influence the performance of the decoder. In Figure 4.5, the optimal performance is obtained when the $d_{\min}$ of the sub-codebooks is higher than that between user sub-codebooks. This reduced erroneous decoding events, where the HM decoder outputs invalid codewords.

4.5 Summary

We proposed an MA decoder with a reduced computational complexity in reference to the two ES-based decoders, MD and ES-C. The proposed decoder combines the Hungarian and Murty algorithms to determine the codewords of the participating transmitters,

from which the transmitted information is recovered. The Hungarian algorithm is used to determine the optimal maximum assignment of the $M \times M$ channel output matrix, while Murty's algorithm finds all the best assignments and ranks them in order of decreasing cost. The m highest costs corresponding to m PCWs are selected as the likely transmitted codewords identifying the respective transmitters. The computational complexity of the two ES-based decoders is $O(M! \cdot M^2)$, while that of the proposed HM decoder is $O(M^4)$. Thus, the proposed HM decoder has a tremendously reduced decoding complexity.

A system model where information is transmitted in the presence of binary asymmetric errors and the AWGN was considered. The proposed HM decoder matches the BLER performance of the ES-C in the absence of AWGN. However, when AWGN is considered, the SD decoding advantage over hard-decision decoding is evident, where the proposed decoder outperforms the ES based decoders in terms of BLER. Additionally, the complexity of the HM decoder increases in the order of a polynomial function, as opposed to an exponential order increase like in ES-based decoders. Ultimately, instead of employing ES-based decoders in WOMA systems using POCs, the proposed HM decoder can be used to attain better performance at lower computational complexity. Although, we specifically apply the HM decoder to a WOMA communication system, this decoder can be applied to other communication channels, since it can take both hard and soft information as input.

CHAPTER 5

Encoder Adaptation for Generalised Space-Time Coded MIMO Systems using a Hungarian-Murty Soft-Decision Decoder

5.1 Introduction

In this chapter, we propose a generalised space-time coded multiple-input and multiple-output (GSTC-MIMO) scheme for a VLC system. Precisely, we propose the use PCs resulting in variable weight (VW) matrices, hence enhancing the system data rate when compared to a system using equal weight (EW) permutation matrices. In the proposed GSTC-MIMO system, we use a low-complexity SD decoder based on the Hungarian and Murty's algorithms, referred to as the HM decoder. We show that apart from reducing the decoding complexity of the space-time coded (STC) system, a signal-to-noise (SNR) gain of over 6 dB, is achieved, when the HM decoder is used. Furthermore, based on the weight properties of the combined PCs, we provide a theorem defining the capability of the HM decoder. Additionally, an adaptation of the space-time (ST) encoder to improve the HM decoder capability, is proposed based on the codebook partitioning scheme. We show that the GSTC-MIMO system using

the decoder-adapted ST encoder outperforms the GSTC-MIMO system using the conventional ST encoder, by an SNR exceeding 5 dB. Finally, based on the HM adapted encoder, we extended the sub-codebooks from the partitioning scheme to a multiple access (MA) system. For practical consideration in an indoor environment, we investigate the impact of transmit element (TE) separation distances from 0.1 m to 1 m, on the MA system's bit error performance.

The ever growing demand of reliable wireless services at high transmission speeds, especially in indoor environments, has been one of the technology evolution drivers, seeking to efficiently use the available communication resources. MIMO, a technique that uses multiple transmit and receive elements, has been widely used in wireless communication systems to achieve these demands [44, 62, 87, 103, 111, 128, 135]. In recent years, optical MIMO has been extended to vehicular technology, where it is applied in inter vehicular or vehicle-to-infrastructure communication, for safety, security and to facilitate the smooth flow of traffic in big, busy cities [69, 97]. An increase of MIMO application areas in vehicular communications, aeronautics, smart cities and hospitals, is expected with the emergence of 5G communication networks.

A significant number of MIMO schemes in literature can basically be classified into three categories namely: precoding by beamforming, spatial multiplexing and spatial diversity. The precoding class aims at mitigating the effects of the continuous changing environment. Effects such as multipath fading on the received signal is reduced by

ensuring that signals emitted from different TEs add up constructively at the receiver. This also increases the gain of the received signal, hence the system reliability is improved. On the other hand, in spatial multiplexing, each TE is assigned independent data symbols, thus the data rate is enhanced, while spatial diversity mainly reduces the bit error rate (BER) by transmitting copies of data symbols simultaneously.

In this work, we focus on the STC- MIMO scheme, a type of the spatial diversity class, where the bit error performance is enhanced by transmitting data symbols over multiple TEs in a particular time period. Several designs achieving the STC-MIMO schemes have been reported [2, 9, 51, 76, 133, 140]. We particularly focus on the permutation aided STC-MIMO scheme and apply it to a VLC system.

Binary matrices mapped from permutation sequences can be used to coordinate the transmission pattern of TEs in a MIMO system. In [76], a MIMO system using permutation-aided space-time shift keying (STSK) modulation in an indoor VLC channel was proposed. The indices of the transmitters were coordinated by antenna matrices using permutations, such that, each transmitter index was selected only once at each transmit time and transmit block. In this way, similar to SM, the inherent high channel correlation of VLC systems [44], was avoided. To increase the data rate of the MIMO scheme in reported in [76], in [81, Chap. 8], more than one LED at each transmit time was activated by using a type of concatenated PCs which generates EW space-time (ST) matrices. In an EW matrix,

the number of the non-zero elements in all rows is equal to that of non-zero elements in all columns. However, the use of concatenated PCs which generate EW ST matrices places a restriction on the allowed codeword combinations. Also the cardinality of the codebook is equal to the length, M, of the PCW and hence limiting the system data rate.

In this work, we extend the idea in [81, Chap. 8] and propose the inclusion and use of concatenated PCs which result in VW matrices, in a generalised ST coded MIMO system. In a VW matrix, the number of non-zero elements in the rows may not equal that of non-zero elements in the columns.

Due to its low decoding complexity, we elect to use the SD decoder in [130], based on the Hungarian [86] and Murty [106] optimization algorithms. The HM decoder considers the receiver output matrix as an assignment problem and the Hungarian method finds the optimal cost matrix on which the Murty's algorithm is applied to rank the cost of all possible costs. The authors in [130] showed that based on the cost rankings of the $\mathcal{K}$ best solutions to the assignment problem, multiple PCWs that make up the transmitted combination, can be deduced.

However, the capability of the HM decoder in a GSTC-MIMO system may be compromised in that VW matrices from specific codeword pairs result into erroneous decoding. Consequently, properties of permutation codeword combinations are investigated in order to

adapt the GSTC-MIMO codebook to the HM decoder, in a way that avoids the use of the codeword combinations whose decoding has a higher probability of error.

Additionally, in order to use the full capacity of a given codebook, including codeword combinations whose decoding has a higher probability of error, we propose an encoding scheme that partitions the main codebook into sub-codebooks based on the combination properties. The sub-codebooks from the partitioning scheme are further applied to an MA system that we use for the investigation of TE separation distance effect on the system performance.

Precisely, the main contributions of this chapter can be summarised as follows:

1. Implementation of a GSTC-MIMO system in which we propose the inclusion and use of concatenated PCs which result in VW matrices. The use of VW matrices increases the cardinality of the PC codebook, ultimately enhancing the system's data rate.

2. For the proposed GSTC-MIMO, we implement a low-complexity system by the use of an SD decoder based on the Hungarian and Murty's optimisation algorithms, which also further enhances the system's reliability.

3. Based on the combination properties of the PCWs, we define a theorem on the capability of SD HM decoder and propose an adaptation of the ST encoder to the HM decoder. This enhances the reliability of the permutation codded GSTC-MIMO system.

4. The ST encoder adaptation results in partitioned codebooks which we then apply in an MA system to enhance distinction of different user information at the receiver. Furthermore, we use the MA system to investigate the impact of TE separation distances, in an indoor environment.

The remainder of the chapter is organised as follows: In Section 5.2, the GSTC-MIMO system models is presented. Section 5.3 is dedicated to the analysis of the pattern combination properties of the PCs from which we present a GSTC-MIMO encoder adapted for the SD HM decoder. In Section 5.4, the simulation results showing the BER performance of the GSTC-MIMO system based on the different codeword combinations, are presented and analysed. Additionally, the energy efficiency (EE) for the STC-MIMO and GSTC-MIMO systems, is evaluated. BER performance results for an MA system where users' information is transmitted in an STC-MIMO scheme, are also presented, for varying TE separation distances. Finally, the chapter summary, is presented in Section 5.5.

5.2 GSTC-MIMO System Model

In GSTC-MIMO N_a out of N_t TEs are activated at a time, where $1 \leq N_a \leq N_t$. Before presenting the GSTC-MIMO system, a brief presentation of the considered VLC channel model is given and then details on the basic STC-MIMO system based on PCs are presented.

5.2.1 MIMO Channel Model for VLC

In the considered VLC channel, only the LOS propagation paths of the Lambertian model, are assumed. The channel gain of the LOS component for a receiver located at a distance, d_{v} and angle of irradiance, θ, with respect to the transmitter, is approximated as (2.7) [53]. For an $N_r \times N_t$ system, where N_r denotes the number of receive elements (REs) at the receiver and N_t denotes the number of TEs, the channel gain matrix is represented as

$$\mathbf{H} = \begin{bmatrix} h_{11} & h_{12} & \dots & h_{1N_t} \\ \vdots & \vdots & \ddots & \vdots \\ h_{N_t1} & h_{N_t2} & \dots & h_{N_rN_t} \end{bmatrix}. \tag{5.1}$$

In (5.1), each h_{n_r,n_t} representing the individual channel gain between a specific TE, n_t and RE, n_r of the wireless VLC link is defined in (2.7). The optical received signal is affected by AWGN with zero-mean and a variance, $\sigma_G^2 = \sigma_{\text{shot}}^2 + \sigma_{\text{thermal}}^2$. Where σ_{shot}^2 and $\sigma_{\text{thermal}}^2$ represents the shot noise variance and the thermal noise variance, respectively. Since every element of the received element is independently affected by noise, n_G can be represented as an $M \times M$ matrix, $\boldsymbol{N}_G$. Considering the transmitted matrix $\boldsymbol{X}$ and $\boldsymbol{H}$, the received matrix can be represented by (2.11).

5.2.2 Space-Time Coded MIMO (STC-MIMO)

5.2.2.1 Permutation Codewords for STC-MIMO

As presented in Section 4.2, a permutation codeword $\boldsymbol{v}_p$, of length M, is a sequence of integers $1, 2, \ldots, M$, belonging to a permutation codebook $\boldsymbol{P}$ of cardinality $|\boldsymbol{P}|$. All the codewords in $\boldsymbol{P}$ can be arranged into a matrix such that each codeword $\boldsymbol{v}_p$ belongs to row p, in $\boldsymbol{P}$. We use the notation $\mathcal{PC}(M, d_{\min})$ to describe $\boldsymbol{P}$ with minimum Hamming distance $d_{\min}$, with each codeword having a length of M. The codeword $\boldsymbol{v}_p$ can be represented as an $M \times M$ codeword matrix, $\boldsymbol{C}_p = [c_{ij}] \in \{0, 1\}$, $(i, j = 1, 2, \ldots, M)$. Each column j in $\boldsymbol{C}_p$ only has one non-zero element which fills the position corresponding to the permutation codeword's integer, while other $M - 1$ elements in j are set to '0'.

5.2.2.2 STC-MIMO System

In Figure 5.1, the incoming message bits are divided in two groups. The first group has $\mathcal{B}$ bits which are directed to the ST encoder and are mapped to their respective predefined $\boldsymbol{v}_p$ corresponding to $\boldsymbol{C}_p$. The second group of $\mathcal{B}'$ bits is mapped to a modulation constellation symbol q, according to the selected M-ary modulation scheme. If a codebook containing any $2^{\mathcal{B}}$ pre-selected codewords belonging to $\boldsymbol{P}$ is available at the ST encoder, then

$$\mathcal{B} = \log_2(|\boldsymbol{P}|). \tag{5.2}$$

Thus, the total number of bits, referred to as $D1$, transmitted per block period when other message bits are mapped to a constellation symbol, is

$$D1 = \mathcal{B}' + \mathcal{B}, \tag{5.3}$$

where $\mathcal{B}' = \log_2(\mathcal{M})$ and $\mathcal{M}$ is the modulation order. Suppose $|\boldsymbol{P}| = 4$ consisting of codewords $\{1234; 1342; 2431; 1432\}$, respectively mapped to $\{00; 01; 10; 11\}$, consequently $N_t = 4$. Now, assuming that the message bits 01 are to be transmitted, then the $\boldsymbol{v}_p = 1342$ is selected for transmission, whose corresponding $\boldsymbol{C}_p$ and consequently $\boldsymbol{X}$ follow as:

$$\boldsymbol{X} = \boldsymbol{C}_p = \begin{bmatrix} 1 & 0 & 0 & 0 \\ 0 & 0 & 0 & 1 \\ 0 & 1 & 0 & 0 \\ 0 & 0 & 1 & 0 \end{bmatrix}.$$

Thus, only one TE is active at each interval, avoiding ICI.

The transmit matrix $\boldsymbol{X}$ is the ST pattern that coordinates the activation of the TEs at each transmit interval in a transmit period, expressed as $\boldsymbol{X} = q \cdot \boldsymbol{C}_p$. In STC-MIMO where only one TE is activated at a time, the non-zero element indicates the TE to be activated at a particular interval in each transmit block period; a transmit block period has M time slots. The i and j of $x_{ij} \in \boldsymbol{X}$ specifies the TE and time slot, respectively. If E_s is the symbol

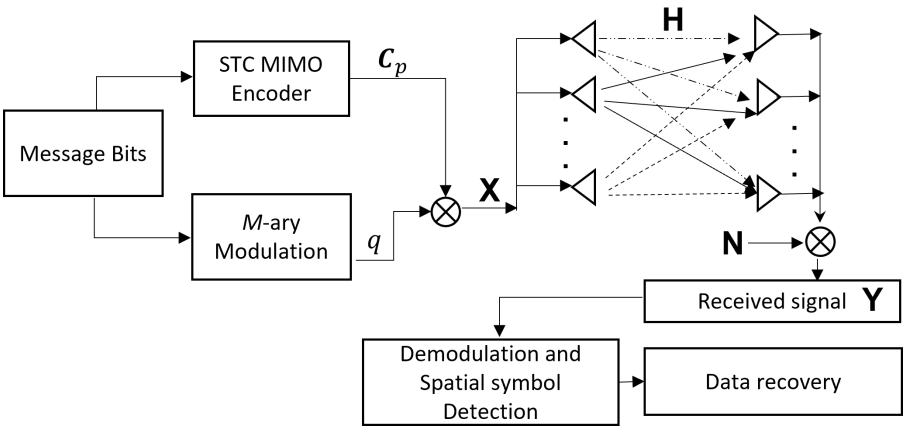

FIGURE 5.1: System model of the permutation-based STC-MIMO communication system

energy of the modulated bits, then

$$x_{ij} = \begin{cases} \sqrt{E_s}, & \text{if } c_{ij} = 1 \\ 0, & \text{otherwise.} \end{cases} \tag{5.4}$$

At the receiver, the transmitted message bits are estimated and recovered after demodulation and estimation of the spatial symbols.

5.2.3 Generalized STC-MIMO System

To increase the data rate of the STC-MIMO system, a generalised system where more than one TE can transmit at any interval, is considered. In GSTC-MIMO, N_a number of PCWs are transmitted per block, thus, $N_a \geq 1$ TEs can be active at each interval. Therefore, the ST pattern is now expressed as

$$\boldsymbol{X} = q \cdot \bigvee_{u=1}^{N_a} \boldsymbol{C}_p^u \quad u = 1, 2, \ldots, N_a, \tag{5.5}$$

where $\bigvee$ denotes an element-by-element Boolean sum. It should be noted that in the symbol $\boldsymbol{C}_p^u$, the superscript u denotes the uth TE and not a power of $\boldsymbol{C}_p$.

Unlike the work in [81], where PCWs which generate EW ST matrices are used, in this study we consider a combination of any codewords that qualify to be in a particular permutation codebook based on the selected minimum Hamming distance $d_{\min}$, thus resulting in VW matrices.

The codeword combination criterion in the GSTC-MIMO in this work is that, any number of codeword matrices added must result in a unique binary matrix, this aids in the decoding process. For EW ST matrices, a minimum Hamming distance $d_{\min} = M$ is required. However, this constraint is eliminated by the use of permutation codebooks with $d_{\min} < M$. We define the weight, w of a matrix as the total number of non-zero elements in that matrix. Examples of EW and VW ST patterns are:

$$EW = \begin{bmatrix} 1 & 0 & 0 & 1 \\ 1 & 1 & 0 & 0 \\ 0 & 1 & 1 & 0 \\ 0 & 0 & 1 & 1 \end{bmatrix}, VW = \begin{bmatrix} 1 & 0 & 0 & 1 \\ 1 & 1 & 0 & 0 \\ 0 & 0 & 1 & 0 \\ 0 & 1 & 0 & 1 \end{bmatrix}.$$

Since at any transmit period, N_a PCWs are combined to form $\boldsymbol{X}$, then unlike in STC-MIMO where information bits are mapped to a single codeword, in GSTC-MIMO they are mapped to a combination of N_a PCWs. Since all possible combinations of the codewords in $\boldsymbol{P}$

taken N_a at a time is $\binom{|\boldsymbol{P}|}{N_a}$, then, the set to which information bits are mapped increases from $|\boldsymbol{P}|$ to $\binom{|\boldsymbol{P}|}{N_a}$. Consequently, if an assumption that M-ary modulation technique is applied, then the total number of bits transmitted per block period, referred to as $D2$, is given by

$$D2 = \mathcal{B}' + \log_2 \binom{|\boldsymbol{P}|}{N_a}. \tag{5.6}$$

In (5.6), $\mathcal{B}'$ is as defined in (5.3). Compared to $D1$ in (5.3), it is shown that the second term in (5.6), has increased, translating in increased data rate. This demonstrates the increased spectral efficiency of the GSTC-MIMO scheme over the STC-MIMO scheme.

5.3 Adapting the GSTC-MIMO Encoder to the HM Decoder Capability

5.3.1 Soft-Decision Hungarian-Murty (HM) Decoder

The SD decoder discussed in this section uses two linear programming (LP) algorithms, Hungarian [86] and Murty [106], to solve and iteratively rank the cost assignments of the received signal matrix until the assignment produces the most likely transmitted codeword $\boldsymbol{v}_p \in \boldsymbol{P}$ [79, 80]. Depending on whether a maximisation or minimisation problem is being solved, the Hungarian algorithm first determines the highest or lowest cost K_1, of the received signal matrix corresponding to the first assignment, A_1. Thereafter, Murty's algorithm iteratively ranks the costs from the second-highest/lowest

cost K_2 to the $\mathcal{K}^{th}$ highest/lowest cost. Each $K_2, K_3, \ldots, K_{\mathcal{K}}$ produces an equivalent assignment $A_2, A_3, \ldots, A_{\mathcal{K}}$ mapped to a permutation sequence. In a GSTC-MIMO system where N_a codewords are transmitted at each period, the HM decoder estimates the N_a highest cost assignments mapped to the likely transmitted permutation codewords.

Remark 5.1. For simplicity, unless otherwise stated, in the whole of Section 5.3, we consider transmission to be only by spatial symbols.

We illustrate the decoding process by examples in which $N_a = 2$ using $\mathcal{PC}(M = 4, d_{\min} = 3)$ shown in Table 5.1. Four examples are shown denoting transmit periods 1, 2, 3 and 4. Suppose message bits are mapped to the following codeword combinations for each transmit period: PCWs 1 and 3, 6 and 11, 1 and 12 and 6 and 9, respectively.

TABLE 5.1: $\mathcal{PC}(M = 4, d_{\min} = 3)$

PCWs 1 - 3	**PCWs 4 - 6**	**PCWs 7 - 9**	**PCWs 10 - 12**
1 2 3 4	4 1 3 2	3 2 4 1	2 4 3 1
2 1 4 3	1 3 4 2	4 2 1 3	3 4 1 2
3 1 2 4	2 3 1 4	1 4 2 3	4 3 2 1

In the first two periods, A_1 corresponding to K_1, is one of the codewords that was transmitted while A_2 corresponding to K_2, is the other transmitted codeword. In the first and second transmit periods, $K_1 = K_2$, while the other likely codewords have lower costs, thus, the HM decoder correctly decodes the transmitted codewords. In the third and fourth periods, it is observed that $K_1 = K_2 = K_3 = K_4$. However, from Table 4.1, the assignments $A_2, A_3 \notin \boldsymbol{P}$ and

Period 1. PCW 1 & 3: (1 2 3 4 & 3 1 2 4)

Cost Matrix G	All possible Assignments	Assignment Ranking	Cost
[0] 0 1 1	1 2 3 4	K1	0
1 [0] 0 1	3 1 2 4	K2	0
0 1 [0] 1	3 2 1 4	K3	1
1 1 1 [0]	2 1 3 4	K4	1
	4 2 3 1	K5	2
	3 2 4 1	K6	2
	3 1 4 2	K7	2

Period 2. PCW 6 & 11: (2 3 1 4 & 3 4 1 2)

Cost Matrix G	All possible Assignments	Assignment Ranking	Cost
1 1 [0] 1	2 3 1 4	K1	0
[0] 1 1 0	3 4 1 2	K2	0
0 [0] 1 1	2 4 1 3	K3	1
1 0 1 [0]	3 2 1 4	K4	1
	3 4 2 1	K5	2
	1 4 2 3	K6	3
	1 2 3 4	K7	3

Period 3. PCW 1 & 12: (1 2 3 4 & 4 3 2 1)

Cost Matrix G	All possible Assignments	Assignment Ranking	Cost
[0] 1 1 0	1 2 3 4	K1	0
1 [0] 0 1	4 2 3 1	K2	0
1 0 [0] 1	1 3 2 4	K3	0
0 1 1 [0]	4 3 2 1	K4	0
	4 3 1 2	K5	2
	4 1 3 2	K6	2
	4 1 2 3	K7	2

Period 4. PCW 6 & 9: (2 3 1 4 & 1 4 2 3)

Cost Matrix G	All possible Assignments	Assignment Ranking	Cost
[0] 1 0 1	1 3 2 4	K1	0
0 1 [0] 1	2 3 1 4	K2	0
1 [0] 1 0	1 4 2 3	K3	0
1 0 1 [0]	2 4 1 3	K4	0
	3 4 2 1	K5	2
	3 4 1 2	K6	2
	4 1 2 3	K7	2

FIGURE 5.2: Examples of codeword pairs in four periods

$A_1, A_4 \notin \boldsymbol{P}$, respectively for Periods 3 and 4. As such, the HM decoder is likely to pick one of the invalid codewords resulting in decoding errors. An invalid codeword is a permutation sequence $\boldsymbol{v}_o \notin \boldsymbol{P}$, of length M. Similarly, the codeword $\boldsymbol{v}_o$ can be represented as an $M \times M$ codeword matrix, $\boldsymbol{C}_o = [(c_o)_{ij}] \in \{0, 1\}$, $(i, j = 1, 2, \ldots, M)$. Each column j in $\boldsymbol{C}_o$ only has one non-zero element which fills the position corresponding to the PCW's integer, while other $M - 1$ elements in j are set to '0'. To reduce decoding errors, a brute force approach can be used to eliminate the invalid codewords. However, this increases receiver's decoding complexity.

5.3.2 Permutation-Codeword Combination Properties

The relationship of any PCW with others PCWs of the same permutation codebook can be described using a permutation cycle τ . For example, suppose we considered a codeword pair consists of PCWs $\boldsymbol{v}_p^1 = 1234$ and $\boldsymbol{v}_p^2 = 3142$ of length $M = 4$, presented as $\binom{1234}{3142}$. The mapping from $\boldsymbol{v}_p^1$ to $\boldsymbol{v}_p^2$ is read as "one maps to three, three maps to four, four maps to two and two maps back to one". The mappings can also be presented as: $1 \mapsto 3 \mapsto 4 \mapsto 2 \mapsto 1$. Since the elements in $\boldsymbol{v}_p^1$ and $\boldsymbol{v}_p^2$ map to each other in a cyclic fashion, this τ, is called a cyclic permutation with a length $\mathfrak{l} = 4$. Note that τ can be written in any cyclic order, for instance (1 3 4 2), (3 4 2 1), (4 2 1 3) or (2 1 3 4). On the other hand, if the considered codeword pair consisting of $\boldsymbol{v}_p^1 = 1234$ and $\boldsymbol{v}_p^2 = 1423$ presented as $\binom{1234}{1423}$, then we have $1 \mapsto 1$ where "one maps to itself" and "two maps to four, four maps to three and three maps back to two", expressed as $2 \mapsto 4 \mapsto 3 \mapsto 2$. The combination of the two permutation cycles, $\tau_1 = (1)$ and $\tau_2 = (2\ 4\ 3)$ can be written as $(1)(2\ 4\ 3)$, referred to as a product of two disjoint permutation cycles of lengths $\mathfrak{l} = 1$ and $\mathfrak{l} = 3$.

From the two combination scenarios between $\boldsymbol{v}_p^1$ and $\boldsymbol{v}_p^2$, we deduce that any mapping between a pair of permutation sequences consisting of $\boldsymbol{v}_p^1$ and $\boldsymbol{v}_p^2 \in \boldsymbol{P}$, can be expressed by either a cyclic permutation of length $\mathfrak{l} = M$ or as a product of disjoint permutation cycles of length $1 \leq \mathfrak{l} < M$ and logically, $\tau \subseteq \boldsymbol{v}_p$.

Theorem 5.2. *A pair of permutation sequences consisting of* $\boldsymbol{v}_p^1$ *and* $\boldsymbol{v}_p^2 \in \boldsymbol{P}$*, is transmitted as an ST pattern* $\boldsymbol{X}$ *obtained by logically adding their corresponding binary matrices,* $\boldsymbol{C}_p^1$ *and* $\boldsymbol{C}_p^2$*, by the Boolean OR operator. The pattern* $\boldsymbol{X}$*, is guaranteed an error-free decoding by the HM decoder, if the mapping between* $\boldsymbol{v}_p^1$ *and* $\boldsymbol{v}_p^2$*, does not result in a product of two disjoint* τ *having equal lengths of*

$$\mathfrak{l} = \begin{cases} \frac{M}{2}, & \text{if } M \text{ is even} \\ \frac{M-1}{2}, & \text{otherwise.} \end{cases} \tag{5.7}$$

Proof. Consider a permutation codebook with PCWs of length M. Referring to (5.7), if a mapping between two PCWs, $\boldsymbol{v}_p^1$ and $\boldsymbol{v}_p^2$, results in a product of two disjoint τ having equal lengths, then the Boolean product (AND) of $\boldsymbol{X}$ and $\boldsymbol{C}_o^u$ corresponding to some $\boldsymbol{v}_o^u \neq \boldsymbol{P}$, will result in a binary matrix of weight $w = M$; where $\boldsymbol{X} = \boldsymbol{C}_p^1 \bigvee \boldsymbol{C}_p^2$. This means there is a probability that this particular $\boldsymbol{v}_o^u \neq \boldsymbol{v}_p^1$ or $\boldsymbol{v}_p^2$ can be decoded. Thus, a decoding error may occur when the HM decoder is used.

On the other hand, if the mapping between $\boldsymbol{v}_p^1$ and $\boldsymbol{v}_p^2$ results in τ of different lengths, then the resultant matrix from the AND operation between $\boldsymbol{X}$ and $\boldsymbol{C}_o^u$ of any other $\boldsymbol{v}_o^u \neq \boldsymbol{v}_p^1$ or $\boldsymbol{v}_p^2$, will have at-most $w = 2$. Two (2) is the $d_{\min}$ of any permutation codebook with cardinality $M!$. Thus, an error-free decoding by the HM decoder is guaranteed because any corresponding binary matrix has $w = M$.

□

For instance, the transmitted ST pattern of Period 4 in Figure 5.2, is mapped from a pair consisting of $\boldsymbol{v}_p^1 = 2314$ and $\boldsymbol{v}_p^2 = 1423$, which decomposes into two disjoint τ of (12)(34) and their resultant ST pattern is:

$$\boldsymbol{X} = \begin{bmatrix} 0 & 0 & 1 & 0 \\ 1 & 0 & 0 & 0 \\ 0 & 1 & 0 & 0 \\ 0 & 0 & 0 & 1 \end{bmatrix} \bigvee \begin{bmatrix} 1 & 0 & 0 & 0 \\ 0 & 0 & 1 & 0 \\ 0 & 0 & 0 & 1 \\ 0 & 1 & 0 & 0 \end{bmatrix} = \begin{bmatrix} 1 & 0 & 1 & 0 \\ 1 & 0 & 1 & 0 \\ 0 & 1 & 0 & 1 \\ 0 & 1 & 0 & 1 \end{bmatrix}. \tag{5.8}$$

The Boolean product of $\boldsymbol{X}$ and the $\boldsymbol{C}_o^u$ matrix corresponding to $\boldsymbol{v}_o^u = 1324$ or $\boldsymbol{v}_o^u = 2413$, will result in $\boldsymbol{C}_o^u$ matrices with $w = M = 4$ as:

$$\boldsymbol{X} = \begin{bmatrix} 1 & 0 & 1 & 0 \\ 1 & 0 & 1 & 0 \\ 0 & 1 & 0 & 1 \\ 0 & 1 & 0 & 1 \end{bmatrix} \bigwedge \begin{bmatrix} 1 & 0 & 0 & 0 \\ 0 & 0 & 1 & 0 \\ 0 & 1 & 0 & 0 \\ 0 & 0 & 0 & 1 \end{bmatrix} = \begin{bmatrix} 1 & 0 & 0 & 0 \\ 0 & 0 & 1 & 0 \\ 0 & 1 & 0 & 0 \\ 0 & 0 & 0 & 1 \end{bmatrix}, \tag{5.9}$$

and

$$\boldsymbol{X} = \begin{bmatrix} 1 & 0 & 1 & 0 \\ 1 & 0 & 1 & 0 \\ 0 & 1 & 0 & 1 \\ 0 & 1 & 0 & 1 \end{bmatrix} \bigwedge \begin{bmatrix} 0 & 0 & 1 & 0 \\ 1 & 0 & 0 & 0 \\ 0 & 0 & 0 & 1 \\ 0 & 1 & 0 & 0 \end{bmatrix} = \begin{bmatrix} 0 & 0 & 1 & 0 \\ 1 & 0 & 0 & 0 \\ 0 & 0 & 0 & 1 \\ 0 & 1 & 0 & 0 \end{bmatrix}, \tag{5.10}$$

where $\wedge$ denotes the Boolean product. The results in (5.9) and (5.10) show that the cost ranking of $\boldsymbol{v}_o^u = 1324$ and $\boldsymbol{v}_o^u = 2413$ is equivalent to that of $\boldsymbol{v}_p^1$ and $\boldsymbol{v}_p^2$, erroneously indicating their presence in $\boldsymbol{X}$,

hence, increasing the probability of error at the HM decoder.

Conversely, the transmitted codeword pair in Period 1 consisting of $\boldsymbol{v}_p^1 = 1234$ and $\boldsymbol{v}_p^2 = 3124$, decomposes into a product of two disjoint τ of different lengths, (132)(4) and their resultant ST pattern is

$$\boldsymbol{X} = \begin{bmatrix} 1 & 0 & 0 & 0 \\ 0 & 1 & 0 & 0 \\ 0 & 0 & 1 & 0 \\ 0 & 0 & 0 & 1 \end{bmatrix} \bigvee \begin{bmatrix} 0 & 1 & 0 & 0 \\ 0 & 0 & 1 & 0 \\ 1 & 0 & 0 & 0 \\ 0 & 0 & 0 & 1 \end{bmatrix} = \begin{bmatrix} 1 & 1 & 0 & 0 \\ 0 & 1 & 1 & 0 \\ 1 & 0 & 1 & 0 \\ 0 & 0 & 0 & 1 \end{bmatrix}. \tag{5.11}$$

Because, the Boolean product of any other $\boldsymbol{C}_o$ or $\boldsymbol{C}_p$ with the resultant ST pattern $\boldsymbol{X}$, results in a binary matrix with $w \leq 2$, then an error-free decoding is guaranteed.

In light of the above, one mitigation measure taken to enhance the performance in a GSTC-MIMO system is to completely avoid the use of the codeword combinations that result in erroneous decoding, in the ST encoder. If $\boldsymbol{\mathcal{P}} \subseteq \boldsymbol{P}$ is the codebook containing only codeword pairs that do not result in decoding errors, and $\mathcal{B}'$ as previously defined in Section 5.2.2.2, then the data rate of the GSTC-MIMO system, which we refer to as $D3$, is given by

$$D3 \ = \mathcal{B}' + \log_2 \binom{|\boldsymbol{\mathcal{P}}|}{N_a}. \tag{5.12}$$

Hence, it is highly likely that $D3 < D2$ because some codeword combinations are completely avoided, which may reduce the codebook

cardinality. However, it is still certain that $D3 > D1$, because information bits are mapped to codeword combinations and not single codewords as the case in STC-MIMO.

5.3.3 GSTC-MIMO Encoder based on Partitioned Codebooks

Based on Theorem 5.2 and its proof presented in Section 5.3.2, we propose a simple encoding scheme where the ST MIMO codebook is partitioned into N_ρ disjoint sub-codebooks $\boldsymbol{\mathcal{P}}_\rho \subseteq \boldsymbol{P}$, enabling the use of all codewords in $\boldsymbol{P}$, where $\rho = 1, 2, \ldots, N_\rho$. The codebook partition is done in such a way that codeword pairs resulting in erroneous decoding at the HM decoder, form a sub-codebook. The message bits to be mapped to PWCs are divided into a group of $\mathcal{B}$ bits, which are further segmented into N_a bit blocks denoted as $\boldsymbol{b}_1, \boldsymbol{b}_2, \ldots, \boldsymbol{b}_{N_a}$. In Figure 5.3, a representation of the adapted GSTC-MIMO encoder for $N_\rho = N_a = 2$ and $\mathcal{PC}(M = 4, d_{\min} = 3)$ is shown. As depicted in Figure 5.3, the message bits are mapped to the indices of the PCWs in each $\boldsymbol{\mathcal{P}}_\rho$ to determine the constituent codewords for the combination. The first block $\boldsymbol{b}_1 = 011$ is mapped to 2431 of $\boldsymbol{\mathcal{P}}_1$, while the second block $\boldsymbol{b}_2 = 11$ is mapped to 4321 from $\boldsymbol{\mathcal{P}}_2$. The HM decoding capability is enhanced since the codebook partition avoids the formation of codeword combinations that result in erroneous decoding. For distinction, we refer to the system using the adapted encoder as AE-GSTC-MIMO system. The data rate for

the AE-GSTC-MIMO system, referred to as D4 is expressed by

$$D4 = \mathcal{B}' + \sum_{\rho=1}^{N_\rho} \log_2(|\boldsymbol{\mathcal{P}}_\rho|). \tag{5.13}$$

Note that N_ρ does not necessarily have to be equal to N_a. However, N_a PCWs are combined every transmit period.

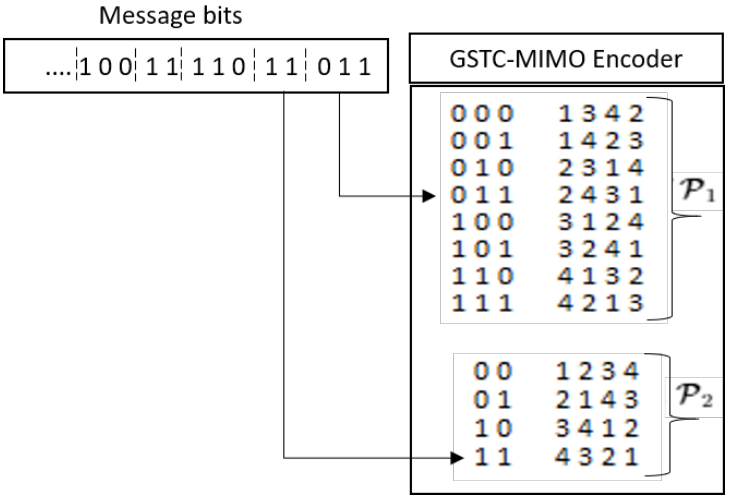

FIGURE 5.3: Adapted GSTC-MIMO Encoder

5.4 Simulation Results and Analysis

An indoor environment is considered with room dimensions of 4.0 m× 4.0 m×3.0 m, where the TEs are placed in a downward orientation at 3.0 m above the floor. A spacing of 0.2 m is assumed between the TE array. A normalized transmitted optical power is assumed at every transmit interval and to ensure a constant mean optical power irrespective of the number of active TEs, the intensity at each transmit interval is divided by N_a, the number of active TEs. The receiver, placed in the center of the room at a height above the floor, in an upward orientation, is composed of an array of four PDs separated

by a distance of 0.05 m in both the x and y directions. Simulation parameters are listed in Table 5.2.

TABLE 5.2: Simulation Parameters

Parameter	**Value**
Room size (W × L × H)	4 m × 4 m × 3 m
Number of TEs	4
TE height from RE plane	2.15 m
Half-power angle, $\Phi_{1/2}$	15°
TE Locations (x,y,z)	(1.9, 1.9, 3), (2.1, 1.9, 3) (1.9, 2.1, 3), (2.1, 2.1, 3)
Transmitted Optical Power	2 W
Receiver plane height from floor	0.85 m
Detector receiver area, A_r	1cm^2
Receiver locations (m) (x,y,z)	(2.0, 2.0, 0.85)
Single detector, FOV	15°

5.4.1 Bit Error Rate (BER) Performance in MIMO Systems

Performance results of the GSTC-MIMO systems in the presence of AWGN, are presented. Message bits are mapped to predefined PCs whose equivalent permutation matrices are transmitted, hence an OOK modulation is assumed. The attenuation effect of each $h_{n_r n_t}$ in (5.1), has to be accounted for in the calculation of the probability of error, P_e [44]. Thus,

$$P_e = \frac{1}{2}\text{erfc}\left(\sqrt{\frac{E_b}{4N_0}\| \boldsymbol{H} \|_F^2}\right), \tag{5.14}$$

where erfc(.), E_b and $\| \ . \ \|_F$ denote the complementary error function, the received electrical bit energy and Frobenius norm, respectively. Considering the room parameters and the positions and locations of the TEs and RE according to Table 5.2, the resulting LOS channel gain is of the order of 10^{-4}, which leads to electrical path loss at the receiver side [44, 87]. Hence, an offset of 70 dB with respect to the received signal-to-noise ratio (SNR), is noticed in the BER performance. In Figure 5.4, we compare the BER performance results of a systems using the HM adapted encoder to those of GSTC-MIMO system using the conventional codebook, for both types of codeword combinations, i.e those that result in error-free decoding and those with a high decoding error probability. We denote the codeword combinations that result in error-free decoding and those with a high decoding error probability by C1 and C2, respectively. To ascertain the SD HM decoder's superior performance over the HD minimum distance (MD) decoder as presented in [130], we first compare the performance comparison of the STC-MIMO system. There after, in all subsequent performance analysis, we focus only on the performance of the HM SD decoder.

In Figure 5.4, the robustness of SD HM decoder against AWGN, over the HD decoder, is seen from the BER performance of the STC-MIMO based systems using these decoders. It is noticed that the HM decoder's BER performance improves with the increasing signal to noise ratio (SNR) faster than that of the MD decoder, hence the HM decoder outperforms the MD decoder. Hence the HM decoder

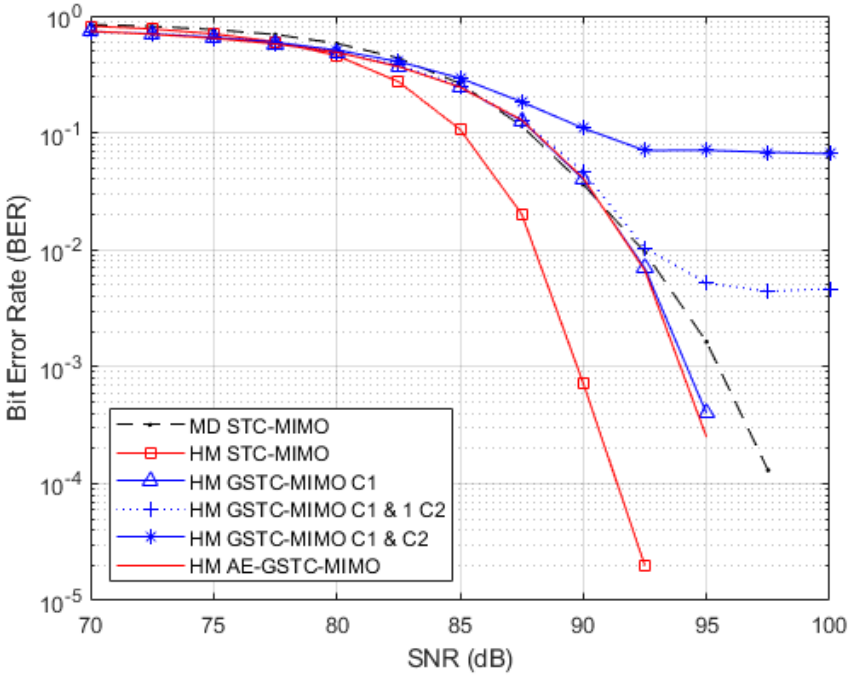

FIGURE 5.4: BER performance, STC and GSTC-MIMO systems.

outperforms the MD decoder, such that an SNR gain of over 5 dB is noticed at a BER of 10^{-3}. Additionally, as presented in [130], the HM decoder has a much lower decoding complexity compared to the MD decoder, as such a twofold gain of reliability and low decoding complexity is achieved with the HM decoder.

From the same Figure 5.4, the reliability performance of the STC-MIMO and GSTC-MIMO schemes with the HM decoder, is compared. The difference in performance between them, where the STC-MIMO scheme performs better than the GSTC-MIMO schemes, demonstrates the advantage of allowing only one active TE at a time, consequently, avoiding the inherent channel correlation effects of VLC systems. At BER of 10^{-3}, approximately 5 dB SNR degradation is noticed in the performance of the GSTC-MIMO system using the HM decoder, in comparison to the STC-MIMO system, using the

same decoder. However, despite the BER degradation, a data rate improvement from $\log_2(|\boldsymbol{P}|)$ to $\log_2\binom{|\boldsymbol{P}|}{N_a}$ bits per period, is achieved for a non partitioned codebook. Whereas a data rate improvement from $\log_2(|\boldsymbol{P}|)$ to $\sum_{\rho=1}^{N_a}\log_2(|\boldsymbol{\mathcal{P}}_\rho|)$ bits per period, is achieved for a partitioned codebook, $\boldsymbol{P}$.

For codebook $\boldsymbol{P}$ of Table 5.1, we simulated the GSTC-MIMO system using the following:

- All error-free combinations with only one combination resulting in erroneous decoding, expressed as: C1 & one (1) C2.
- Use of all possible $\binom{|\boldsymbol{P}|}{2}$ combinations, i.e all C1 and C2.
- Codebooks $\boldsymbol{\mathcal{P}}_1$ and $\boldsymbol{\mathcal{P}}_2$ partitioned from $\boldsymbol{P}$.
- Only C1 combinations from $\boldsymbol{P}$.

The robustness of the system with a partitioned codebook is seen from the performance results in Figure 5.4, where the BER results match those of the un-partitioned codebook using only error-free combinations, C1. For data rate enhancement, longer codes yielding larger codebooks that are partitioned into higher number of sub-codebooks can be used. The effects of the codeword combination properties presented in Section 5.3.2, are observed in the BER performance in the presence of AWGN. It is observed from the BER performance improvement when only C1 combinations are used, that the mitigation strategy of avoiding the use of C2 combinations in a GSTC-MIMO system yields good results. As such, the codeword

combination investigation presented in this chapter aids in adapting ST codes to decoders, such as the HM decoder.

5.4.2 Energy Efficiency Evaluation and Comparison

Every modulated message bit requires an energy $E_b = E_s / \mathcal{B}'$ to be transmitted. Hence, the EE can be determined by the ratio of the message bits conveyed by indices of the PWCs to the total number of bits transmitted [67]. As such, the EE for STC-MIMO system can be expressed as

$$EE_{\text{STC}} = \frac{\mathcal{B}}{\mathcal{B} + \mathcal{B}'} \times 100 \tag{5.15}$$

Further, if $\varpi = D4 - D1$, then $D4 = \mathcal{B} + \varpi + \mathcal{B}'$. Consequently, the EE for the AE-GSTC-MIMO system can be expressed as

$$EE_{\text{AE-GSTC}} = \frac{\mathcal{B} + \varpi}{\mathcal{B} + \varpi + \mathcal{B}'} \times 100. \tag{5.16}$$

From the respective EE expressions of the STC and AE-GSTC schemes, in (5.15) and (5.16), the AE-GSTC-MIMO system saves about

$$\text{Energy saving} = \frac{(\mathcal{B} + \varpi)(\mathcal{B} + \mathcal{B}')}{\mathcal{B}(\mathcal{B} + \varpi + \mathcal{B}')}, \tag{5.17}$$

more energy compared to the STC-GSTC MIMO system. This shows that the technique of mapping some message bits to indices of permutation codewords helps reduce the system's total required energy for transmission. Therefore, two evident gains of the GSTC-MIMO

over STC-MIMO are the enhancement in the efficiency of both energy and spectrum.

5.4.3 Multiple Access STC-MIMO (MA STC-MIMO) System

Based on the results presented in Section 5.4.1 of adapting the GSTC-MIMO encoder to the HM decoder, a reliable multiple access STC-MIMO system can be achieved. We simulated a two user MA STC-MIMO system and assigned codebooks $\boldsymbol{\mathcal{P}}_1$ and $\boldsymbol{\mathcal{P}}_2$ partitioned from $\boldsymbol{P}$, to users 1 and 2, respectively. This way, C1 combinations are strategically assigned to one of the two users. As such all possible codeword pairs belonging to $\boldsymbol{P}$ are used in the MA system.

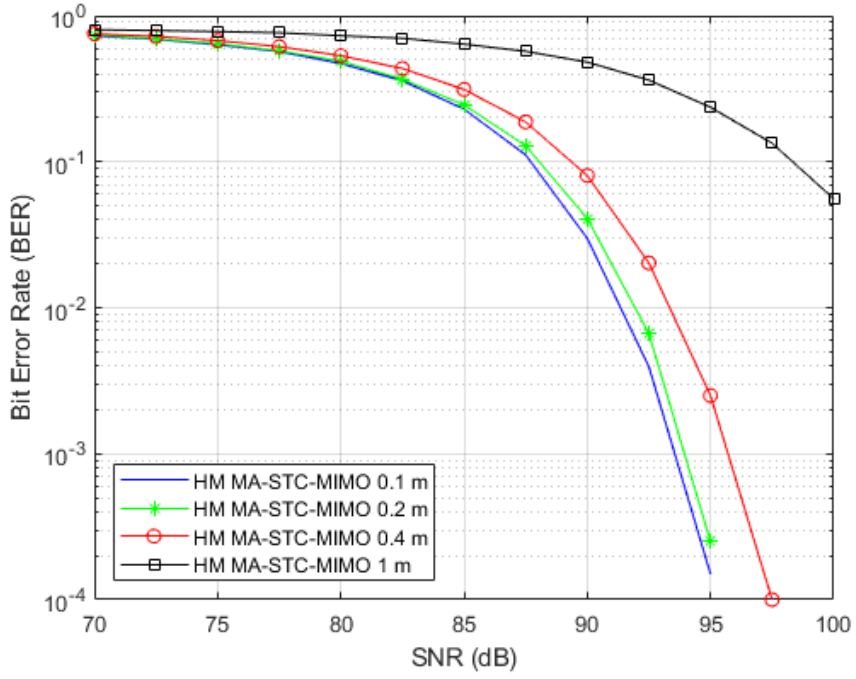

FIGURE 5.5: Bit error rate (BER) performance of the MA STC-MIMO system with varying user TE separation

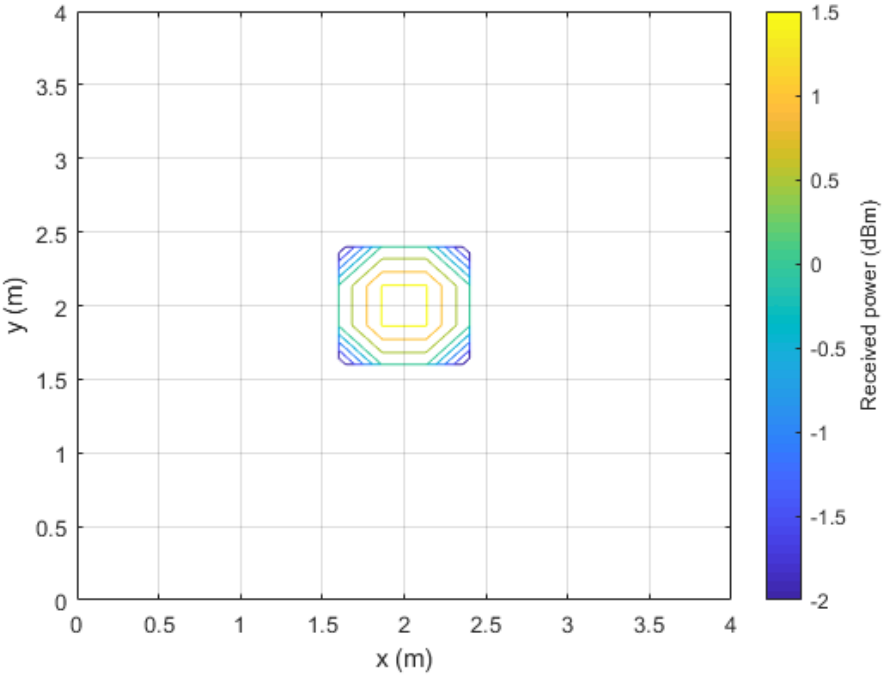

(a)

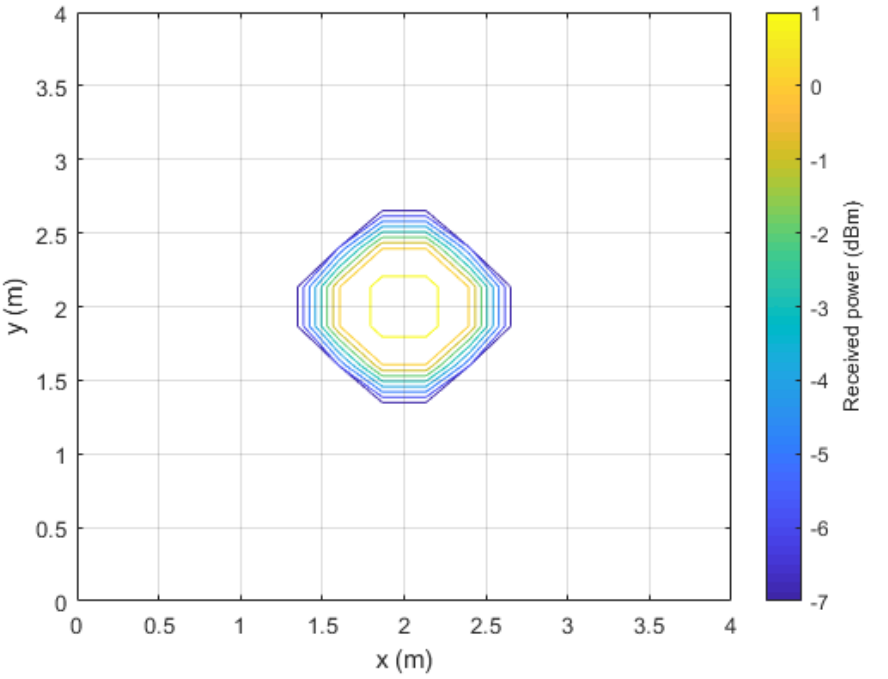

(b)

FIGURE 5.6: Representation of power distribution from the TEs for varying Δd. (a) $\Delta d = 0.1$ m (b) $\Delta d = 0.2$ m .

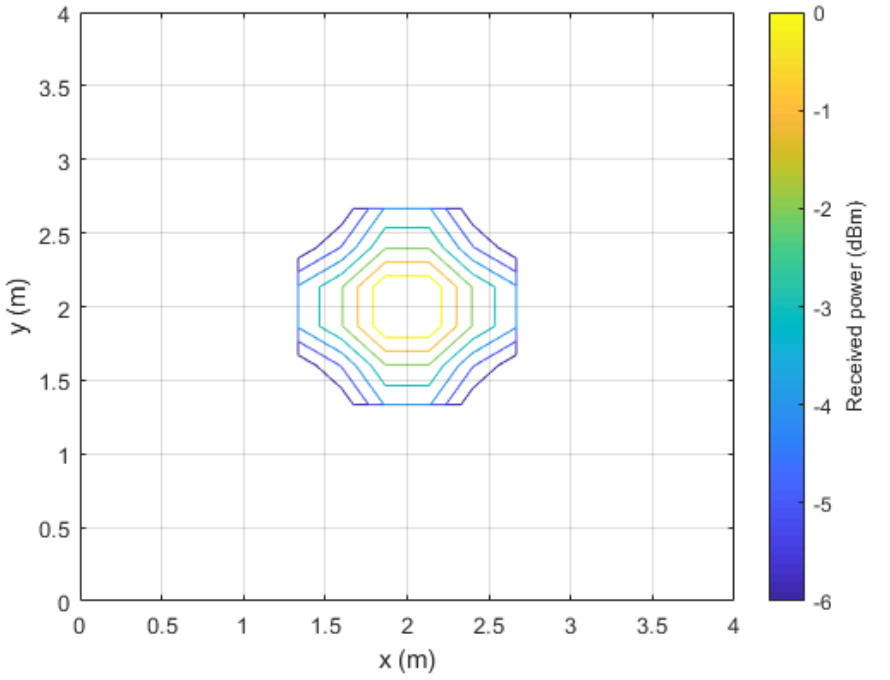

(a)

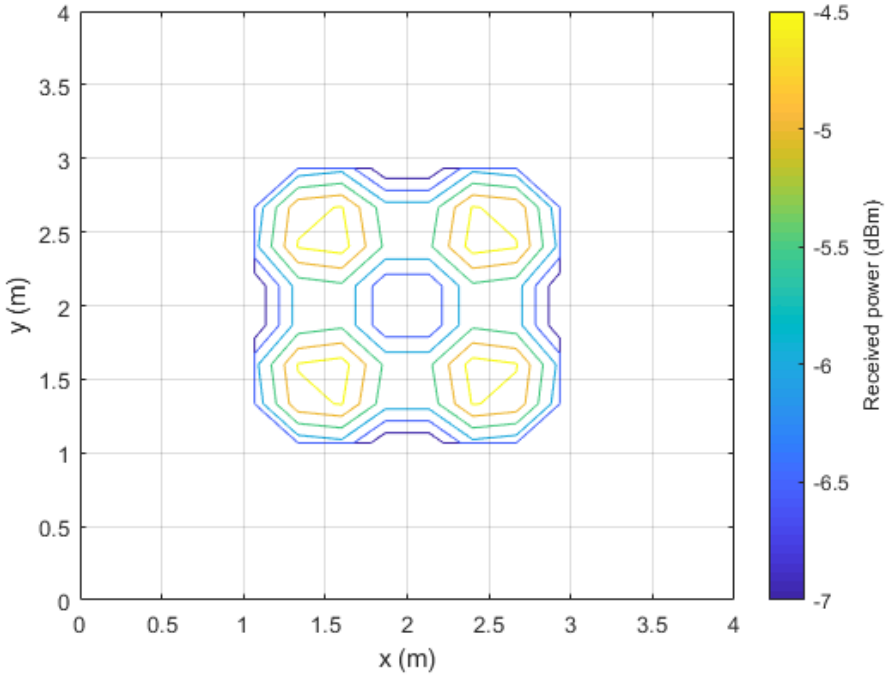

(b)

FIGURE 5.7: Representation of power distribution from the TEs for varying Δd. (a) $\Delta d = 0.4$ m. (b) $\Delta d = 1$ m.

In indoor environments like air crafts where the light of a communication/illumination device from one passenger is not suppose to dazzle the next passenger, illumination devices are designed to be highly directional having narrow $\Phi_{1/2}$. In such environments, optical TE and RE positioning is of the essence. We use the MA STC-MIMO system to investigate the performance effect of the separation distance, Δd, between TEs. The value of Δd is varied as $\Delta d = 0.1$ m, 0.2 m, 0.4 m and 1 m, while the RE position is fixed. In Figure 5.5, we notice that in this scenario where only the LOS is considered with LEDs having narrow $\Phi_{1/2}$ and the RE is stationary, it is desirable to maintain a reasonable short distance between the TEs. These shorter distances between TEs result in lower path loss and the optical energy is concentrated within the receiver's field of view. As such, the system performance degrades with the increase in Δd.

The fact that not all TEs are activated at the same time, then the conditions that will avoid correlation between the MIMO links still reasonably hold. This can be likened to the link blockage scheme in [44]. Thus, the reason the system performs better for shorter Δd, in Figure 5.5, is mainly attributed to the received power.

A representation of the received power, $P_r = P_t \cdot \boldsymbol{H}$, for varying Δd, is shown in Figure 5.6 and Figure 5.7; where $\boldsymbol{H}$ is the channel gain matrix in (5.1) and P_t the optical power from each TE. For the illustration in Figure 5.6 and Figure 5.6, $P_t = 2$W is assumed. The profile of the P_r distribution can explain the reason the system having $\Delta d = 0.1$ m, performs better. Noting that the receiver position

was kept constant at the centre, we see that as Δd increases, the power at the centre of the room where the RE is placed, reduces. In Figure 5.7(b), which shows the power distribution of the largest Δd, the highest power from the LEDs is concentrated away from the centre, thus the RE receives low energy which results in decoding errors.

5.5 Summary

A VLC GSTC-MIMO system using a low-complexity SD decoder based on the Hungarian and Murty's algorithm, referred to as the HM decoder, was studied. The inclusion and use of PCs resulting in VW matrices was proposed for data rate enhancement. Based on the properties of the PCW combinations, a theorem defining the capability of HM decoder was provided and an adaptation of the ST encoder to the HM decoder capability, based on the codebook partitioning scheme, was proposed. The performance of the system using all codewords of the codebook as a result of the adapted ST encoder based on the codebook partitioning scheme, performed as well as the GSTC-MIMO system using only codewords resulting in combinations with lower probability of error. The adapted ST encoder scheme was extended to an MA system where the sub-codebooks were assigned to separate users, thus avoiding the codeword combinations that would cause decoding errors at the HM decoder. An investigation on the impact of TE distance separation, on the performance of the system was conducted. It was shown that for LEDs

with narrow half-power angles, the system's BER worsens as the TE separation distances, Δd increases. It was also shown that the GSTC based system is robust against the correlation effects that MIMO links are prone to. This is due to the fact that not all TEs are activated at every transmit interval.

CHAPTER 6

Generalised Permutation Coded OFDM-MFSK in Hybrid Powerline and Visible Light Communication

---

This chapter is based on the following publication: *Mulundumina Shimaponda-Nawa, Oluwafemi Kolade, and Ling Cheng*, "Generalised Permutation Coded OFDM-MFSK in Hybrid Powerline and Visible Light Communication". *IEEE Access Journal, 10:20783-20792, 2022.*

The author of this thesis conceptualized the work, performed the simulations, analyzed the results and wrote the paper.

6.1 Introduction

The use of OFDM in various communication technologies [65, 75, 105, 138], including HPV [82, 93], has been welcomed because it enhances the spectral efficiency and is a reliable mitigation scheme against ISI. In classical OFDM, each OFDM sub-carrier symbol carries a message symbol modulated using a single-carrier modulation technique, such as M-QAM or M-PSK. Furthermore, to enhance

the data rate and the spectral efficiency of OFDM-based systems, several modulation options for OFDM-based systems such as index-based, sub-carrier number-based and shape-based OFDM schemes, have been exploited [16, 17, 40, 49, 64, 65]. Variants of index-based OFDM include OFDM with index modulation (OFDM-IM) and spatial modulation OFDM (SM-OFDM) [16, 17, 49]. In OFDM-IM, the indices of the sub-carriers in an OFDM symbol are used to send additional information. Whereas in SM-OFDM, some information bits are mapped to and sent by the indices of antennas, while other information bits are conventionally modulated and conveyed via the activated antenna.

On the other hand, in sub-carrier number modulation OFDM (OFDM-SNM), some sub-carriers are exploited to convey additional information [64], whereas, in shape-based OFDM, the shape of pulses is exploited to convey additional information. Examples of the shaped-based OFDM modulation schemes are reported in [24, 46].

It is worth noting that the work mentioned above focused only on wireless communication systems and some noise effects inherent in other fast varying channels such as the PLC, were not considered. Examples of such noise types are narrow-band interference and impulse noise which affect multiple frequencies in the narrow-band region [58, 100, 101, 132]. In [58], where extensive measurements were carried out for a residential power line channel, impulse noise was observed to occur in bursts and lasting for a maximum period of

about 0.1 ms. In such channels, a series of signal bits may be affected in time domain or a frequency may be affected over a period of time. Therefore, in the application of index modulation (IM) of OFDM or its variants, to channels prone to narrow-band interference and impulse noise noise effects, a special consideration in the implementation, is required.

Since impulse noise affects a range of frequencies in a short period [1, 6, 33, 58, 132], then schemes that activate only some frequencies for data transmission at each transmit period would well mitigate this noise. This is because there is a probability that frequencies affected by the impulse noise may not be carrying information at a particular transmit period. Hence, schemes such as MFSK where information symbols are mapped to one of the M available frequencies are good candidates for impulse noise mitigation because only one of the M sub-carrier frequencies carries information at each sampling period.

A combination of OFDM and MFSK (OFDM-MFSK) proposed in [114, 155, 157], was exploited for impulse noise mitigation in a PLC system [75]. When OFDM-MFSK, which is a variant of OFDM-IM is used, frequency sub-carriers in the OFDM symbol are segmented in groups of M, where M denotes the order of the frequency shift keying (FSK) modulation. As such, at any transmit interval, only one sub-carrier is activated in each group of M. Thus, the effects of impulse noise are mitigated. In light of this, we extend the OFDM-MFSK scheme to an HPV system to exploit the benefits of impulse noise mitigation, which can result in enhanced system reliability.

In [74, 75], a coded OFDM-MFSK in a PLC system was achieved with the use of PCs, whose codeword length is equal to M, the FSK modulation order. The length of a non-binary permutation codeword (PCW) is the number of integers in the codeword. In the scheme proposed in [75], a one-to-one mapping of data symbols and PCWs, was used. The non-binary PCWs' integers then determine which sub-carriers would be activated in each OFDM-MFSK sub-carrier sub-block. Each activated subcarrier conveys a set of modulated message bits and those mapped to the PCW. In this scheme, only one codeword is selected for each OFDM symbol. Therefore, all the activated sub-carriers convey the same data symbols. Therefore, if a subcarrier is affected by noise, subcarrier decoding can assist with recovering the information of the affected subcarrier.

To improve the data rate of the permutation aided OFDM-MFSK scheme applied in the HPV system, we propose to select more than one codeword for each OFDM-MFSK symbol. Thus, a generalised permutation coded (GPC) OFDM-MFSK HPV system is achieved and is denoted as GPC OFDM-MFSK. Since the GPC OFDM-MFSK activates a few sub-carriers, it can be considered as a type of the recently reported sparse index modulation (SIM) [60, 123]. However, unlike SIM, where a certain number of sub-carriers are selected irrespective of the order of selection, the pattern of sub-carrier activation in GPC matters and is influenced by the positions of the integers in each selected PCW. Furthermore, since multiple PCWs are used for each OFDM symbol, the SD low-complexity HM decoder

proposed in [130] to simultaneously detect multiple PCWs, is used.

Precisely, the contributions in this chapter can be summarised as:

- To the best of our knowledge, we, for the first time propose and present the use of the OFDM-MFSK scheme in an HPV system to enhance the system's performance by impulse noise mitigation.
- Increasing the OFDM-MFSK data rate by implementing a GPC scheme where k message symbols are mapped to k PCWs to be simultaneously transmitted per OFDM-MFSK symbol.
- Application of an SD HM decoder for a reduced decoding complexity and for further enhancement of the error rate performance of the HPV system.

The rest of the chapter is organised as follows: In the following section, an overview of the OFDM-MFSK based system is presented, including the system and channel models. In Section 6.3, the GPC OFDM-MFSK based HPV system is presented and a brief description of the SD decoding method based on the HM decoder, is also included. Then the simulation results and analysis of the different schemes considered in this work are presented in Section 6.4, after which a summary of this chapter, is presented in Section 6.5.

6.2 OFDM-MFSK based HPV System

This section first provides an overview of the basic principles of the OFDM-MFSK scheme applied to the HPV system. Later, a downlink transmission system in which the receiver is placed in a room served by a VLC transmitter installed in the ceiling, which also provides illumination, is considered. The VLC transmitter receives the information from the PLC channel and then re-transmits the information to the VLC receiver located at some position in the room of consideration.

6.2.1 An Overview of the OFDM-MFSK

In M-FSK modulation, information symbols are mapped to one of the M available frequencies, such that at each sampling time, one of the M frequencies is transmitted. This results in $\mathcal{B}_1 = \log_2 M$ bits being transmitted at each sampling time. Thus, the the bandwidth utilisation, η_1, for MFSK is given as [121],

$$\eta_1 = \frac{\mathcal{B}_1}{M}. \tag{6.1}$$

On the other hand, in OFDM modulation, information symbols are mapped to N orthogonal sub-carriers in an OFDM array and simultaneously transmitted in the PLC channel. If a signal constellation symbol has $\mathcal{Q}$ information bits, then $\mathcal{B}_2 = \mathcal{Q}N$ bits are transmitted per OFDM symbol. The OFDM bandwidth utilisation, η_2, can be

expressed as:

$$\eta_2 = \frac{N}{N + N_{\text{cp}}}, \tag{6.2}$$

where N_{cp} is the number of sub-carriers used for the cyclic prefix (CP) of the OFDM symbol. A CP is inserted at the beginning of the OFDM signal to maintain orthogonality among sub-carriers. The CP consists of a cyclic extension from the end of the OFDM signal, whose length is mainly influenced by the delay spread of the channel. Thus, to eliminate ISI, inter-carrier interference (ICI) and maintain orthogonality between sub-carriers, the length of the CP is chosen to be longer than the delay spread of the channel as this ensures that all the samples from the previous OFDM symbols fall within the CP duration.

In the OFDM-MFSK scheme, N sub-carriers are divided into groups of M sub-carriers. Only one sub-carrier from each group is activated for transmission, hence no energy is transmitted on the other $M-1$ sub-carriers in each group. Let $g = 1, 2, \ldots, G$ denote the different groups of M sub-carriers and $\varsigma = 1, 2, \ldots, M$ denote the indices of one of the M frequencies in group g. Then, each of the symbols at any activated sub-carrier can be represented as $x_{g\varsigma}$. Then, a vector representation of the whole OFDM-MFSK symbol to be transmitted per channel use via the PLC channel is

$$\boldsymbol{x} = 0 \ldots \underbrace{x_{1\varsigma}}_{\text{Group 1}} \ldots 0, 0 \ldots \underbrace{x_{2\varsigma}}_{\text{Group 2}} \ldots 0, \ldots, 0 \ldots \underbrace{x_{G\varsigma}}_{\text{Group G}} \ldots 0. \tag{6.3}$$

Thus, the total number of bits per OFDM-MFSK symbol is

$$\mathcal{B}_3 = G \log_2 M = G \cdot \mathcal{B}_1. \tag{6.4}$$

Considering (6.1) and (6.2), the bandwidth utilisation, η_3, of the OFDM-MFSK scheme can therefore be expressed as:

$$\eta_3 = \frac{\mathcal{B}_1}{M} \frac{N}{N + N_{\text{cp}}}. \tag{6.5}$$

Thus, the bandwidth utilisation for the MFSK, OFDM and OFDM-MFSK schemes can be compared as, $\eta_1 \leq \eta_3 < \eta_2$, indicating that the OFDM-MFSK scheme enhances the spectral efficiency of the MFSK scheme, however, it is lower than that of the classical OFDM scheme.

6.2.2 System Model

In Figure 6.1, a system block diagram highlighting the major sections, such as the transmitter, receiver, PLC/VLC integration module and the channels, of the OFDM-MFSK HPV system, is shown.

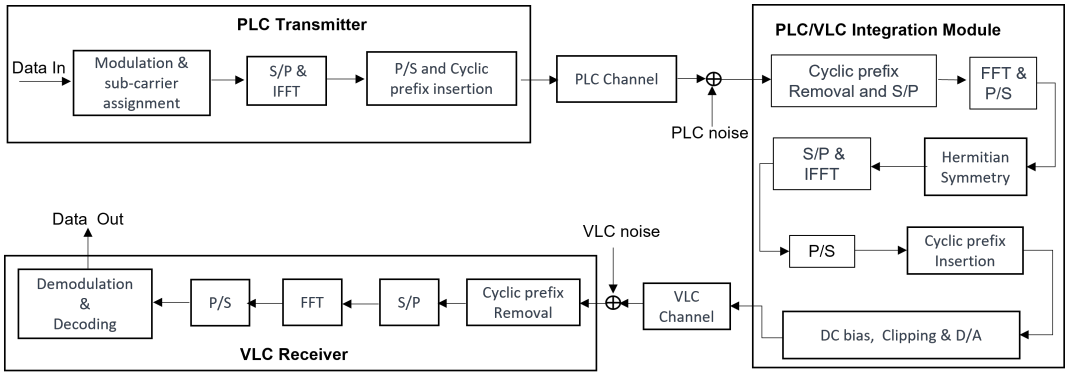

FIGURE 6.1: System block diagram of OFDM-MFSK based HPV system

6.2.2.1 PLC Section and the Integration Unit

The incoming modulated symbols are segmented into $G = \frac{N}{M}$ groups and each information symbol in a particular group determines the sub-carrier index to be activated for transmission. The frequency domain signals are converted to time domain via the IFFT block and transmitted via the PLC channel. At the PLC-VLC integration module, the output signal from the PLC channel is given by

$$\boldsymbol{y}_{\mathrm{p}} = \boldsymbol{s} \cdot e^{j\phi} + \boldsymbol{n}_{\mathrm{p}}. \tag{6.6}$$

In (6.6), $\boldsymbol{s}$ is the complex transmitted signal, $\boldsymbol{n}_{\mathrm{p}} = \boldsymbol{n}_{\mathrm{G}} + \boldsymbol{n}_{\mathrm{I}}\sqrt{z}$, is the noise component in the PLC channel comprising the background noise $\boldsymbol{n}_{\mathrm{G}}$ modelled as AWGN (a complex component with zero-mean and variance of $\sigma_{\mathrm{G}}^2 = 2N_0$, where N_0 is the noise power spectral density) and the impulse noise, $\boldsymbol{n}_{\mathrm{I}}$, which follows a Poisson distribution and has a variance σ_{G}^2/A. A is the impulsive index determining the frequency of occurrence of $\boldsymbol{n}_{\mathrm{I}}$ and z is a variable imposing the Poisson distribution on $\boldsymbol{n}_{\mathrm{I}}$. If the AF relaying protocol is applied, the received PLC signal $\boldsymbol{y}_{\mathrm{p}}$ is demodulated, scaled and re-modulated [93]. The resulting signal is re-transmitted by VLC transmitters. On the other hand, the DF relaying protocol will also decode the received PLC signal before re-modulation for transmission by the VLC transmitters. In this work, the AF relaying protocol is assumed for its simplicity.

6.2.2.2 VLC Section

The signal $\boldsymbol{y}_{\mathrm{p}}$ at the FFT output, in the integration unit, is complex. Since the VLC section of the HPV system employs IM/DD, then $\boldsymbol{y}_{\mathrm{p}}$ is not suitable to modulate the intensity of the VLC transmitters due to the constraint that light intensity cannot be negative. To obtain optical IM/DD compatible signals, the HS property to generate real OFDM signals has widely been used [15, 93, 95].

In an HS structure, a message symbol is duplicated in the form of its complex conjugate. For the N frequency domain symbols obtained from the FFT operation on PLC output signal, the general expression relating the message symbols X, their complex conjugate X^* components and their positions due to the HS constraint is given as:

$$X_{(\xi+2)} = X^*_{(2N-\xi)}, \;\; \xi = 0, 1, 2, \ldots, N-2. \tag{6.7}$$

Thus, the HS structure is formed by concatenating the original vector of message symbols with the vector of their complex conjugate symbols. From (6.7), it can be seen that in VLC, $2N$ sub-carriers are required due to the HS constraint. If the same number of sub-carriers is maintained between the PLC and VLC channels, then the symbols from the PLC would be transmitted in two transmit periods. Another way would be to apply the HS constraint at the PLC section. Then, the same number of sub-carriers would be maintained between the two channels. In the HS structure, the first and $(N+1)^{\mathrm{th}}$

components are set to zero, to avoid any DC shift or any residual complex component in the time domain signal, ($X_{(0)} = X_{(N+1)} = 0$).

After the HS block, the signal is again converted to a time domain signal $\boldsymbol{x}_{\mathrm{v}}$ by the IFFT after which a CP is inserted at the beginning of the OFDM signal to maintain orthogonality among subcarriers. The signal $\boldsymbol{x}_{\mathrm{v}}$ is real-valued and bipolar with a random-like variation often characterized by a high peak-to-average power ratio (PAPR) [36, 93]. The high PAPR leads to signal distortions due to the non-negativity constraint for the optical time-domain signal and a reduced energy efficiency for practical LED drivers with limited dynamic ranges [93]. As such, a DC bias is then added to $\boldsymbol{x}_{\mathrm{v}}$ in order to make the signal compatible with IM/DD channel and avoid the PAPR problem. Additionally, before modulating the LED, peaks of time domain OFDM signals may be clipped at the voltage which corresponds to permissible pulsed currents recommended by the manufacturer [36]. However, this may introduce clipping noise, as will be shown in Section 6.4. After the digital-to-analog (D/A) operation, $\boldsymbol{x}_{\mathrm{v}}$ modulates the LEDs transmitters for transmission via the VLC wireless channel. The transmitters are assumed to have a Lambertian propagation model.

In this chapter, only the LOS component is assumed as it accounts for a greater portion of the transmitted optical signal [59, 105]. The channel gain, considering LOS propagation between a transmitter and a receiver located at a distance of d_{v} and angle of irradiance θ, with respect to the transmitter, can be approximated as (2.7) [68].

The received optical signal at any receiver element is expressed as [34]

$$\boldsymbol{y}_{\mathrm{v}} = \boldsymbol{x}_{\mathrm{v}} \cdot h_{los} + \boldsymbol{n}_{\mathrm{Gv}} \tag{6.8}$$

where $\boldsymbol{n}_{\mathrm{Gv}}$ denotes the noise which is modelled as AWGN with zero-mean and variance σ^2_{Gv}. At the VLC receiver, the CP is first removed and the signal is passed through a serial-to-parallel (S/P) converter before the FFT is performed on the signal.

The estimation of the likely transmitted symbols can be achieved by maximum likelihood (ML) detection. In [116] envelope detection was used for estimating MFSK in AWGN, while the analysis in [114] suggests that the decision for estimating the transmitted signal is made in favour of the maximum absolute value of the components of $\boldsymbol{y}_{\mathrm{v}}$. As these are similar, the analysis and expression in [114] is adopted and the vector $\hat{\boldsymbol{y}}_{\mathrm{v}}$ consisting of the estimated transmitted symbols is given as:

$$\hat{\boldsymbol{y}}_{\mathrm{v}} = \underset{\boldsymbol{x}_{\mathrm{v}} \in F}{\arg\max} \, |\boldsymbol{y}_{\mathrm{v}} \boldsymbol{x}_{\mathrm{v}}|^2. \tag{6.9}$$

Note that $\boldsymbol{x}_{\mathrm{v}}$ is a vector consisting of different $x_{\mathrm{v}_{g\varsigma}}$, elements from one of the activated sub-carriers in the OFDM array F, where variables g and ς denote the group and sub-carrier index in that group.

The bit error probability, P_e of OFDM-MFSK, for the energy per bit, E_b, is said to be the same as that of MFSK [75] and is defined:

$$P(e) = \sum_{\varsigma=1}^{M-1} \frac{(-1)^{\varsigma+1}}{\varsigma+1} \binom{M-1}{\varsigma} e^{\left(-\frac{\varsigma \log_2 M}{M+1} \frac{E_b}{N_0} \right)}. \tag{6.10}$$

Larger M values would enhance the error performance of the system, however, they degrade the spectral efficiency. Hence, a trade-off between error performance and spectral efficiency is inevitable.

6.3 Generalised Permutation-Coded OFDM-MFSK based HPV System

In this section, we present a method to improve the data rate of the OFDM-MFSK HPV system by employing PCs. Precisely, the use of PCs is considered in order to also aid the use of a soft-decision method of identifying the activated sub-carriers of the OFDM-MFSK scheme. First, the model of a permutation-coded OFDM-MFSK (PC OFDM-MFSK) system is presented and then the generalisation method is presented.

6.3.1 Permutation-Coded OFDM-MFSK based HPV System

In [74, 75], a subcarrier coding of the OFDM-MFSK scheme was proposed for impulse noise mitigation in PLC channels. In this section, the idea of sub-carrier coding is extended to the HPV system introduced in Section 6.2. The BER performance of the PC OFDM-MFSK HPV system is compared to that of the uncoded OFDM-MFSK presented in Section 6.2. A permutation code $\boldsymbol{P}$ consists of $|\boldsymbol{P}|$ codewords of length M [153]. All $|\boldsymbol{P}|$ codewords in $\boldsymbol{P}$ are row vectors denoted in this work by $\boldsymbol{v}_p$ and contain M different integers

$1, 2, \ldots, M$, as symbols, while $p = 1, 2, \ldots, |\boldsymbol{P}|$. Hence,

$$\mathrm{b}_1 = \lfloor \log_2 |\boldsymbol{P}| \rfloor, \tag{6.11}$$

bits are mapped per each codeword $\boldsymbol{v}_p$, where $\lfloor . \rfloor$ denotes the floor function. Each $\boldsymbol{v}_p \in \boldsymbol{P}$ can be converted to an equivalent $[0, 1]^{M \times M}$ codeword matrix $\boldsymbol{C}_p = [c_{ij}]$ such that in each column of $\boldsymbol{C}_p$, a '1' fills the position which corresponds to the codeword's integer, while other $M - 1$ values in the column are set to '0'.

6.3.1.1 System Model for the Permutation-Coded OFDM-MFSK based HPV System

In PC OFDM-MFSK, b_1 information bits are mapped to a predefined permutation codeword, $\boldsymbol{v}_p$. Note that in this work, the length of PCWs and the MFSK order are assumed equal, that is they both have the same value of M. Therefore, even in PC OFDM-MFSK, G groups of sub-carriers are formed by $\frac{N}{M}$ and each integer symbol in $\boldsymbol{v}_p$ indicates the index of the active subcarrier in each of the G groups [75]. The sequence of b_1 bits is repeated over each active sub-carrier. Therefore, in addition to information bits mapped to modulation constellation symbols, the PC OFDM-MFSK data rate is enhanced by b_1 bits mapped to each index of the activated sub-carrier. As such, the total number of transmitted bits $\mathcal{B}_4$ in a PC OFDM-MFSK, per channel use is,

$$\mathcal{B}_4 = b_1 + \mathcal{B}_3 = b_1 + G \cdot \mathcal{B}_1, \tag{6.12}$$

6.3.1.2 Soft-Decision Decoding for PC OFDM-MFSK HPV System

If the transmitted information symbols are mapped to both conventional modulation constellations and the index of the permutation codeword, then the receiver's task is to be able to estimate the digitally modulated information symbols and those mapped to permutation codewords. The digitally modulated symbols are conventionally demodulated and estimated according to the appropriate scheme matching the modulation technique that was used at the transmitter, while those mapped to permutation codewords are recovered after the detection of the corresponding codewords. An iterative SD decoder based on the Hungarian and Murty's algorithms described in [130], is employed to enhance decoding reliability as well as reduce the decoding complexity of the PC OFDM-MFSK HPV system.

The SD decoders in [79, 130] considers the signal input as an assignment problem, such that a linear programming algorithm based on the Hungarian method [86], is employed for decoding. The mathematical model of an assignment problem [86], can be expressed as:

$$K = \sum_{i=1}^{M} \sum_{j=1}^{M} c_{ij} (y_{\mathrm{v}})_{ij}, \tag{6.13}$$

subject to the constraints

$$\sum_{i=1}^{M} c_{ij} = \sum_{j=1}^{M} c_{ij} = 1, \;\; (i, j = 1, 2, \ldots, M), \tag{6.14}$$

where K in (6.13) is the cost of the assignment, $(y_{\mathrm{v}})_{ij}$ the cost of assigning a resource to an activity.

From the model in (6.13), the Hungarian algorithm of the HM decoder iteratively finds an $M \times M$ matrix $\boldsymbol{R} = [r_{ij}] \in \mathbb{R}$ that produces the maximum cost K corresponding to $\boldsymbol{v}_p$. If the produced codeword $\boldsymbol{v}_p \in \boldsymbol{P}$, then the decoder stops and the produced codeword is assumed to be the transmitted codeword. However, if the produced codeword does not belong to $\boldsymbol{P}$, then from $\boldsymbol{R}$, using the Murty's algorithm, the decoder finds the next highest $\mathcal{K}$ costs and ranks them in order of decreasing cost. The highest ranking cost corresponding to one of $\boldsymbol{v}_p \in \boldsymbol{P}$, is then selected to be the transmitted codeword. Let $\boldsymbol{y}_{\mathrm{v}} = vec(\boldsymbol{Y}_{\mathrm{v}})$ denote the HM decoder input. The HM decoding algorithm can be summarised and presented as follows:

Algorithm 4 HM decoding in PC OFDM-MFSK HPV system

Input: Channel output matrix $\boldsymbol{Y}_{\mathbf{v}} = [(y_{\mathbf{v}})_{ij}] \in \mathcal{C}^{M\times M}$ in

Output: Permutation codeword $\boldsymbol{v}_p$ out

1: By Hungarian method, find matrix $\boldsymbol{R} = [r_{ij}] \in \mathbb{R}$

2: **if** $\boldsymbol{v}_p \in \boldsymbol{P}$ **then**

3: $\boldsymbol{v}_p$ is the transmitted permutation codeword

4: Stop decoder process

{Complexity order of $O(M^3)$ [90]}

5: **else**

6: By Murty's algorithm, find the best $\mathcal{K}$ permutation codewords and rank them in order of increasing cost.

7: Select $\boldsymbol{v}_p$ corresponding to the highest ranking cost as the transmitted codeword

{Complexity order of $O(M^4)$[30]}

8: **end if**

{Overall worst case decoder complexity order is $O(M^4)$}

6.3.2 Generalisation of the PC OFDM-MFSK based HPV System

In generalising the PC OFDM-MFSK scheme, N sub-carriers are divided into $G = \frac{N}{M}$ groups of M sub-carriers each, similar to the PC OFDM-MFSK scheme. However, the G groups are further divided into $k = \frac{G}{M}$ groups. Each k group is mapped to a sequence of b_1 bits. As such a set of $k > 1$ codeword indices are transmitted at a time. Consequently, the number of bits mapped to PCWs is improved by a factor of k. Hence

$$\mathrm{b}_2 = k\lfloor \log_2 |\boldsymbol{P}| \rfloor = k \cdot \mathrm{b}_1. \tag{6.15}$$

Therefore, the total number of transmitted bits $\mathcal{B}_5$ in a GPC OFDM-MFSK, per channel use is,

$$\mathcal{B}_5 = b_2 + \mathcal{B}_3 = k \cdot \mathrm{b}_1 + G \cdot \mathcal{B}_1. \tag{6.16}$$

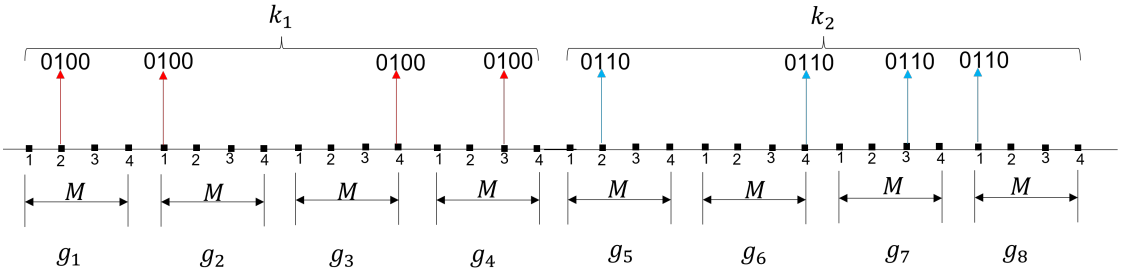

FIGURE 6.2: Representation of encoded bits mapped to PCs in a GPC OFDM-MFSK. $N = 32$, $k = 2$, $M = 4$. The encoded bits 0100 and 0110 are mapped to 2143 and 2431, respectively.

When decoding by HD, minimum distance decoding is used, where the sequence of the received vector is compared to all possible combination sequences. However, this method exponentially increases in complexity with the increase in code length M and k. In this work, because multiple codewords are transmitted for each OFDM-MFSK symbol, we elect to use the SD HM decoder applied in a multiple access system in [130]. At the receiver, elements from each k group are represented as $M \times M$ matrices, after which all the matrices are added together to form $\boldsymbol{Y}_{\mathrm{v}} = [(y_{\mathrm{v}})_{ij}]$, the decoder input. Then Algorithm 4 is applied as in the case of the PC OFDM-MFSK system. However, unlike, the decoding in Section 6.3.1.2, where the decoder can stop at the Hungarian stage, when the HM decoder is applied to the GPC-OFDM-MFSK, the Murty's algorithm is mandatory, because the decoder selects the k highest cost corresponding to the k

codewords mapped to the message symbols. Nevertheless, the decoding complexity in the GPC system is still $O(M^4)$.

6.4 Simulation and Results Analysis

A series of performance simulations for the classical OFDM, OFDM-MFSK, PC OFDM-MFSK and GPC-OFDM-MFSK systems, are carried out and their results compared. A VLC transmitter controlled and receiving information from the powerline is installed at a height of 3 m above the floor. The transmitter has a half-power angle of $(\Phi_{1/2}) = 15^\circ$. The receiver placed at 0.85m above the floor is a photo-detector with an angle of incidence $\psi = 70^\circ$ while $A_r = 1 \times 10^{-4}$ m. For all coded systems, we apply a permutation codebook defined by $\mathcal{PC}(M = 4, d_{\min} = 3)$.

6.4.1 BER Performance Comparison of OFDM HPV and OFDM-MFSK HPV Systems

In Figure 6.3, the BER performance the OFDM-MFSK HPV system is presented and compared to that of the classical OFDM HPV system. The simulation was carried out for $N = 32$ and 512, using two simple DC biasing methods referred to as DC1 and DC2. In the DC1 biasing method, the DC bias added to all the components at the output of the IFFT block is equal to the minimum absolute value of the real bipolar signal at the output of the IFFT block, DC1= $\min(|\boldsymbol{x}_{\text{v}}|)$. On the other hand, DC2 biasing refers to a bias of $10\log_{10}(\zeta^2+1)$ [8],

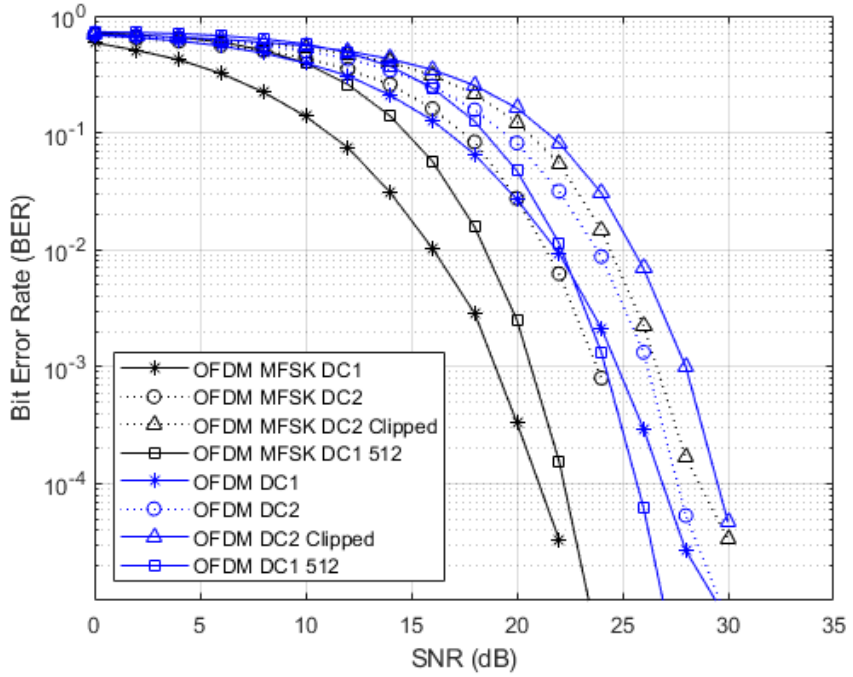

FIGURE 6.3: BER performance comparison of OFDM and OFDM-MFSK for varying sub-carrier window sizes, N

where ζ, refers to the clipping factor. The robustness against impulse noise offered by MFSK in the OFDM-MFSK based HPV system is evident as all the performance graphs show its superior performance over that of classical OFDM-based HPV system. For instance, at a BER of 10^{-3} over 5 dB and 3 dB differences are recorded for the DC1 graphs using $N = 32$ and 512, respectively. A trade-off between higher data rates and system reliability is inevitable, evidenced by the better performance obtained when smaller values of N are used, for signal-to-noise ratio (SNR) values below 20 dB. The performance difference at 10^{-3} between the OFDM-MFSK systems of $N = 32$ to that of $N = 512$ is over 1 dB. However, at higher SNR, the performance of systems with larger values of N shows a better reliability, especially for the classical system.

6.4.2 DC Biasing and Clipping Effects on BER Performance of the OFDM HPV and OFDM-MFSK HPV Systems

The impact of the two DC biasing methods mentioned in Section 6.4.1 and clipping, on the BER performance, are analysed. In Figure 6.3, the DC1 method achieves better results than the DC2 method. This could be attributed to the fact that when DC2 is used, there are some signal components with negative picks that are clipped to zero, resulting in information loss. For the OFDM-MFSK that only activates only a subset of sub-carriers, the ratio of information loss would higher. In light of the performance results of the two DC biasing methods, the subsequent simulations are based on the DC1 method since it achieves better results.

6.4.3 Coded and Uncoded OFDM-MFSK based HPV System

Figure 6.4 shows the BER performance of the permutation coded and uncoded systems, labelled OFDM-MFSK and PC OFDM-MFSK. Both systems use the HD decoder. The performance of the two systems are comparable, which can be attributted to the fact that both systems, allow the activation of only one sub-carrier in each group of M, hence the effect on the impulse noise mitigation is similar.

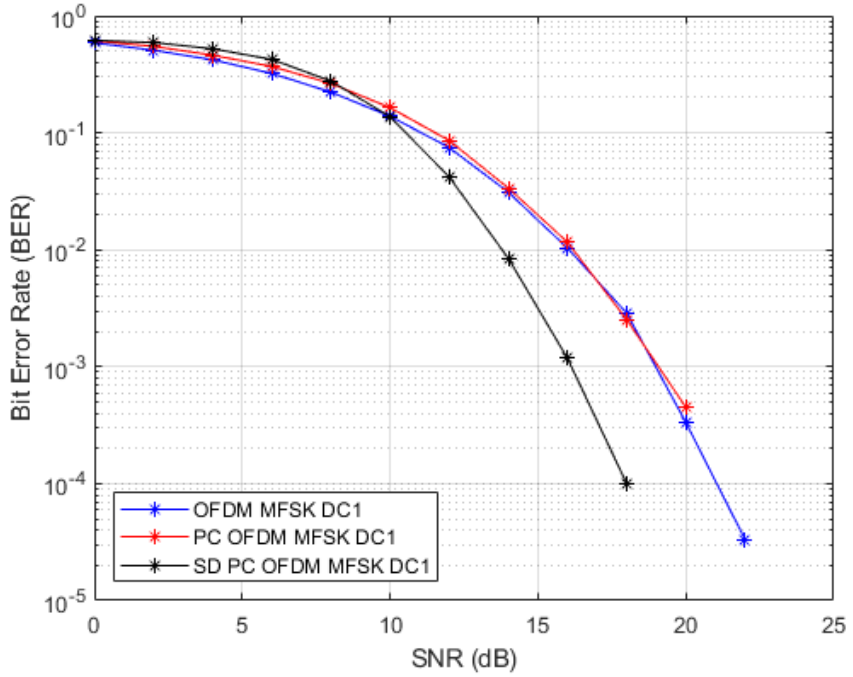

FIGURE 6.4: Hard-decision versus soft-decision decoding. $A = 0.1$

Furthermore, an SD decoder was employed and its performance compared to that of the HD based decoders. Because of the iterative feature of the Hungarian based SD decoder, its reliability is enhanced compared to that using the HD decoder. Additionally, as presented in [130], the complexity of the HD decoder is exponential with respect to the length of the permutation code, while that of the SD decoder based on the Hungarian and Murty's algorithms is polynomial. Hence the use of the SD decoder enhances the system reliability and offers a lower decoding complexity.

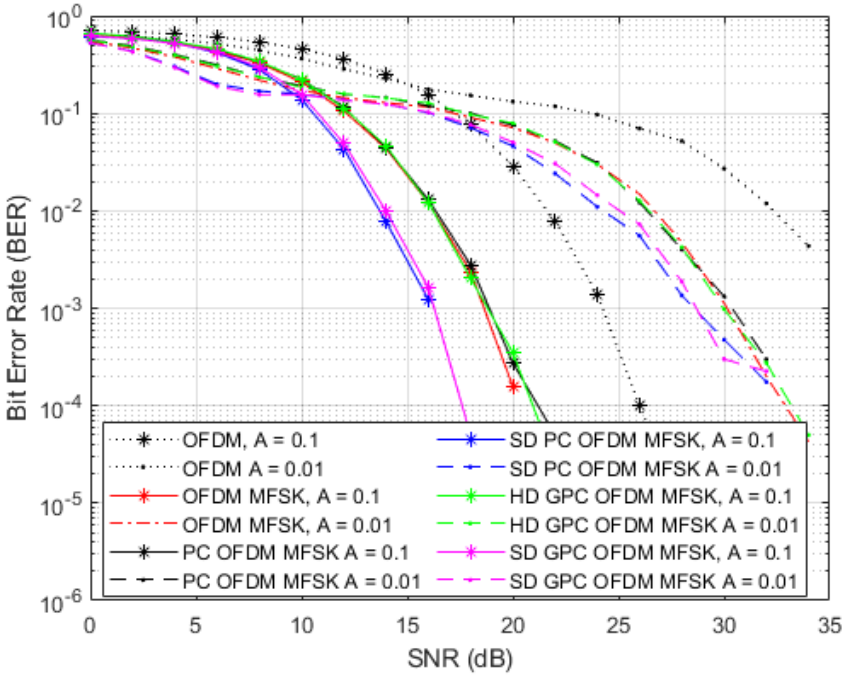

FIGURE 6.5: Effect of varying A values on BER performance for the OFDM, coded and uncoded OFDM-MFSK based HPV systems, including the GPC based system

6.4.4 Impulse Noise Effects

In Figure 6.5, the system reliability of the investigated schemes for different values of the parameter A, is presented. The results in Figure 6.5 can be seen to depict the system reliability at different times of the day for indoor environments. Values of $A = 0.01$ and 0.1 were simulated. At lower SNR values, systems simulated with $A = 0.01$ show a lower probability of error. However, as the SNR increases, the independence on A in multi-carrier modulations mentioned in [132] is evident, where the performance of the systems modelled with $A = 0.1$ show an improvement.

6.4.5 GPC OFDM-MFSK HPV System Performance

6.4.5.1 Bit Error Rate Performance

The performance of the GPC OFDM-MFSK based HPV system is included in Figure 6.5. The BER performance is simulated only for information symbols mapped to the PCWs, without including those from a modulation constellation. We notice that for both HD and SD decoders, the GPC graphs simulated with $A = 0.1$ and 0.01, almost match those of the PC OFDM-MFSK based systems. This could be attributed to the fact that there is no increase in the number of sub-carriers activated in each group of M. Hence, the impulse noise mitigation feature of MFSK is preserved, howbeit with increased system data rate.

6.4.5.2 Data Rate Comparison

A data rate comparison for OFDM-MFSK, PC OFDM-MFSK and GPC OFDM-MFSK schemes, for $\mathcal{PC}(M = 4, d_{\min} = 3)$ and varying N is shown in Figure 6.6. Due to the fact that bits mapped to PCWs are repeated for all activated sub-carriers, the data rate enhancement of the PC OFDM-MFSK scheme does not show a significant difference over the OFDM-MFSK scheme. However, it is noticed that with increasing N values for the same M, generalising the PC OFDM-MFSK scheme enhances the system data rate. For instance, for $N = 2048$, the data rate ratio increase for $\mathcal{B}_5$ to $\mathcal{B}_4$, is approximately 0.4. Thus, with the BER performance matching that

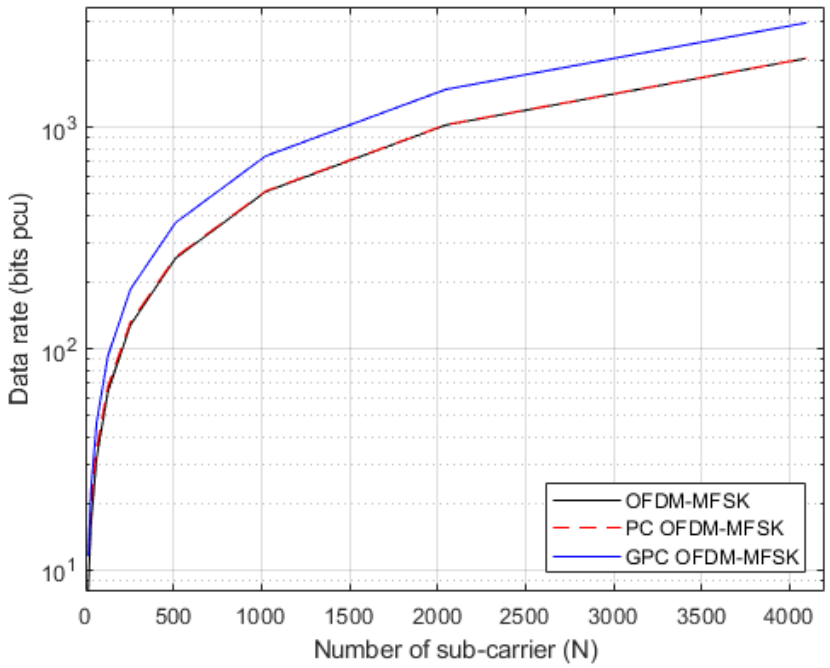

FIGURE 6.6: Data rate comparison for OFDM-MFSK, PC OFDM-MFSK and GPC OFDM-MFSK scheme for $\mathcal{PC}(M = 4, d_{\min} = 3)$ and varying N.

of the PC OFDM-MFSK as shown in Figure 6.5, using the GPC OFDM-MFSK scheme for the HPV system would enhance both the reliability and data rate.

6.5 Summary

The use of OFDM-MFSK enhances the BER performance of the HPV communication system. In the OFDM-MFSK, only a selected set of sub-carriers are activated to transmit information bits for each OFDM symbol, hence the ratio of sub-carriers that can be affected in each g group, is reduced to $\frac{1}{M}$. The robustness of the OFDM-MFSK scheme against impulse noise enhances the system reliability in comparison to that using the classical OFDM scheme. An SNR gain of 5 dB was achieved at a BER of 10^{-3}. Further, in order to

use the soft-decision low-complexity decoder based on the Hungarian and Murty's algorithms, PCs were used to determine the sub-carriers to be activated for each transmitted OFDM symbol. In addition, the issue of the reduced data rate in the HPV system employing the OFDM-MFSK scheme is addressed by the implementation of a GPC scheme. In the GPC scheme, the data rate is enhanced by a factor k which denotes the number of permutation codewords that can simultaneously be transmitted per OFDM-MFSK symbol and can uniquely be decoded. Since the GPC scheme also activates only one sub-carrier per group of M as in the PC OFDM-MFSK scheme, the OFDM-MFSK feature is maintained, hence impulse noise is still well mitigated. Moreover, the system complexity is maintained when the HM SD decoder is used.

CHAPTER 7

Impulse Noise Mitigation by Time-Diversity Hermitian Symmetry scheme in HPV Systems

---

This chapter is based on the following publication: *Mulundumina Shimaponda-Nawa, Oluwafemi Kolade, Jianhua He , Wenbo Ding and Ling Cheng*, "Impulse Noise Mitigation by Time-Diversity Hermitian Symmetry scheme in HPV Systems". *Under review with The IEEE Internet of Things Journal.*

The author of this thesis conceptualized the work, performed the simulations, analyzed the results and wrote the paper.

7.1 Introduction

smart mines, wearables and connected cars are just but a few areas where the IoT has developed and will continue to grow [77, 136, 160]. This growth demands increasingly wide coverage areas, high capacities and data rates to maintain reliable and ubiquitous connectivity of several smart devices and machines, regardless of their environment and geographical locations. Thereby presenting a challenge on the current commonly used standalone RF networks. Therefore,

hybrid networks where various communication technologies complement each other to achieve the device-to-device and device-to-infrastructure connectivity, have been proposed [18, 32, 63, 77, 112, 122]. Some of the common communication technologies studied for hybrid networks include RF, VLC and PLC. VLC is a type of optical wireless communication technology that uses the electromagnetic wavelengths within the visible spectrum. Thus, VLC is capable of providing illumination and data communication simultaneously. On the other hand, the powerline provides power to the VLC transmitters and also works as an information backbone [84, 88, 139, 162].

Figure 7.1 depicts some areas where hybrid networks consisting of either a pair of or all of the three technologies previously mentioned, have been applied with potential for optimisation. For example, hospitals have areas where an RF solution could be undesirable, thus VLC can be used as an access point solution, whose information is provided via the PLC channel. Figure 7.1 also shows a smart transport system, where the RF and VLC technologies complement each other to achieve the vehicle-to-vehicle (V2V) and vehicle-to-infrastructure (V2X) communication involving traffic lights and security/speed cameras installed on the road. Furthermore, a hybrid of RF, PLC and VLC is assumed for achieving the smart home, shown in Figure 7.1. Additionally, a hybrid configuration is shown for a smart car whose powerline network is integrated to its VLC enabled lights. All these scenarios show that hybrid networks are inevitable in achieving several simultaneous smart device connectivity.

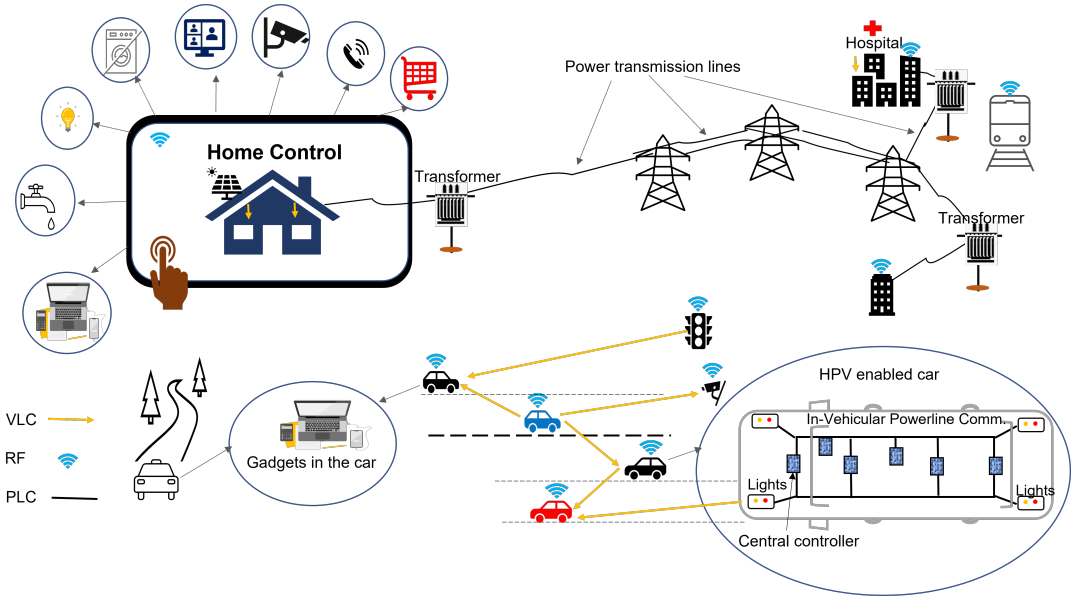

FIGURE 7.1: A depiction of hybrid networks of RF, PLC and VLC technologies for infrastructure and device interconnection.

The presence of the powerline in most locations of Figure 7.1, makes PLC a strong candidate for championing the IoT campaign, for smart cities and homes[23, 32, 63, 77]. Additionally, because high power efficient solid state lighting is being rolled out for both outdoor and indoor illumination, it is possible to have VLC wherever the installation of solid state lighting is available. Hence, VLC has also been proposed to be one of the main technologies that enable the full realisation of IoT [20, 63, 94]. Motivated by the relevance of both PLC and VLC in the IoT domain and the drive towards hybrid networks, in this work, we investigate the hybrid configuration of PLC and VLC, we refer to as the HPV system in this thesis.

Since the first demonstration of VLC [84, 139], LEDs became the highly considered VLC transmitters due to their advantages of low cost, energy efficient, durability and their ability to be modulated at high speed. Apart from the much desired wide unlicensed spectrum

in order of several hundred terahertz (THz), some notable advantages attributed to VLC technology are its non-subjection to interference by electromagnetic sources, congestion, as well as high level of security since it does not penetrate through walls. Potential application areas for VLC include, but not limited to hospitals where RF could be undesirable, smart transport systems, smart lighting of smart buildings and underwater communication.

Like VLC, PLC has an advantage of having ubiquitous presence in indoor environments which is a desirable communication network feature for coverage enhancement. Some of the applications of PLC include providing remote meter reading services, voice communication, data acquisition and intra-vehicle communication [23, 32, 88].

In light of the above, the integration of PLC and VLC is naturally achievable based on the fact that lighting devices always need power supply and that powerlines are ubiquitously available in environments such as houses, hospitals, office spaces, server rooms and high busy trading areas such as shopping malls [34, 83, 95]; resulting in a cost-effective implementation of the HPV system.

Being an emerging and developing integrated scheme, various areas of the HPV system still require optimisation. Hence, since the first demonstration of an HPV system [83], a significant number of studies with regards to integration schemes between PLC and VLC, hybrid channel models, coverage optimisation, modulation, multiplexing, MA, as well as spectrum and power efficiency schemes, have been

reported. For instance, simulated HPV channel models based on PLC and VLC practical measurements are presented in [109, 110], while authors in [38, 78] derived the HPV channel models using a semi-hidden Markov model (SHMM) with the aid of a Fritchman channel state representation model. Measurements obtained from different positions were used in an indoor VLC environment, aided by software-defined radios. Integration techniques of the two channels is also an area that has received a lot of attention, with the two main protocols identified as AF and DF [22, 78, 92, 104]. For the AF protocol, the signal received from the PLC channel is scaled and amplified, before modulating the VLC transmitters. On the other hand, in the DF protocol, the signal is decoded and subjected to the AF processes before being re-transmitted by the VLC transmitters.

In [87, 128], the BER performance of an HPV system with MIMO configurations at the VLC sections, is presented with practical indoor considerations. It was established that channel effects from both PLC and VLC have an influence on the BER performance of the HPV system. Moreover, the location and positions of the transmitters and receivers at the VLC section also have an influence on the BER performance of the system. Furthermore, single carrier M-ary modulation schemes such as phase shift-keying, multicarrier modulation such as orthogonal frequency division multiplexing (OFDM) and multiplexing schemes such as color shift-keying (CSK) and bit division multiplexing (BDM) have been investigated for HPV systems [22, 50, 82, 107]. Additionally, both orthogonal

and non-orthogonal MA techniques have also been considered for the HPV system [45, 93, 141], demonstrating the hybrid scheme's potential to be used in high speed networks and ultimately, for IoT. With such significant ongoing research work, HPV systems are not only projected to complement, but in some application areas, projected to substitute the existing RF solutions.

7.2 Problem statement and Motivation

Despite their merits, HPV systems are prone to channel noise. Precisely, in an indoor environment where electrical appliances are randomly plugged in the powerline, noise impulses are injected affecting the communication signals that are transmitted over the PLC channel. In literature, impulse noise has been shown to occur in random bursts [26, 33, 39, 48, 102, 121, 132, 147], affecting either a group of frequencies over a period of time or data symbols in a sequence of time-slots.

Several methods to combat the effects of the impulse noise and narrow-band interference in the fast time-varying PLC channel have been proposed. For instance, the simple method of suppressing the impulse noise effects by preceding the OFDM receiver with clipping or blanking [161] has been successfully applied in PLC systems to enhance the performance of the OFDM receiver [100, 119]. The work in [161] demonstrated that simultaneously exploiting the advantages of the clipping and blanking schemes by combining them yields better

results, compared to using the two schemes independently. While, in [119], pre-processing the signal at the transmitter was proposed and shown to enhance the performance of the blanking/clipping-based techniques for impulse noise mitigation in powerline channels. In [55], simple iterative impulsive noise suppression algorithms that exploit the noise structure in the time and frequency domain, were shown to improve the performance of the OFDM receiver. Further, in [100], the performance of the PLC system was enhanced by preceding the iterative algorithms discussed in [55] with a clipping and nulling technique. In addition to clipping, blanking, nulling and iterative algorithm techniques mentioned above, coding techniques have been exploited for impulse noise mitigation [151]. For instance, PCs combined with a non-coherent detection scheme such as MFSK, makes the communication system robust against permanent frequency disturbances and impulse noise [151]. Whereas in [152], the use of MFSK was shown to mitigate the narrow-band interference and impulse noise in fast time-varying channels. In addition, a combination of PCs and MFSK was proposed and shown to also mitigate the effects of the burst noise in PLC channels [74, 75, 129].

Time-diversity (TD) schemes have also been applied in different communication technologies for performance reliability enhancement [26, 128]. In TD schemes, information bits or symbols are repeatedly transmitted such that the receiver has multiple copies of the transmitted signal, from which different decoding schemes such as

maximum ratio combining (MRC), majority rule scheme or any comparison based technique, can be applied. In [26], a TD permutation coding scheme for narrow-band interference powerline channels was proposed. In the proposed TD scheme of [26], the same information symbol is repeatedly sent over the channel at different times to mitigate the effects of impulse noise. Because the time between repeated information symbols is adjusted to be longer than the length of a typical error burst, then the probability of the repeated information symbol to be affected by the same burst error is reduced. Hence, the unaffected information symbol can be used to recover the transmitted signal.

In this work, a novel TD scheme based on the HS structure is proposed and implemented at the PLC section of the HPV system. The TD scheme aims at improving the overall BER performance of an HPV system by mitigating the effects of impulse noise in the PLC channel. Unlike the schemes discussed above that exploit the noise structure in the channel or the effects of the employed modulation techniques to mitigate the impulse noise, in this work, we exploit the HS, a fundamental signal property, that has commonly been used to generate real OFDM signals in optical systems. In a cascaded system like HPV, the achieved data rate is proportional to the data rate of the constituent technology with the lower data rate capability. Thus, the use of the HS window at the PLC section, which is twice that of the conventional system does not in any way affect the system data-rate. Moreover, in this work where optical OFDM is applied

at the VLC section, the HS structure is required to ensure that the signals to modulate the VLC transmitters are intensity-modulation direct-detection (IM/DD) compatible. Therefore, the TDHS scheme with an enhanced reliability, offers the same data rate capability as the conventional system because of the HS constraint at the integration unit. By conventional HPV system, we refer to the system where the information symbols are transmitted without being subjected to the HS structure, at the PLC section. Furthermore, the proposed TDHS scheme uses the AF relaying protocol. Therefore, the implementation is simplified and less complex in comparison to an integration unit using the DF relaying protocol.

Since impulse noise occurs in short bursts and can affect data symbols in sequence of time-slots, then a scheme that only activates a selected and spaced number of time-slots to carry information would further enhance the system's BER performance. As such, PCs are used to attain a systematic pattern of time-slot activation. We note from literature that PCs can be used in an MA system to identify different users [130, 151], hence the TDHS scheme with PCs is extended to an MA HPV system. We also note that the MA schemes in literature are mostly applied to the VLC section of the HPV system only. However, in this work, by using PCs, we apply the MA scheme at the PLC section and show that the message can be correctly decoded at the VLC receiver, while the need for decoding at the PLC/VLC unit is eliminated. While most of the impulse noise

mitigation schemes mentioned above focus on application of the impulse noise mitigation schemes to multi-carrier modulated signal in the PLC channel, the TDHS scheme can be applied to both single and multi-carrier modulated signals.

Precisely, the contributions in this chapter can be summarised as follows:

- Design and investigation of a novel time diversity scheme based on the Hermitian symmetry to effectively mitigate the inherent impulse noise in PLC channels.
- We then propose a permutation coded TDHS system and use a soft-decision decoder based on the Hungarian and Murty's optimisation algorithms, for further performance enhancement.
- Unlike most literature on HPV systems where the MA scheme is implemented at the VLC transmitter section, we extend the permutation coded TDHS scheme to an MA system implemented from the PLC transmitter section.
- We provide an analysis of the performance of the proposed TDHS scheme, in terms of BER and goodput, and further compare the results of the HPV system using the TDHS scheme to the results of the conventional HPV systems using both AF and DF protocols.

The rest of the chapter is organised as follows: Section 7.3 gives the details of the TDHS-based HPV system model as well as the permutation coded TDHS (PC TDHS) system. Under the PC TDHS subsection, the decoding process of the applied SD HM decoder is also presented. Additionally, the principle of the impulse noise detector used at the PLC/VLC integration unit is described. The final part of Section 7.3 introduces an MA scheme implemented as an extension of the permutation coded TDHS system. In Section 7.4, the details of the conducted simulations and results analysis of the considered systems are presented, after which the chapter summary is provided in Section 7.5.

7.3 Time Diversity Hermitian Symmetry based HPV System Models

An HPV system where a single carrier modulation (SCM) scheme is implemented in the PLC section while a multi-carrier modulation scheme, precisely OFDM, is implemented at the VLC section, is considered. The use of an SCM in the PLC section avoids the complexity of the use of the fast Fourier transform (FFT) and its inverse at the PLC/VLC integration unit and PLC input, respectively. To reduce the system complexity due to the decoding process at the integration unit, the AF relaying protocol, is employed.

7.3.1 TDHS based HPV System

7.3.1.1 System Model Overview

In the investigated TDHS based HPV system, the structure of the HS is exploited as a TD mitigation method against impulse noise in the PLC channel. $\frac{N}{2}-1$ information symbols are transmitted from the PLC side in each transmit period; N is the length of the HS window. The $\frac{N}{2}-1$ symbols are arranged in an HS structure before they are transmitted over the PLC channel, such that, a message symbol x_n is duplicated in the form of its complex conjugate x_n^*, for $n = 2, 3, \ldots, \frac{N}{2}$, where the superscript $*$ denotes the complex conjugate. For N time-slots, the general expression relating the message symbols, their complex conjugate and their positions due to the HS constraint is given as:

$$x_{(\xi+2)} = x^*_{(N-\xi)}, \;\; \xi = 0, 1, 2, \ldots, \frac{N}{2} - 2. \tag{7.1}$$

Thus, the HS structure is formed by concatenating the original vector of message symbols with the vector of their complex conjugate symbols as, $[0, x_2, x_3, \ldots, x_{(N/2)}, 0, x^*_{(N/2)}, \ldots, x^*_3, x^*_2]$. Equivalent symbols, x_n and x_n^*, are therefore separated enough to avoid the effect of impulse noise which occurs in short bursts. The first and $(\frac{N}{2}+1)^{\text{th}}$ components in the HS structure are set to zero, to avoid any DC shift or any residual complex component in the time domain signal.

As shown in Figure 7.2, the transmitted signal is affected by PLC

noise. Hence, the output signal vector, $\boldsymbol{y}_{\mathrm{p}}$, from the PLC channel is

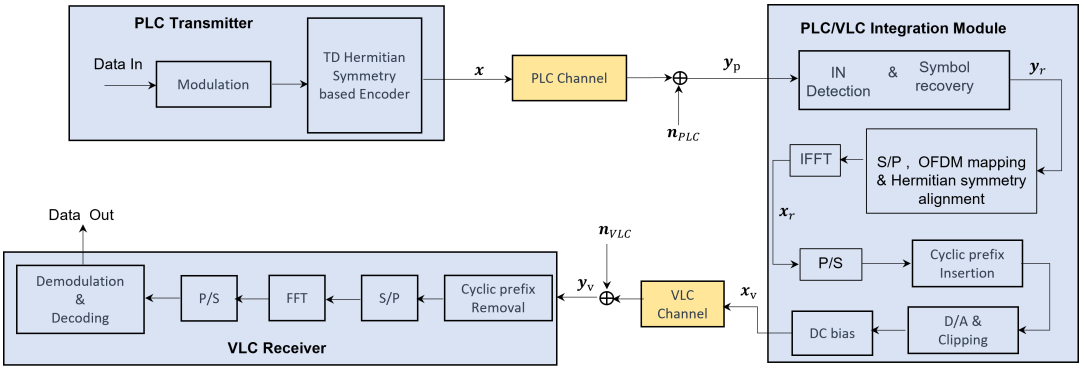

FIGURE 7.2: Block diagram for TDHS based HPV system

given as

$$\boldsymbol{y}_{\mathrm{p}} = \boldsymbol{x}e^{j\phi} + \boldsymbol{n}_{\mathrm{p}}, \tag{7.2}$$

where p is used to denote the signals in the PLC section. In (7.2), $\boldsymbol{x} = [0, x_2, x_3, \ldots, x_{(N/2)}, 0, x^*_{(N/2)}, \ldots, x^*_3, x^*_2]$ denotes the complex input message symbols in the HS window, transmitted via the PLC channel. The output signal vector, $\boldsymbol{y}_{\mathrm{p}} = [y_{\mathrm{p}1}, y_{\mathrm{p}2}, y_{\mathrm{p}3}, \vdots, y_{\mathrm{p}(\frac{N}{2})}, y_{\mathrm{p}(\frac{N}{2}+1)}, y^{\dagger}_{\mathrm{p}(\frac{N}{2})}, \ldots, y^{\dagger}_{\mathrm{p}3}, y^{\dagger}_{\mathrm{p}2}]$. Due to the effect of the PLC noise, the complex conjugate feature does not hold. However, the position of the elements in the received vector are still assumed. Thus, to differentiate the elements from the complex conjugate notation, the superscript, † is used. In addition, $\boldsymbol{n}_{\mathrm{p}} = \boldsymbol{n}_{\mathrm{G}} + \boldsymbol{n}_{\mathrm{I}}\sqrt{D}$ denotes the noise component in the PLC channel comprising the background noise $\boldsymbol{n}_{\mathrm{G}}$ and the impulse noise, $\boldsymbol{n}_{\mathrm{I}}$. The background noise is modelled as additive white Gaussian noise (AWGN) (a complex component with zero-mean and variance of $\sigma^2_{\mathrm{G}} = 2N_0$, where N_0 is the noise power spectral density) and impulse noise is assumed to have a Poisson distribution with a variance

σ_{G}^2/A. A is the impulsive index determining the frequency of occurrence of $\boldsymbol{n}_{\mathrm{I}}$ and D is a variable imposing the Poisson distribution on $\boldsymbol{n}_{\mathrm{I}}$.

The signal received from the PLC channel is passed to the impulse noise threshold detector (see Section 7.3.1.2) where, if a transmitted symbol, $y_{\mathrm{p}(n)}$, was affected by impulse noise, then the appropriate symbol amplitude is recovered from the element, $y^{\dagger}_{\mathrm{p}(n)}$. It should be noted that elements in the first and $(\frac{N}{2}+1)^{\mathrm{th}}$ positions of $\boldsymbol{y}_{\mathrm{p}}$ are basically noise components since zeros were transmitted in these positions. Thus, there are $\frac{N}{2}-1$ recovered complex symbols on which OFDM will be applied. We denote the vector of these recovered symbols as $\boldsymbol{y}_{\mathrm{r}}$. Precisely, if the zero that was transmitted in the first position is included and occupies the first position again, then $\boldsymbol{y}_{\mathrm{r}} = [0, y_{\mathrm{r}2}, y_{\mathrm{r}3}, \ldots, y_{\mathrm{r}(\frac{N}{2})}]$.

In this work, IM/DD is employed, as such, the OFDM signal modulates the current of the VLC transmitter and a photo-detector is used for detection, at the receiver. To ensure IM/DD compatibility and obtain real OFDM signals, frequency symbols to which $\boldsymbol{y}_{\mathrm{r}}$ is mapped, are forced to satisfy the Hermitian symmetry constraint (7.1), before the inverse fast Fourier transform (IFFT) is performed, as depicted in Figure 7.2. An expansion of the S/P, OFDM mapping & Hermitian symmetry alignment block of Figure 7.2, is shown in Figure 7.3, with details of the processed signal from each stage. The frequency domain signal $\boldsymbol{Y}_{\mathrm{r}}$, at the input of the IFFT block

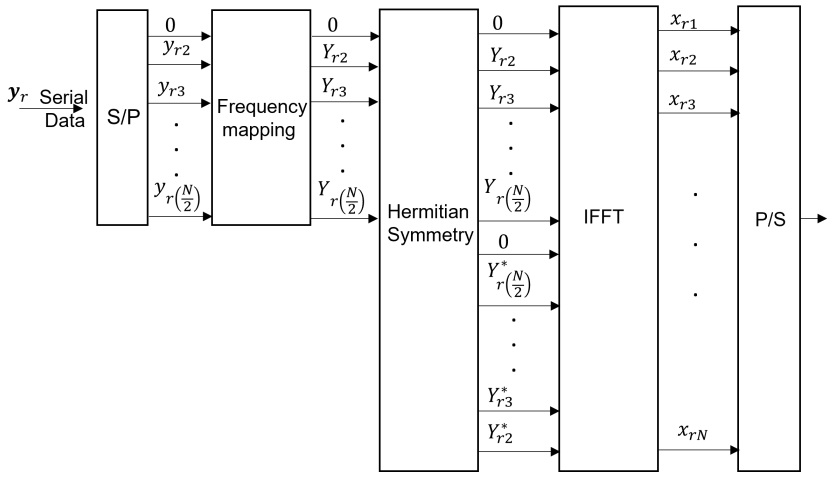

FIGURE 7.3: Block diagram showing the signal output from the S/P, OFDM mapping & Hermitian symmetry alignment and the IFFT blocks of Figure 7.2.

is expressed as $[0, Y_{\mathrm{r}2}, Y_{\mathrm{r}3}, \ldots, Y_{\mathrm{r}(\frac{N}{2})}, 0, Y^*_{\mathrm{p}(\frac{N}{2})}, \ldots, Y^*_{\mathrm{r}3}, Y^*_{\mathrm{r}2}]^{\mathrm{T}}$; where the function $[.]^T$ denotes vector transposition.

The bipolar real-valued, time domain symbols obtained after the IFFT block are serially aligned and can be expressed as $\boldsymbol{x}_{\mathrm{r}} = [x_{\mathrm{r}1}, x_{\mathrm{r}2}, x_{\mathrm{r}3}, \ldots, x_{\mathrm{r}N}]$. The cyclic prefix (CP) is then added to $\boldsymbol{x}_{\mathrm{r}}$ for inter-carrier and inter-symbol interference mitigation, after which, DC biasing is applied to achieve the uni-polar signals required to modulate the current of the VLC transmitters. We denote the signal from the VLC transmitters as $\boldsymbol{x}_{\mathrm{v}}$, where v is specifically used to denote the signals in the VLC section. Thus, $\boldsymbol{x}_{\mathrm{v}}$ is transmitted by the VLC transmitters having a Lambertian radiation pattern influenced by the channel gain element h between the transmitting LED and the corresponding receiving photo-diode. Consequently, the received signal at the VLC receiver can be expressed as:

$$\boldsymbol{y}_{\mathrm{v}} = h\boldsymbol{x}_{\mathrm{v}} + \boldsymbol{n}_{\mathrm{v}}, \tag{7.3}$$

where the AWGN affecting the received optical signal is denoted by $\boldsymbol{n}_{\mathrm{v}}$ and h expressed as (2.7) denotes the channel gain.

At the VLC receiver, the analogue signal is converted to digital signal, the CP is removed and the serial sequence is converted to parallel sub-carriers, after which the fast Fourier transform (FFT) is performed on the received signal. Demodulation and decoding then follow, to recover the transmitted signal. We assume that the receiver has perfect knowledge of the channel and maximum likelihood detection is used to estimate the likely transmitted message symbols. Therefore, the $\hat{\boldsymbol{x}}_{\mathrm{v}}$ which minimises the Euclidean distance between the actual received signal vector $\boldsymbol{y}_{\mathrm{v}}$ and all potential received signals is accepted as the transmitted vector and is expressed as,

$$\hat{\boldsymbol{x}}_{\mathrm{v}} = \arg\min_{\boldsymbol{x}_{\mathrm{v}}} ||\boldsymbol{y}_{\mathrm{v}} - h\boldsymbol{x}_{\mathrm{v}}||_{\mathrm{F}}^{2}, \tag{7.4}$$

where ||.||F denotes the Frobenius norm.

7.3.1.2 Impulse Noise Detection

At the PLC channel output, a simple impulse noise threshold detector which compares the magnitudes of $y_{\mathrm{p}(n)}$ and $y_{\mathrm{p}(n)}^{\dagger}$, is used to determine whether an information symbol was affected by impulse noise. In this work the threshold, θ, is assumed to be five times the average transmitted power. The component between $y_{\mathrm{p}(n)}$ and $y_{\mathrm{p}(n)}^{\dagger}$, with a lower magnitude with respect to (wrt) θ, is assumed to be the symbol that was not affected by impulse noise and is selected for

re-transmission by the VLC transmitter. Thus, for $n = 2, 3, \ldots \frac{N}{2}$, the symbol to be transmitted must satisfy

$$y_{\mathrm{r}(n)} = \min(y_{\mathrm{p}(n)}, y^{\dagger}_{\mathrm{p}(n)}) < \theta. \tag{7.5}$$

At any transmit interval, the following are probable:

1. None of $y_{\mathrm{p}(n)}$ and $y^{\dagger}_{\mathrm{p}(n)}$ are affected by impulse noise,
2. Both $y_{\mathrm{p}(n)}$ and $y^{\dagger}_{\mathrm{p}(n)}$ are affected by impulse noise,
3. Either $y_{\mathrm{p}(n)}$ or $y^{\dagger}_{\mathrm{p}(n)}$ is affected by impulse noise.

If '1' is used to indicate that a symbol was affected by impulse noise, while '0' indicates otherwise, then an impulse noise error table can be represented as a logic AND truth table shown in Table 7.1. From

TABLE 7.1: Impulse Noise Error Probabilities on the received signal components from PLC

$y_{\mathrm{p}n}$	$y^{\dagger}_{\mathrm{p}(n)}$	Output	Symbol recovery (Yes/No)
0	0	0	Yes
0	1	0	Yes
1	0	0	Yes
1	1	1	No

Table 7.1, we observe that transmitting a copy of the information symbol in the form of its complex conjugate contributes to the $\frac{3}{4}$ outcomes when the output is '0'. Since, either $y_{\mathrm{p}(n)}$ or $y^{\dagger}_{\mathrm{p}(n)}$ can be selected for re-transmission at the VLC section, the probability of transmitting impulse noise affected data symbols, is drastically reduced by 75%. In instances when both $y_{\mathrm{p}(n)}$ and $y^{\dagger}_{\mathrm{p}(n)}$ are affected by impulse noise, then $y_{\mathrm{p}(n)}$ is clipped to zero, to avoid transmitting

signals with higher peaks which could increase the peak-to-average power ratio (PAPR).

7.3.2 Permutation Coded Time-Diversity Hermitian Symmetry (PC-TDHS) based HPV System

Since impulse noise occurs in short random bursts, then spacing the information carrying time-slots can be another method to enhance the robustness of the system against impulse noise. In light of this, a PC-TDHS scheme is introduced to enhance the reliability of the HPV system. A further reduction in the complexity of the system is implemented by the use of SD decoder instead of using HD decoders whose computational complexity increases exponentially with an increase in code-length and cardinality, as shown in [130]. It is noted that the implementation of the PC-TDHS scheme reduces the spectral efficiency of the system. However, for applications where a trade-off between reliability and data-rate is tolerated, the PC-TDHS based system is a potential candidate.

As presented in previous chapters, a permutation code $\boldsymbol{P}$ consists of $|\boldsymbol{P}|$ codewords of length M. All $|\boldsymbol{P}|$ codewords in $\boldsymbol{P}$ are row vectors consisting M different integers $1, 2, \ldots, M$, as symbols and denoted in this work by $\boldsymbol{v}_p$, where $p = 1, 2, \ldots, |\boldsymbol{P}|$. We use the notation $\mathcal{PC}(M, d_{\min})$ to describe $\boldsymbol{P}$ with minimum Hamming distance $d_{\min}$, with each codeword having a length of M. Hence, $b = \lfloor \log_2 |\boldsymbol{P}| \rfloor$ bits are mapped per $\boldsymbol{v}_p$, where $\lfloor . \rfloor$ denotes the floor function. In the PC-TDHS scheme, a sequence of N time-slots are divided into G groups

of M time-slots and only one of the M time-slots in each group, is selected to carry information symbols. This has the potential to mitigate impulse noise which occurs in short bursts, in that the probability of impulse noise affecting an information symbol in a group of M time-slots, is $\frac{1}{M}$.

Information symbols consisting of b message bits have a one-to-one mapping with one of $|\boldsymbol{P}|$ codewords. Each information symbol with b bits is repeated over all the selected time-slots in the $\frac{G}{2}$ groups. Further, $\frac{G}{2} \cdot \mathcal{Q}$ bits can be modulated and $\mathcal{Q}$ bits assigned to each selected time-slot in each of the $\frac{N}{2}$ groups. Therefore, the total number of bits $\mathcal{B}_{\mathrm{t}}$ per transmission period is

$$\mathcal{B}_t = \log_2 |\boldsymbol{P}| + \frac{G}{2} \cdot \mathcal{Q}, \tag{7.6}$$

Let $g = 1, 2, \ldots, \frac{G}{2}$ denote the different groups consisting of M time-slots, and let $l = 1, 2, \ldots, M$ denote the different time-slots in group g. It is worth noting that $M = \frac{G}{2}$, therefore, $g = 1, 2, \ldots, M$. Thus, the vector $\boldsymbol{x}_{\mathrm{p}}$ denoting the symbols to be transmitted via the PLC channel in the PC-TDHS scheme is

$$\boldsymbol{x}_{\mathrm{p}} = \underbrace{0 \ldots x_{\mathrm{p}_{1l}} \ldots 0}_{\text{Group 1}}, \underbrace{0 \ldots x_{\mathrm{p}_{2l}} \ldots 0}_{\text{Group 2}}, \ldots, \underbrace{0 \ldots x_{\mathrm{p}_{(G/2)l}} \ldots 0}_{\text{Group G/2}} \tag{7.7}$$

In the TDHS scheme, the complex conjugate elements, ${x^*}_{\mathrm{p}_{gl}}$, of vector in (7.7) are generated to occupy the other $\frac{N}{2}$ time-slots, forming a HS structure. The transmission process till the VLC receiver is similar to that described in Section 7.3.1.

Considering (7.3)and the structure of (7.7), we can express the received signal at the VLC receiver of the PC-TDHS HPV system after the FFT operation, as a matrix $\boldsymbol{Y}_{\mathrm{v}} = [(y_{\mathrm{v}})_{gl}] \in \mathcal{C}^{M\times M}$, where g and l will denote the rows and columns in the matrix. As in the uncoded TDHS system, maximum likelihood detection is used to estimate the constellation vector $\hat{\boldsymbol{x}}_{\mathrm{v}}$. If hard-decision (HD) by a threshold detector is used, then a threshold value τ to which the received signal is subjected to, is set. Consequently,

$$(\hat{y}_{\mathrm{v}})_{gl} = \begin{cases} 1, & \text{if } |(y_{\mathrm{v}})_{gl}| \geq \tau, \\ 0, & \text{otherwise.} \end{cases} \tag{7.8}$$

where $(\hat{y}_{\mathrm{v}})_{gl} = 0$ and $(\hat{y}_{\mathrm{v}})_{gl} = 1$ is an indication of inactive and active time-slots in each group. Each $\boldsymbol{v}_p \in \boldsymbol{P}$ can be converted to an equivalent $[0,1]^{M\times M}$ codeword matrix $\boldsymbol{C}_p = [c_{gl}]$ such that in each column of $\boldsymbol{C}_p$, a '1' fills the position which corresponds to the codeword's integer, while other $M-1$ values in the column are set to '0'. Therefore, the estimated matrix, $\hat{\boldsymbol{Y}}_{\mathrm{v}} = [(\hat{y}_{\mathrm{v}})_{gl}]^{M\times M} \in \{0,1\}$, is compared with all likely $\boldsymbol{C}_p$ matrices at the receiver and then a decision is made based on the minimum distance.

7.3.2.1 Permutation Codes and Soft-Decision Decoding

When PCs are used, the low-complexity SD HM decoder [76, 80, 130], can be used. In this type of decoder, the Hungarian algorithm solves an assignment problem, where the objective is to assign a number of resources to an equal number of activities [86]. Thus, minimising the

total cost or maximising the total profit by such an allocation. The Hungarian algorithm assigns a job to each worker such that a worker can only be assigned one task. Thus, when the Hungarian algorithm is applied to a permutation coded communication system, the aim will be to find the optimal solution of the cost of the likely transmitted PCW. The mathematical model of an assignment problem [80, 86, 130], can be expressed as:

$$K = \sum_{g=1}^{M} \sum_{l=1}^{M} c_{gl} |(y_{\mathrm{v}})_{gl}|, \tag{7.9}$$

subject to the constraints $\sum_{g=1}^{M} c_{gl} = \sum_{l=1}^{M} c_{gl} = 1, (g, l = 1, 2, \ldots, L)$, where K in (7.9) is the cost of the assignment and $(y_{\mathrm{v}})_{gl}|$ denotes the cost of assigning a resource to an activity.

From the model in (7.9), the Hungarian algorithm of the HM decoder iteratively finds an $M \times M$ matrix $\boldsymbol{R} = [r_{gl}] \in \mathbb{R}$ that produces the maximum cost K corresponding to $\boldsymbol{v}_p$. If the produced codeword is $\boldsymbol{v}_p \in \boldsymbol{P}$, then the decoder stops and the produced codeword is assumed to be the transmitted codeword. However, if the produced codeword does not belong to $\boldsymbol{P}$, then from $\boldsymbol{R}$, using the Murty's algorithm, the decoder finds the next highest $\mathcal{K}$ costs and ranks them in order of decreasing cost. The highest ranking cost corresponding to one of $\boldsymbol{v}_p \in \boldsymbol{P}$, is then selected to be the transmitted codeword. The HM decoding algorithm can be summarised and presented as follows:

Algorithm 5 HM decoding in PC-TDHS based HPV system

Input: Channel output matrix $\boldsymbol{Y}_{\mathbf{v}}$ in

Output: PCW $\boldsymbol{v}_p$ out

1: By Hungarian method, find matrix $\boldsymbol{R} = [r_{gl}] \in \mathbb{R}$

2: **if $\boldsymbol{v}_p \in \boldsymbol{P}$ then**

3: $\boldsymbol{v}_p$ is the transmitted PCW

4: Stop decoder process

{Complexity order of $O(M^3)$ [90]}

5: **else**

6: By Murty's algorithm, find the best $\mathcal{K}$ PCWs and rank them in order of increasing cost.

7: Select $\boldsymbol{v}_p$ corresponding to the highest ranking cost as the transmitted codeword

{Complexity order of $O(M^4)$[30]}

8: **end if**

{Overall worst case decoder complexity order is $O(M^4)$}

7.3.3 Multiple Access for PC-TDHS based HPV System

The PC-TDHS based HPV is a basis for the consideration of a MA scheme for TDHS HPV system shown in Figure 7.4. Simultaneous transmission from multiple users may compromise the gains of the single user PC-TDHS based system, however the spectral efficiency of the MA is enhanced as multiple users are able to access the channel. In the MA scheme, disjoint codebooks are assigned to multiple users, whereby information bits from users are mapped to specific codewords of their respective codebooks. The codewords in-turn determine the specific time-slot to carry the modulated symbols, similar to the PC-TDHS scheme.

In an MA scheme, the computational complexity at the receiver increases exponentially, when HD decoders are used. Hence, for reduced decoding complexity at the VLC receiver, we employ the SD decoder based on the Hungarian and Murty's algorithms as presented in [130], whose decoding process differs only slightly compared to the description in Section 7.3.2.1. The difference is that when applied to an MA system, the decoder not only selects one best optimal solution from Murty's ranking, but the highest ranked m solutions, where m denotes the number of allowed active users.

The system block diagram of the PC-TDHS based MA HPV system is shown in Figure 7.4. Each user is assigned a set of codewords forming the user codebook, $\boldsymbol{P}_u$, where $u = 1, 2, \ldots, T$ and T is the number of users in the network. The $b_u = \log_2(|\boldsymbol{P}_u|)$ bits from a user's sequence of message bits, are mapped to each codeword $\boldsymbol{v}_p(u) \in \boldsymbol{P}_u$, where $p = 1, 2, \ldots, (|\boldsymbol{P}_u|)$. Each integer symbol of the user's codeword indicates which time-slot is activated for data transmission.

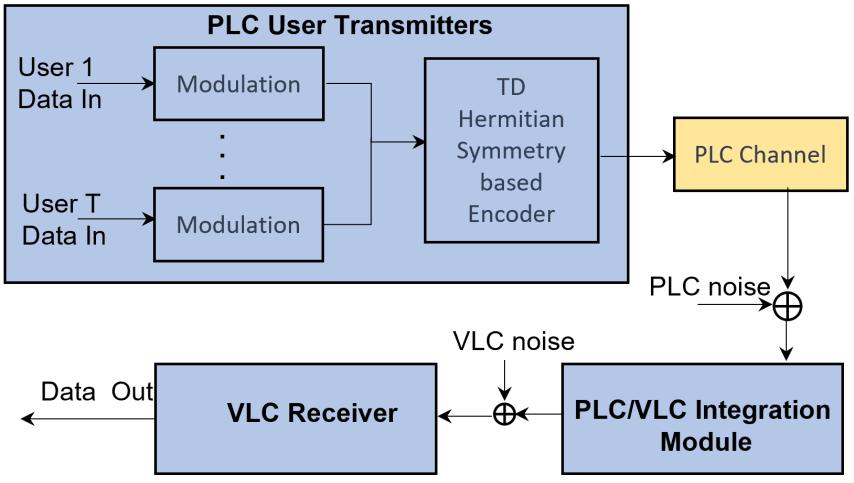

FIGURE 7.4: Block diagram for TDHS MA HPV Communication System

Assuming block synchronisation of the participating users, the users' input signals are added together forming what is referred to as a composite signal, which is then passed to the TDHS encoder. An example of the time-slot activation pattern due to $m = 2$ is demonstrated in Figure 7.5. For simplicity, in Figure 7.5, the subscripts denote the user number and integer positions of the respective user codewords. For instance, in v_{ul}, u is the user number while l the integer position. Additionally, v_{ul}, v_{ul} indicates that both users used the same time-slot number for transmission. The TDHS encoder arranges the composite signal in an HS structure before transmission to the PLC/VLC integrator module, via the PLC channel. For unique decodability by the HM SD decoder at the receiver, the minimum Hamming distance between codeword of different users and the cyclic properties of the combined PCWs, are cardinal as demonstrated in [131] and Chapter 5.

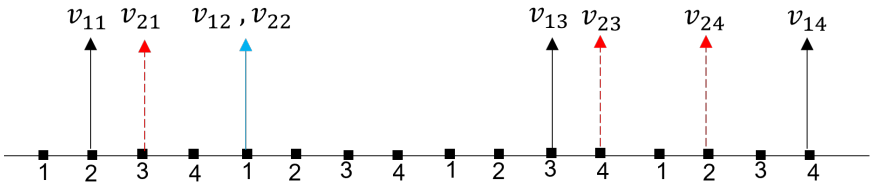

FIGURE 7.5: Time-slot activation representation in a multiple access PC-TDHS HPV system. User information symbols for two users mapped to user PCWs 2134 and 3142 for the two users.

The output signal vector, $\boldsymbol{y}_{\mathrm{p}}$, from the PLC channel affected by the channel noise is given as:

$$\boldsymbol{y}_{\mathrm{p}} = \sum_{u=1}^{m} \boldsymbol{x}_{\mathrm{p}}^{u} e^{j\phi} + \boldsymbol{n}_{\mathrm{p}}, \quad u = 1, 2, \ldots, m, \tag{7.10}$$

where $\boldsymbol{x}_{\mathrm{p}}^{u}$ is a vector consisting of the complex input information symbols from user u in the composite transmitted signal. As in (7.2), $\boldsymbol{n}_{\mathrm{p}} = \boldsymbol{n}_{\mathrm{G}} + \boldsymbol{n}_{\mathrm{I}}\sqrt{D}$ is the noise component in the PLC channel comprising the background noise $\boldsymbol{n}_{\mathrm{G}}$ modelled as AWGN with zero-mean and variance of $\sigma_{\mathrm{G}}^2 = 2N_0$ and the impulse noise $\boldsymbol{n}_{\mathrm{I}}$ which follows a Poisson distribution and has a variance σ_{G}^2/A. At the PLC/VLC integration module, the process described in Section 7.3.1, regarding impulse noise detection and making the signal IM/DD compatible, is applied.

7.4 Simulation Results and Analysis

On the VLC section, an indoor environment is considered. The transmitter is placed in a downward orientation at 3.0 m above the floor, and the receiver is at 0.85 m above the floor, directly under the transmitter, in an upward orientation. In all the simulations, OFDM modulation is used at the VLC section and an array of $N = 32$ time-slots and sub-carriers are assumed for the PLC and VLC sections respectively. In addition, quadrature amplitude modulation (QAM), precisely 4-QAM, is used. For all coded systems, we apply a permutation codebook defined by $\mathcal{PC}(M = 4, d_{\min} = 3)$. Simulations for various system scenarios are conducted to obtain the BER and goodput performances. Precisely, the following are simulated:

1. The HPV system where the TDHS scheme is not applied; this is referred to as the non-TDHS HPV system.

2. The TDHS-based HPV system.

3. The permutation coded non-TDHS and TDHS HPV systems denoted as PC non-TDHS and PC TDHS, respectively; employing HD and SD decoding techniques. While the AF protocol is applied in all the above mentioned systems, we additionally simulate a PC non-TDHS system employing the DF protocol.

4. A multiple-access PC-TDHS HPV system.

7.4.1 Impact of the A-Value on System Performance

The system performance in terms of BER as a function of the SNR, is simulated for varying A-values. The simulated A-values of 0.1, 0.05 and 0.01 could depict different times of the day or different events in a day inducing varying levels of impulse noise in terms of the frequency of occurrence. An observation of superior performance for low A-values at lower SNR values is noticed. This, as was pointed out in [132], could be attributed to the use of SCM in the PLC channel, where very few symbols are affected, hence the low probability of error no matter the strength (or average variance) of the impulse noise. For all the A-values, the performance of the TDHS scheme is compared with the non-TDHS system.

From Figure 7.6, it is observed that the TDHS based systems, perform better than the conventional system at lower SNR values, which is a desirable feature for a communication system. The robustness of the TDHS based system at low SNR values can be attributed to

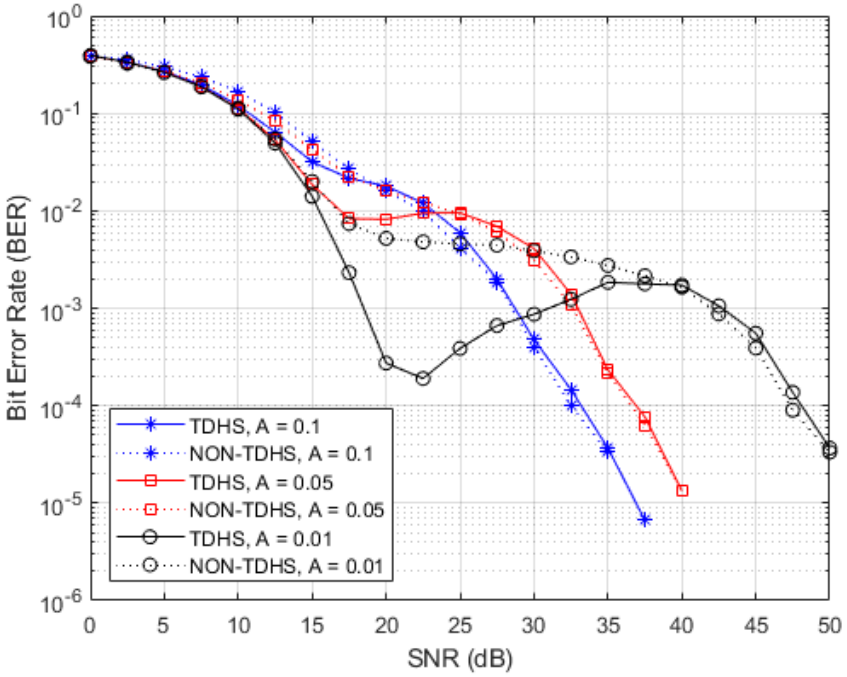

FIGURE 7.6: BER performance for TDHS and non-TDHS system for varying A-values.

the transmission time difference between the original data symbol and its complex conjugate component, as well as the fact that each copy of the information symbol has an independent probability of being affected by a different impulse noise event. As demonstrated in Section 7.3.1, the implementation of TDHS scheme offers a 75% reduction in the probability of of data symbol being affected by impulse noise. This performance shown in Figure 7.6 demonstrates the effectiveness of the proposed TDHS scheme for impulse noise mitigation in HPV systems. Only at high SNR values does the conventional system begin to show slight better performance than the TDHS based systems.

Furthermore, we notice the effect that the different A-values have on the range of the SNR values beyond which the conventional system

begins to performs better than the TDHS based system. In this case, upto 20 dB, 25 dB and 40 dB, for A-values of 0.1, 0.05 and 0.01, respectively.

7.4.2 BER Performance Comparison Between Uncoded TDHS and PC-TDHS Single User HPV Systems using HD and SD Decoders

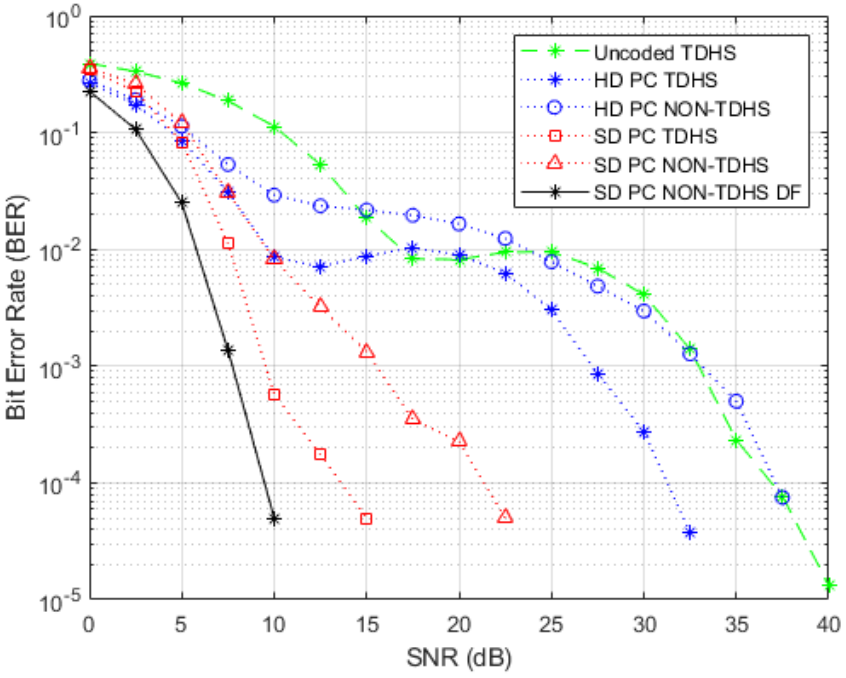

FIGURE 7.7: BER performance comparison between TDHS and Non-TDHS based HPV systems for coded and uncoded schemes. $A = 0.05$, $M = 4$ for coded systems.

A further comparison of the uncoded systems to the coded systems using the HD decoder, is made. Despite the reduction in the spectral efficiency, a superior BER performance of the PC-TDHS based system over the uncoded TDHS system, is noticed. This performance enhancement is due to the feature that the permutation code introduces in the time slot activation pattern, where only some time-slots

are activated to carry the modulated information bits, as a result the probability of the impulse noise effect on the activated time-slot is reduced.

The performance of the coded TDHS HPV system is further enhanced in terms of reliability and decoding computation reduction by the use of the HM-based SD decoder. In Figure 7.7, it is interesting to note the superior performance influenced by the HM SD decoder. For instance, at SNR values greater than 10 dB, PC non-TDHS employing the HM SD decoder performs better than the PC-TDHS system using an HD decoder. Considering the positive effect of the HM decoder on the coded non-TDHS system, it is conceived that a combination of the TDHS scheme and the HM decoder on a coded system will provide further performance enhancement. Suffice to say, the BER performance of a PC-TDHS HPV system using the HM SD decoder, is also shown in Figure 7.7, with an enhanced performance. About 7 dB SNR gain is noticed at the BER of 10^{-4} when the PC-TDHS and PC non-TDHS system employs the HM decoder, while over 17 dB gain is noticed at 10^{-4}, when compared to the TDHS system using the HD decoder.

7.4.3 Performance Comparison Between HPV Systems Employing Amplify-And-Forward (AF) and Decode-And-Forward (DF) Relaying Protocols

All except one plot in Figure 7.7 are results from HPV systems simulated with the AF relaying protocol. The exception shows the BER

performance of the PC non-TDHS system employing the DF protocol. A difference of about 4 dB SNR gain at 10^{-4} is noticed between the BER performance of the PC non-TDHS system employing the DF relaying protocol and the PC TDHS system employing the AF relaying protocol. The superior BER performance of the coded non-TDHS system using the DF relaying protocol over that of the coded TDHS system using the AF protocol, translates into a superior goodput performance, as depicted in Figure 7.8. In this work, the definition of the system goodput is given as the difference between the total transmitted data blocks and the block error rate (BLER); where BLER is a ratio of the number of erroneous blocks to the total number of blocks transmitted. Thus, we express goodput as $1 - \text{BLER}$. The superior performance of the non-TDHS HPV sys-

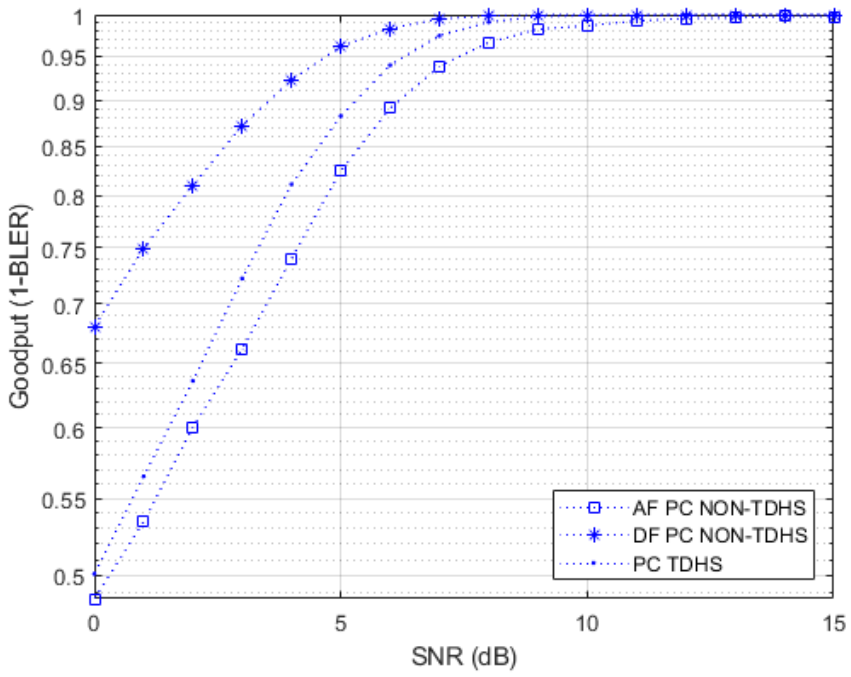

FIGURE 7.8: Goodput performance comparison for coded TDHS and non-TDHS systems employing AF and DF relaying protocols. SD decoding was used for all the systems.

TDHS AF System Processes	Non-TDHS DF System Processes
Encode and Modulation	
Hermitian symmetry	-
PLC Channel	
-	Demodulate
IN detection $\min(y_n, y_n^{\dagger}) < \theta$ Complexity: $O(M^2)$	Decoding with complexities: $O(M^4)$ for SD $O(M!\,M^2)$ for HD.
-	Encode
-	Modulate
Signal preparation for transmission via VLC channel	

FIGURE 7.9: Comparison of major signal processes between TDHS system using the AF relaying protocol and non-TDHS system using the DF relaying protocol. Grey portions depict common processes, while white portions indicate processes not applicable to a particular system. Blue and orange portions depict processes applicable only to either the TDHS or the non-TDHS system, respectively.

tem using the DF relaying protocol over the TDHS system, is due to the fact that information received from the PLC channel is only forwarded to the destination if the decoding is deemed successful by the error detection code. However, the enhanced performance over AF enabled schemes is achieved at higher computational complexity. While the TDHS scheme using the AF relaying protocol only detects if the transmitted data was affected by impulse noise with a complexity of $O(M^2)$, the DF scheme as seen in Figure 7.9 requires several signal processes before re-transmission to the VLC receiver. In addition to the computational complexities of the demodulation, encoding and modulation of the considered coded system, the decoding complexities are $O(M^4)$ and $O(M!\cdot M^2)$ for SD and HD decoding, respectively [130]. Hence, with a difference of less than 5 dB SNR gain at a BER of 10^{-4}, shown in Figure 7.7, the proposed TDHS scheme would be a cost-effective option.

7.4.4 BER Performance PC-TDHS based MA HPV Systems

The BER performance of the TDHS based multiple access HPV system using the HM decoder, is shown in Figure 7.10. As expected, from the trend in Figs. 7.6 and 7.7, the TDHS MA HPV system outperforms that of the conventional MA HPV system. For example, over 6 dB difference in SNR at 10^{-4} is noticed. Furthermore, since multiple time-slots are activated in each G group, the number of time-slots prone to the impulse noise effect also increases. Hence, it is noticed that the single user PC-TDHS system also using the HM decoder, outperforms the system with MA scheme. However, MA implementation increases the channel utilisation, hence a trade-off between the BER performance and the spectral efficiency is inevitable.

7.5 Summary

In this chapter, an investigation on the reliability performance of a hybrid technology system identified to be critical for continued development of IoT, was conducted. Precisely, a novel scheme for impulse noise mitigation in an HPV communication system has been presented. The scheme is based on a time-diversity concept that uses the Hermitian symmetry structure to introduce data repetition and recover information symbols that are likely to have been affected by

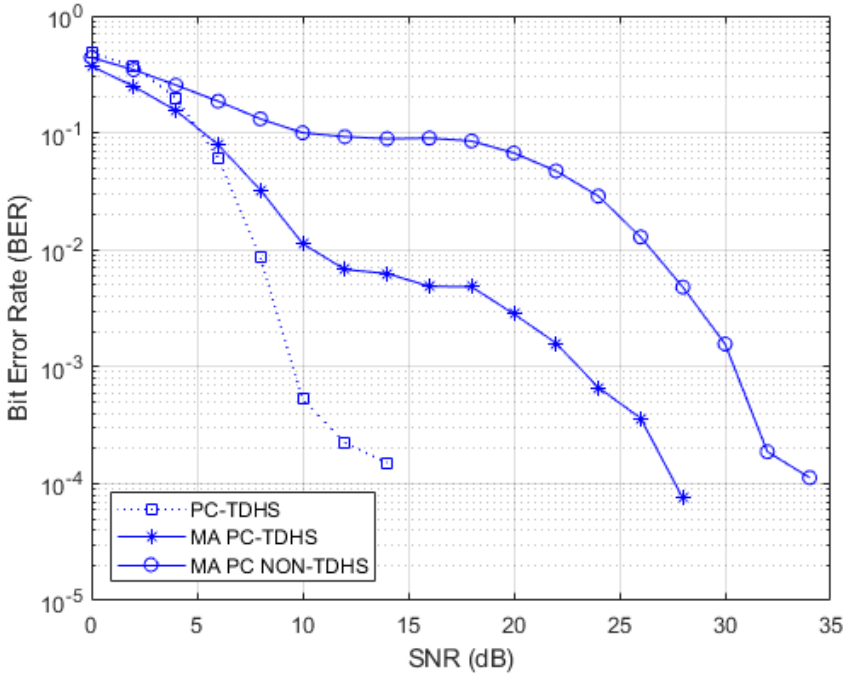

FIGURE 7.10: BER performance of the multiple access HPV system using the permutation coded TDHS. $A = 0.05$, $L = 4$, $m = 2$.

impulse noise. Thus, referred to as time-diversity Hermitian symmetry (TDHS) scheme for impulse noise mitigation. The use of the TDHS scheme results in a 75% chance to recover impulse noise affected data symbols at the PLC/VLC integration unit. In comparison to the conventional system, the TDHS based HPV system has a better BER performance that is attributed to the fact that information symbols affected by impulse noise could be recovered using their respective copies that are simultaneously transmitted with them, in complex conjugate form.

Further, the TDHS scheme was implemented over a permutation coded HPV system using soft decision decoding. Compared to the uncoded TDHS HPV system, the PC TDHS based system demonstrated enhanced reliability where an SNR gain of over 7 dB at a

BER of 10^{-4} for both HD and SD decoders, was achieved. The use of the an SD HM decoder with the TDHS scheme further improved the BER when compared to the one employing the HD decoder. Despite the poorer performance when compared to a PC non-TDHS system using the DF protocol, the proposed TDHS based HPV system using the AF protocol has acceptable performance metrics in terms of BER and goodput, yet with a lower computational complexity. Furthermore, PCs provided a base for the implementation of a permutation coded MA HPV system whose decoding complexity is reduced by employing an SD HM decoder.

CHAPTER 8

Conclusion and Future Work

8.1 Conclusion

It is a fact that emerging alternative communication technologies like VLC and the HPV systems may not only have to complement, but in some applications areas, replace the use of the well established RF technology. Hence, the need for communication systems based on these alternative technologies to perform as well as or even better than the RF-based solutions. In this work, an HPV system was investigated with an objective of enhancing its performance in terms of error rate and computational complexity. Noise mitigation schemes, MIMO, MA and decoding techniques applied to the various sections of the HPV system were presented.

Indoor illumination using solid state lighting is normally achieved with multiple LEDs, thus naturally providing an easy way of enabling MIMO techniques for VLC systems. However, indoor O-MIMO links are usually correlated resulting in minor gains to influence the system performance positively. This work showed that the use of STC-MIMO techniques such as the ASTC technique with

ImRs forms a more robust system compared an ATSC system using NImRs. The STC-MIMO enhances the system performance as it provides transmit diversity of the message signal, while the ImR decorrelates MIMO links. It was also shown that the error performance of the system improves as the number of pixels of the ImR increases.

MA techniques provide one of the most desired features of a communication system of allowing resource sharing among users. Thus, effectively utilising some of the scarce channel resources like timeslots ad frequency bandwidth. Coded MA techniques based on PCs have been studied. However, the computational complexity of existing commonly used MA decoders based on HD exhaustive search methods, increase exponentially. By interpreting the output of the channel as an assignment problem, it was shown that the SD decoder based on the Hungarian and Murty's optimization algorithms can achieve an SD decoder. In this work, we proposed and showed that based on the cost rankings from the HM decoder, multiple MA codewords from multiple users can be decoded. Thus, achieving an SD MA decoder that can be applied in PLC, VLC or HPV systems. In this work, it was shown that the complexity of the SD HM decoder is of a polynomial order, thus lower than that based on exhaustive methods. The use of the SD HM decoder was also shown to enhance the reliability of the MA system compared to those using ES methods, thus contributing to the achievement of the main study objective.

An encoder adapted for the SD HM decoder was proposed to further enhance the performance of the system when PCs are used. The investigation was aided by considering a generalised STM-MIMO system where PCWs were used to determine the TE activation patterns. Multiple PCWs, whose combination results in VW matrices were simultaneously selected for transmission, thus increasing the rate of data transmission. An adaptation of the encoder to the HM decoder was achieved by a derived theorem that defined the capability of the HM decoder based on the weight properties of the combined PCWs. In the adapted encoder, the main codebook is partitioned into sub-codebooks based on the codeword combination properties. The advantage of using the adapted encoder was demonstrated by the superior BER performance of the GSTC-MIMO system using the adapted encoder compared to the one using the conventional ST encoder. Furthermore, the adapted encoder was applied to an MA system where each sub-codebook is assigned to a user. In this way, codeword combinations that have a high error probability are avoided. This results in enhanced reliability. Furthermore, the impact on the BER performance of TE positioning with respect to their separation distance was investigated, for an MA using STC-MIMO.

Mitigation of the channel effects is another way to enhance the performance of the HPV system. To this effect, two schemes that mitigate the impulse noise that affect the signals in PLC channels were proposed for the HPV system. The first scheme is a combination

of OFDM and MFSK aided with PCs to enable the use of the low-complexity HM decoder. This PC OFDM-MFSK scheme achieves a better system reliability compared to a system where only OFDM is used. To enhance the data rate of the PC OFDM-MFSK, a generalisation of the PC OFDM-MFSK scheme, that does not increase the decoding complexity of the system, is introduced. As such, the objective to enhance the reliability performance and reduce the computational complexity of the HPV system is achieved.

The final section of this thesis presented the second impulse noise mitigation scheme based on TD using the HS structure. The novel TDHS scheme exploits the Hermitian symmetry structure to introduce data repetition and recover information symbols that are likely to have been affected by impulse noise. The TDHS scheme, therefore, reduces the probability of re-transmitting data symbols affected by impulse noise from the PLC section to the VLC section of the HPV system. Based on the studied codeword combination properties in Chapter 5 and the SD HM decoder, an MA scheme is the applied to the TDHS HPV system. Compared to a conventional HPV MA system, simulation results show that the TDHS-based MA system has an enhanced BER performs.

8.2 Future Work

In Chapters 3 and 5, indoor environment setups in which VLC was assumed, were considered for stationary TEs and REs. However,

different room setups and scenarios that also consider user mobility still need to be investigated in order to refine the implementation of the VLC system for MA and MIMO techniques. This would especially be ideally investigated in a laboratory setting, where real and practical indoor conditions would be accounted for. A combination of MA and STC/GSTC-MIMO where separate TEs are considered for each user, are specifically recommended for investigation. Additionally, given that part of the diversity gain of STBC is in the time dimension, it is intuitive that if the channel is correlated in time over longer periods, successive symbols could equally be correlated, leading to effective decoding and resulting in better performance. This could especially be beneficial for VLC systems which are prone to shadowing and deep fading when mobility is considered. As such, investigation to ascertain the extent of the expected performance enhancement in such scenarios, is important.

Since the use of PCs in conjunction with the SD HM decoder, implemented over the impulse noise mitigation schemes in Chapters 6 and 7, enhance the reliability of system, howbeit with a data rate penalty, it becomes necessary to investigate other novel schemes of increasing the data rate. In Chapter 6, a simple approach of generalisation of the permutation coded system was exploited for data rate enhancement. However, we suggest that other index modulation schemes and dimensions must be exploited, in order to fully benefit from that reliability gains of the two impulse noise mitigation

schemes, presented in Chapters 6 and 7. In addition, other potentially less complex detection methods based on the sparse nature of the activated sub-carriers, can be considered for future work.

References

[1] Ghaith Al-Juboori, Evgeny Tsimbalo, Angela Doufexi, and Andrew R Nix. A comparison of OFDM and GFDM-based MFSK modulation schemes for robust IoT applications. In *2017 IEEE 85th Vehicular Technology Conference (VTC Spring)*, pages 1–5. IEEE, 2017.

[2] Siavash M Alamouti. A simple transmit diversity technique for wireless communications. *IEEE Journal on selected areas in communications*, 16(8):1451–1458, 1998.

[3] Abdulmalik Alwarafy, Mohammed Alresheedi, Ahmad Fauzi Abas, and Abdulhameed Alsanie. Performance evaluation of space time coding techniques for indoor visible light communication systems. In *2018 International Conference on Optical Network Design and Modeling (ONDM)*, pages 88–93. IEEE, 2018.

[4] Yuta Amano, Koji Kamakura, and Takaya Yamazato. Alamouti-type coding for visible light communication based on direct detection using image sensor. In *2013 IEEE Global Communications Conference (GLOBECOM)*, pages 2430–2435. IEEE, 2013.

[5] P Amirshahi and Mohsen Kavehrad. Broadband access over medium and low voltage power-lines and use of white light emitting diodes for indoor communications. In *IEEE Consumer Communications & Networking Conference*, 2006.

[6] Nikoleta Andreadou and Fotini-Niovi Pavlidou. PLC channel: Impulsive noise modelling and its performance evaluation under different array coding schemes. *IEEE Transactions on Power Delivery*, 24(2):585–595, 2009.

[7] Jean Armstrong. Alamouti coding for indoor optical wireless communications using ACO-OFDM. In *2009 Conference Record of the Forty-Third Asilomar Conference on Signals, Systems and Computers*, pages 1650–1654. IEEE, 2009.

[8] Jean Armstrong and Brendon JC Schmidt. Comparison of asymmetrically clipped optical OFDM and DC-biased optical OFDM in AWGN. *IEEE Communications Letters*, 12(5):343–345, 2008.

[9] MK Arti. A novel downlink interference alignment method for multi-user MIMO system with no CSIT: A space-time coding approach. *IEEE Transactions on Vehicular Technology*, 69(10):10937–10948, 2020.

[10] Ruowen Bai, Rui Jang, Jiandong Tan, and Jinguo Quan. Performance comparison of VLC MIMO techniques considering

indoor illuminance with inclined LEDs. In *2016 IEEE International Conference on Wireless for Space and Extreme Environments (WiSEE)*, pages 105–110. IEEE, 2016.

[11] Vladimir B Balakirsky and AJ Han Vinck. Constructions of specific permutation codes for multi-user communication. In *Proceedings 2001 IEEE Information Theory Workshop (Cat. No. 01EX494)*, pages 79–81. IEEE, 2001.

[12] Vladimir B Balakirsky and AJ Han Vinck. Potential performance of PLC systems composed of several communication links. In *International Symposium on Power Line Communications and Its Applications, 2005.*, pages 12–16. IEEE, 2005.

[13] Vladimir B Balakirsky and H Vinck. On the performance of permutation codes for multi-user communication. *Problems of Information Transmission*, 39(3):239–254, 2003.

[14] Sami Barmada, Antonino Musolino, and Marco Raugi. Innovative model for time-varying power line communication channel response evaluation. *IEEE journal on selected areas in communications*, 24(7):1317–1326, 2006.

[15] Fatima Barrami, Yannis Le Guennec, Emil Novakov, Jean-Marc Duchamp, and Pierre Busson. A novel FFT/IFFT size efficient technique to generate real time optical OFDM signals compatible with IM/DD systems. In *2013 European microwave conference*, pages 1247–1250. IEEE, 2013.

[16] Ertugrul Basar. Index modulation techniques for 5G wireless networks. *IEEE Communications Magazine*, 54(7):168–175, 2016.

[17] Ertuğrul Başar, Ümit Aygölü, Erdal Panayırcı, and H Vincent Poor. Orthogonal frequency division multiplexing with index modulation. *IEEE Transactions on signal processing*, 61(22):5536–5549, 2013.

[18] Dushyantha A. Basnayaka and Harald Haas. Hybrid RF and VLC systems: Improving user data rate performance of VLC systems. In *2015 IEEE 81st Vehicular Technology Conference (VTC Spring)*, pages 1–5, 2015.

[19] Sarah S Bawazir, Paschalis C Sofotasios, Sami Muhaidat, Yousof Al-Hammadi, and George K Karagiannidis. Multiple access for visible light communications: Research challenges and future trends. *IEEE Access*, 6:26167–26174, 2018.

[20] Alessandro Bazzi, Barbara M Masini, Alberto Zanella, and Alex Calisti. Visible light communications as a complementary technology for the internet of vehicles. *Computer Communications*, 93:39–51, 2016.

[21] Alexander Graham Bell, WG Adams, WH Preece, et al. Discussion on" the photophone and the conversion of radiant energy into sound". *Journal of the Society of Telegraph Engineers*, 9(34):375–383, 1880.

[22] K Bhavya, Nidhi Gangrade, and Navin Kumar. Simplified integration of power line and visible light communication. In *2018 3rd International Conference on Communication and Electronics Systems (ICCES)*, pages 129–132. IEEE, 2018.

[23] Ândrei Camponogara, H. Vincent Poor, and Moisés V. Ribeiro. The complete and incomplete low-bit-rate hybrid PLC/wireless channel models: Physical layer security analyses. *IEEE Internet of Things Journal*, 6(2):2760–2769, 2019.

[24] Evren Catak and Lütfiye Durak-Ata. An efficient transceiver design for superimposed waveforms with orthogonal polynomials. In *2017 IEEE International Black Sea Conference on Communications and Networking (BlackSeaCom)*, pages 1–5. IEEE, 2017.

[25] Robert W Chang. Synthesis of band-limited orthogonal signals for multichannel data transmission. *Bell System Technical Journal*, 45(10):1775–1796, 1966.

[26] Ling Cheng and Hendrik C Ferreira. Time-diversity permutation coding scheme for narrow-band power-line channels. In *2012 IEEE International Symposium on Power Line Communications and Its Applications*, pages 120–125. IEEE, 2012.

[27] Fan RK Chung, Jawad A Salehi, and Victor K Wei. Optical orthogonal codes: design, analysis and applications. *IEEE Transactions on Information theory*, 35(3):595–604, 1989.

[28] CommScope. Indoor wireless in mobile society: Research reveals gap between expectations of wireless consumers and those who design and manage buildings. 19 November, 2015.

[29] José Antonio Cortés-Arrabal et al. Modulation and multiple access techniques for indoor broadband power-line communications. 2007.

[30] Ingemar J Cox, Matt L Miller, Roy Danchick, and GE Newnam. A comparison of two algorithms for determining ranked assignments with application to multitarget tracking and motion correspondence. *IEEE Transactions on Aerospace and Electronic Systems*, 33(1):295–301, 1997.

[31] Peter de Laval and Shakir Abdul-Jabbar. Decoding of superimposed codes in multi-access communication. In *8th European Conference on Area Communication, EUROCON*, 1988.

[32] Leonardo de MBA Dib, Victor Fernandes, Mateus de L Filomeno, and Moises V Ribeiro. Hybrid PLC/wireless communication for smart grids and internet of things applications. *IEEE internet of things Journal*, 5(2):655–667, 2017.

[33] Luca Di Bert, Peter Caldera, David Schwingshackl, and Andrea M Tonello. On noise modeling for power line communications. In *2011 IEEE International Symposium on Power Line Communications and Its Applications*, pages 283–288. IEEE, 2011.

[34] Wenbo Ding, Fang Yang, Hui Yang, Jintao Wang, Xiaofei Wang, Xun Zhang, and Jian Song. A hybrid power line and visible light communication system for indoor hospital applications. *Computers in Industry*, 68:170–178, 2015.

[35] Ivan B Djordjevic and Bane Vasic. Novel combinatorial constructions of optical orthogonal codes for incoherent optical CDMA systems. *Journal of Lightwave Technology*, 21(9):1869–1875, 2003.

[36] Hany Elgala, Raed Mesleh, and Harald Haas. An LED model for intensity-modulated optical communication systems. *IEEE Photonics Technology Letters*, 22(11):835–837, 2010.

[37] John Fakidis, Dobroslav Tsonev, and Harald Haas. A comparison between DCO-OFDMA and synchronous one-dimensional OCDMA for optical wireless communications. In *2013 IEEE 24th Annual International Symposium on Personal, Indoor, and Mobile Radio Communications (PIMRC)*, pages 3605–3609. IEEE, 2013.

[38] Ayokunle D Familua, Alain Richard Ndjiongue, Kehinde Ogunyanda, Ling Cheng, Hendrik C Ferreira, and Theo G Swart. A semi-hidden markov modeling of a low complexity FSK-OOK in-house PLC and VLC integration. In *2015 IEEE International Symposium on Power Line Communications and Its Applications (ISPLC)*, pages 199–204. IEEE, 2015.

[39] Ayokunle Damilola Familua and Ling Cheng. First and second-order semi-hidden fritchman markov models for a multi-carrier based indoor narrowband power line communication system. *Physical Communication*, 29:55–66, 2018.

[40] Rui Fan, Ya Jun Yu, and Yong Liang Guan. Generalization of orthogonal frequency division multiplexing with index modulation. *IEEE transactions on wireless communications*, 14(10):5350–5359, 2015.

[41] Tekla D Farkas, Tamás Király, Tamás Pardy, Toomas Rang, and Galina Rang. Application of power line communication technology in street lighting control. 2018.

[42] Muhammad Zubair Farooqui and Poompat Saengudomlert. Transmit power reduction through subcarrier selection for MC-CDMA-based indoor optical wireless communications with IM/DD. *EURASIP Journal on Wireless Communications and Networking*, 2013(1):138, 2013.

[43] Thilo Fath, Marco Di Renzo, and Harald Haas. On the performance of space shift keying for optical wireless communications. In *2010 IEEE Globecom Workshops*, pages 990–994. IEEE, 2010.

[44] Thilo Fath and Harald Haas. Performance comparison of MIMO techniques for optical wireless communications in indoor environments. *IEEE Transactions on Communications*, 61(2):733–742, 2013.

[45] Simeng Feng, Tong Bai, and Lajos Hanzo. Joint power allocation for the multi-user NOMA-downlink in a power-line-fed VLC network. *IEEE Transactions on Vehicular Technology*, 68(5):5185–5190, 2019.

[46] Gerhard Fettweis, Marco Krondorf, and Steffen Bittner. GFDM-generalized frequency division multiplexing. In *VTC Spring 2009-IEEE 69th Vehicular Technology Conference*, pages 1–4. IEEE, 2009.

[47] Ryoh Fuji-Hara and Ying Miao. Optical orthogonal codes: Their bounds and new optimal constructions. *IEEE Transactions on Information theory*, 46(7):2396–2406, 2000.

[48] Stefano Galli and Thomas Banwell. A novel approach to the modeling of the indoor power line channel-Part II: Transfer function and its properties. *IEEE Transactions on Power Delivery*, 20(3):1869–1878, 2005.

[49] Sudharsan Ganesan, Raed Mesleh, Harald Ho, Chang Wook Ahn, and Sangboh Yun. On the performance of spatial modulation OFDM. In *2006 Fortieth Asilomar Conference on Signals, Systems and Computers*, pages 1825–1829. IEEE, 2006.

[50] Junnan Gao, Fang Yang, and Wenbo Ding. Novel integrated power line and visible light communication system with bit division multiplexing. In *2015 International Wireless Communications and Mobile Computing Conference (IWCMC)*, pages 680–684. IEEE, 2015.

[51] D. Gesbert, M. Shafi, Da shan Shiu, P.J. Smith, and A. Naguib. From theory to practice: an overview of MIMO space-time coded wireless systems. *IEEE Journal on Selected Areas in Communications*, 21(3):281–302, 2003.

[52] Fritz R Gfeller and Urs Bapst. Wireless in-house data communication via diffuse infrared radiation. *Proceedings of the IEEE*, 67(11):1474–1486, 1979.

[53] Zabih Ghassemlooy, Wasiu Popoola, and Sujan Rajbhandari. *Optical wireless communications: system and channel modelling with Matlab®*. CRC press, 2017.

[54] Lajos Hanzo, Harald Haas, Sándor Imre, Dominic O'Brien, Markus Rupp, and Laszlo Gyongyosi. Wireless myths, realities, and futures: from 3G/4G to optical and quantum wireless. *Proceedings of the IEEE*, 100(Special Centennial Issue):1853–1888, 2012.

[55] Jürgen Häring and AJ Han Vinck. OFDM transmission corrupted by impulsive noise. In *Proceedings of the 2000 International Symposium on Power-Line Communications and its Applications, Limerick, Ireland*, pages 5–7, 2000.

[56] Timothy Healy. Coding and decoding for code division multiple user communication systems. *IEEE transactions on communications*, 33(4):310–316, 1985.

[57] Daniel G Holmes, Ling Cheng, Mulundumina Shimaponda-Nawa, Ayokunle D Familua, and Adnan M Abu-Mahfouz.

Modelling noise and pulse width modulation interference in indoor visible light communication channels. *AEU-International Journal of Electronics and Communications*, 106:40–47, 2019.

[58] Olaf G Hooijen. On the channel capacity of the residential power circuit used as a digital communications medium. *IEEE Communications Letters*, 2(10):267–268, 1998.

[59] Ahmed Taha Hussein and Jaafar MH Elmirghani. 10 Gbps mobile visible light communication system employing angle diversity, imaging receivers, and relay nodes. *Journal of Optical Communications and Networking*, 7(8):718–735, 2015.

[60] Hany S. Hussein, Ahmed S. Mubarak, Osama A. Omer, Usama S. Mohamed, and Mostafa Salah. Sparse index OFDM modulation for IoT communications. *IEEE Access*, 8:170044–170056, 2020.

[61] Naoki Ishikawa, Rakshith Rajashekar, Shinya Sugiura, and Lajos Hanzo. Generalized-spatial-modulation-based reduced-RF-chain millimeter-wave communications. *IEEE Transactions on Vehicular Technology*, 66(1):879–883, 2016.

[62] Mohammad Vahid Jamali, Pooya Nabavi, and Jawad A. Salehi. MIMO underwater visible light communications: Comprehensive channel study, performance analysis, and multiple-symbol detection. *IEEE Transactions on Vehicular Technology*, 67(9):8223–8237, 2018.

[63] Manan Jani, Parul Garg, and Akash Gupta. On the performance of a cooperative PLC-VLC indoor broadcasting system consisting of mobile user nodes for IoT networks. *IEEE Transactions on Broadcasting*, 67(1):289–298, 2020.

[64] Ahmad M Jaradat, Jehad M Hamamreh, and Huseyin Arslan. OFDM with subcarrier number modulation. *IEEE Wireless Communications Letters*, 7(6):914–917, 2018.

[65] Ahmad M Jaradat, Jehad M Hamamreh, and Hüseyin Arslan. Modulation options for OFDM-based waveforms: Classification, comparison, and future directions. *IEEE Access*, 7:17263–17278, 2019.

[66] C Jenila and RK Jeyachitra. Green indoor optical wireless communication systems: Pathway towards pervasive deployment. *Digital Communications and Networks*, 7(3):410–444, 2021.

[67] Georges Kaddoum, Yogesh Nijsure, and Hung Tran. Generalized code index modulation technique for high-data-rate communication systems. *IEEE Transactions on Vehicular Technology*, 65(9):7000–7009, 2015.

[68] Joseph M Kahn and John R Barry. Wireless infrared communications. *Proceedings of the IEEE*, 85(2):265–298, 1997.

[69] Johan Karedal, Fredrik Tufvesson, Nicolai Czink, Alexander Paier, Charlotte Dumard, Thomas Zemen, Christoph F Mecklenbrauker, and Andreas F Molisch. A geometry-based

stochastic MIMO model for vehicle-to-vehicle communications. *IEEE transactions on wireless communications*, 8(7):3646–3657, 2009.

[70] Mohamed Kashef, Mohamed Abdallah, Naofal Al-Dhahir, and Khalid Qaraqe. On the impact of PLC backhauling in multi-user hybrid VLC/RF communication systems. In *2016 IEEE Global Communications Conference (GLOBECOM)*, pages 1–6. IEEE, 2016.

[71] William Kautz and Roy Singleton. Nonrandom binary superimposed codes. *IEEE Transactions on Information Theory*, 10(4):363–377, 1964.

[72] Latif Ullah Khan. Visible light communication: Applications, architecture, standardization and research challenges. *Digital Communications and Networks*, 3(2):78–88, 2017.

[73] Sung-Man Kim, Myeong-Woon Baek, and Seung Hoon Nahm. Visible light communication using TDMA optical beamforming. *EURASIP Journal on Wireless Communications and Networking*, 2017(1):56, 2017.

[74] Oluwafemi Kolade, Adnan M. Abu-Mahfouz, and Ling Cheng. A subcarrier permutation scheme for noise mitigation and multi-access in powerline channels. In *2021 IEEE International Symposium on Power Line Communications and its Applications (ISPLC)*, pages 19–24, 2021.

[75] Oluwafemi Kolade and Ling Cheng. Impulse noise mitigation using subcarrier coding of OFDM-MFSK scheme in powerline channel. In *2019 IEEE International Conference on Communications, Control, and Computing Technologies for Smart Grids (SmartGridComm)*, pages 1–6. IEEE, 2019.

[76] Oluwafemi Kolade and Ling Cheng. Permutation-aided space-time shift keying for indoor visible light communication. In *2019 IEEE International Conference on Communications, Control, and Computing Technologies for Smart Grids (SmartGridComm)*, pages 1–6. IEEE, 2019.

[77] Oluwafemi Kolade and Ling Cheng. Memory channel models of a hybrid PLC-VLC link for a smart underground mine. *IEEE Internet of Things Journal*, pages 1–11, 2021.

[78] Oluwafemi Kolade, Ayokunle Damilola Familua, and Ling Cheng. Indoor amplify-and-forward power-line and visible light communication channel model based on a semi-hidden markov model. *AEU-International Journal of Electronics and Communications*, 124:153108, 2020.

[79] Oluwafemi Kolade, Mulundumina Shimaponda-Nawa, Daniel JJ Versfeld, and Ling Cheng. Optimization algorithms for improving the performance of permutation trellis codes. *Physical Communication*, 44:101237, 2021.

[80] Oluwafemi Kolade, Jaco Versfeld, and Michael Van Wyk. Soft-Decision decoding of permutation block codes in AWGN

and Rayleigh fading channels. *IEEE Communications Letters*, 21(12):2590–2593, 2017.

[81] Oluwafemi Ibrahim Kolade. *Soft-decision decoding techniques for permutation modulation in powerline and visible light communication*. PhD thesis, 2020.

[82] Toshihiko Komine, Shinichiro Haruyama, and Masao Nakagawa. Performance evaluation of narrowband OFDM on integrated system of power line communication and visible light wireless communication. In *2006 1st International Symposium on Wireless Pervasive Computing*, pages 6–pp. IEEE, 2006.

[83] Toshihiko Komine and Masao Nakagawa. Integrated system of white LED visible-light communication and power-line communication. *IEEE Transactions on Consumer Electronics*, 49(1):71–79, 2003.

[84] Toshihiko Komine and Masao Nakagawa. Fundamental analysis for visible-light communication system using LED lights. *IEEE transactions on Consumer Electronics*, 50(1):100–107, 2004.

[85] Toshihiko Komine and Masao Nakagawa. Performance evaluation of visible-light wireless communication system using white LED lightings. In *iscc*, pages 258–263. IEEE, 2004.

[86] Harold W Kuhn. The Hungarian method for the assignment problem. *Naval research logistics quarterly*, 2(1-2):83–97, 1955.

[87] Ajit Kumar and Swapan Kumar Ghorai. BER performance analysis of OFDM-based integrated PLC and MIMO-VLC system. *IET Optoelectronics*, 14(5):242–251, 2020.

[88] Lutz Lampe, Andrea M Tonello, and Theo G Swart. *Power Line Communications: Principles, Standards and Applications from multimedia to smart grid*. John Wiley & Sons, 2016.

[89] Kwonhyung Lee, Hyuncheol Park, and John R Barry. Indoor channel characteristics for visible light communications. *IEEE communications letters*, 15(2):217–219, 2011.

[90] Lantao Liu and Dylan A Shell. Assessing optimal assignment under uncertainty: An interval-based algorithm. *The International Journal of Robotics Research*, 30(7):936–953, 2011.

[91] Shihe Long, Mohammad-Ali Khalighi, Mike Wolf, Salah Bourennane, and Zabih Ghassemlooy. Channel characterization for indoor visible light communications. In *Optical Wireless Communications (IWOW), 2014 3rd International Workshop in*, pages 75–79. IEEE, 2014.

[92] Hao Ma, Lutz Lampe, and Steve Hranilovic. Integration of indoor visible light and power line communication systems. In *2013 IEEE 17th International Symposium on Power Line Communications and Its Applications*, pages 291–296. IEEE, 2013.

[93] Hao Ma, Lutz Lampe, and Steve Hranilovic. Hybrid visible light and power line communication for indoor multiuser downlink. *IEEE/OSA Journal of Optical Communications and Networking*, 9(8):635–647, 2017.

[94] Shang Ma, Qiong Liu, and Phillip C-Y Sheu. Foglight: Visible light-enabled indoor localization system for low-power IoT devices. *IEEE Internet of Things Journal*, 5(1):175–185, 2017.

[95] Xu Ma, Junnan Gao, Fang Yang, Wenbo Ding, Hui Yang, and Jian Song. Integrated power line and visible light communication system compatible with multi-service transmission. *IET Communications*, 11(1):104–111, 2017.

[96] YH Ma, PL So, and E Gunawan. Comparison of CDMA and OFDM systems for broadband power line communications. *IEEE Transactions on power delivery*, 23(4):1876–1885, 2008.

[97] Konstantinos Maliatsos, Leonidas Marantis, Petros S Bithas, and Athanasios G Kanatas. Hybrid multi-antenna techniques for V2X communications—prototyping and experimentation. In *Telecom*, volume 1, pages 80–95. Multidisciplinary Digital Publishing Institute, 2020.

[98] Hanaa Marshoud, Vasileios M Kapinas, George K Karagiannidis, and Sami Muhaidat. Non-orthogonal multiple access for visible light communications. *IEEE photonics technology letters*, 28(1):51–54, 2015.

[99] Samvel Martirosyan and Han AJ. A construction for optical orthogonal codes with correlation 1. *IEICE TRANSACTIONS on Fundamentals of Electronics, Communications and Computer Sciences*, 85(1):269–272, 2002.

[100] Anil Mengi and AJ Han Vinck. Successive impulsive noise suppression in OFDM. In *ISPLC2010*, pages 33–37. IEEE, 2010.

[101] David Middleton. Statistical-physical models of electromagnetic interference. *IEEE transactions on Electromagnetic Compatibility*, (3):106–127, 1977.

[102] David Middleton. Statistical-physical models of electromagnetic interference. *IEEE transactions on Electromagnetic Compatibility*, (3):106–127, 1977.

[103] Abbas Mohammadi and Fadhel M Ghannouchi. *RF transceiver design for MIMO wireless communications*, volume 145. Springer Science & Business Media, 2012.

[104] Mohammed SA Mossaad, Steve Hranilovic, and Lutz Lampe. Amplify-and-forward integration of power line and visible light communications. In *2015 IEEE Global Conference on Signal and Information Processing (GlobalSIP)*, pages 1322–1326. IEEE, 2015.

[105] Mohammed SA Mossaad, Steve Hranilovic, and Lutz Lampe. Visible light communications using OFDM and multiple LEDs.

IEEE Transactions on Communications, 63(11):4304–4313, 2015.

[106] Katta G Murty. Letter to the editor—an algorithm for ranking all the assignments in order of increasing cost. *Operations research*, 16(3):682–687, 1968.

[107] Alain Richard Ndjiongue, Hendrik C Ferreira, and Telex MN Ngatched. Constellation design for cascaded MPSK-CSK systems. In *2017 IEEE International Conference on Communications Workshops (ICC Workshops)*, pages 17–22. IEEE, 2017.

[108] HQ Nguyen, J-H Choi, Moonsoo Kang, Zabih Ghassemlooy, DH Kim, S-K Lim, T-G Kang, and Chung Ghiu Lee. A matlab-based simulation program for indoor visible light communication system. In *Communication Systems Networks and Digital Signal Processing (CSNDSP), 2010 7th International Symposium on*, pages 537–541. IEEE, 2010.

[109] Stephane M Nlom, Alain R Ndjiongue, and Khmaies Ouahada. Cascaded PLC-VLC channel: An indoor measurements campaign. *IEEE Access*, 6:25230–25239, 2018.

[110] Stephane M Nlom, Alain Richard Ndjiongue, Khmaies Ouahada, Hendrik C Ferreira, AJ Han Vinck, and Thokozani Shongwe. A simplistic channel model for cascaded PLC-VLC systems. In *2017 IEEE International Symposium on Power Line Communications and its Applications (ISPLC)*, pages 1–6. IEEE, 2017.

[111] Dominic O'Brien. Multi-input multi-output MIMO indoor optical wireless communications. In *2009 Conference Record of the Forty-Third Asilomar Conference on Signals, Systems and Computers*, pages 1636–1639. IEEE, 2009.

[112] Q. W. Pan and A. Kathnaur. Power-line networks to extend ranges of 2.4 GHz wireless communications inside multistorey buildings. In *2010 IEEE Radio and Wireless Symposium (RWS)*, pages 621–624, 2010.

[113] Niovi Pavlidou, AJ Han Vinck, Javad Yazdani, and Bahram Honary. Power line communications: state of the art and future trends. *IEEE Communications magazine*, 41(4):34–40, 2003.

[114] Eva Peiker-Feil, Matthias Wetz, Werner G Teich, and Juergen Lindner. OFDM-MFSK as a special case of noncoherent communication based on subspaces. In *OFDM 2012; 17th International OFDM Workshop 2012 (InOWo'12)*, pages 1–5. VDE, 2012.

[115] Thanh V Pham, Hoa Le-Minh, and Anh T Pham. Multi-user visible light communication broadcast channels with zero-forcing precoding. *IEEE Transactions on Communications*, 65(6):2509–2521, 2017.

[116] John G Proakis and Masoud Salehi. *Digital communications*, volume 4. McGraw-hill New York, 2001.

[117] Yang Qiu, Hsiao-Hwa Chen, and Wei-Xiao Meng. Channel modeling for visible light communications—a survey. *Wireless*

Communications and Mobile Computing, 16(14):2016–2034, 2016.

[118] Khaled M Rabie, Bamidele Adebisi, Ebtihal HG Yousif, Haris Gacanin, and Andrea M Tonello. A comparison between orthogonal and non-orthogonal multiple access in cooperative relaying power line communication systems. *IEEE Access*, 5:10118–10129, 2017.

[119] Khaled M Rabie and Emad Alsusa. Improving blanking/clipping based impulsive noise mitigation over powerline channels. In *2013 IEEE 24th Annual International Symposium on Personal, Indoor, and Mobile Radio Communications (PIMRC)*, pages 3413–3417. IEEE, 2013.

[120] Michael B Rahaim, Anna Maria Vegni, and Thomas DC Little. A hybrid radio frequency and broadcast visible light communication system. In *2011 IEEE GLOBECOM Workshops (GC Wkshps)*, pages 792–796. IEEE, 2011.

[121] A Rajesh and R Nakkeeran. Performance analysis of integrated system under impulse noise and multipath channel using turbo coded OFDM. In *2008 16th International Conference on Advanced Computing and Communications*, pages 254–259. IEEE, 2008.

[122] Yeduri Sreenivasa Reddy, Meenakshi Panda, Ankit Dubey, Abhinav Kumar, Trilochan Panigrahi, and Khaled M Rabie. Optimisation of indoor hybrid PLC/VLC/RF communication systems. *IET Commun.*, 14(1):117–126, 2020.

[123] Mostafa Salah, Osama A. Omer, and Usama S. Mohammed. Spectral efficiency enhancement based on sparsely indexed modulation for green radio communication. *IEEE Access*, 7:31913–31925, 2019.

[124] Jawad A Salehi. Code division multiple-access techniques in optical fiber networks. I. Fundamental principles. *IEEE transactions on communications*, 37(8):824–833, 1989.

[125] Jawad A Salehi and Charles A Brackett. Code division multiple-access techniques in optical fiber networks. II. Systems performance analysis. *IEEE Transactions on communications*, 37(8):834–842, 1989.

[126] Angeliki M Sarafi, Artemis C Voulkidis, and Panayotis G Cottis. Optimal tdma scheduling in tree-based power-line communication networks. *IEEE Transactions on Power Delivery*, 29(5):2189–2196, 2014.

[127] Abdullah Sevincer, Aashish Bhattarai, Mehmet Bilgi, Murat Yuksel, and Nezih Pala. LIGHTNETs: Smart LIGHTing and mobile optical wireless networks—a survey. *IEEE Communications Surveys & Tutorials*, 15(4):1620–1641, 2013.

[128] Mulundumina Shimaponda-Nawa, Shamin Achari, Dushantha Nalin K Jayakody, and Ling Cheng. Visible light communication system employing space time coded relay nodes and imaging receivers. *SAIEE Africa Research Journal*, 111(2):56–64, 2020.

[129] Mulundumina Shimaponda-Nawa, Oluwafemi Kolade, and Ling Cheng. Generalized permutation coded OFDM-MFSK in hybrid powerline and visible light communication. *IEEE Access*, 10:20783–20792, 2022.

[130] Mulundumina Shimaponda-Nawa, Oluwafemi Kolade, Wenbo Ding, Dushantha Nalin K. Jayakody, and Ling Cheng. Soft-decision decoding of permutation-based optical codes for a multiple access system. *IEEE Communications Letters*, 25(9):2824–2828, 2021.

[131] Thokozani Shongwe, Ulrich Speidel, Theo G Swart, and Hendrik C Ferreira. The effect of Hamming distances on permutation codes for multiuser communication in the power line communications channel. In *IEEE Africon'11*, pages 1–5. IEEE, 2011.

[132] Thokozani Shongwe, AJ Han Vinck, and Hendrik C Ferreira. A study on impulse noise and its models. *SAIEE Africa Research Journal*, 106(3):119–131, 2015.

[133] Marvin K Simon and Victor A Vilnrotter. Alamouti-type space-time coding for free-space optical communication with

direct detection. *IEEE Transactions on Wireless Communications*, 4(1):35–39, 2005.

[134] David Slepian. Permutation modulation. *Proceedings of the IEEE*, 53(3):228–236, 1965.

[135] Yuhang Song, Weichao Lu, Bin Sun, Yang Hong, Fengzhong Qu, Jun Han, Wei Zhang, and Jing Xu. Experimental demonstration of MIMO-OFDM underwater wireless optical communication. *Optics Communications*, 403:205–210, 2017.

[136] John A Stankovic. Research directions for the internet of things. *IEEE Internet of Things Journal*, 1(1):3–9, 2014.

[137] Andrew Stok and Edward H Sargent. Comparison of diverse optical CDMA codes using a normalized throughput metric. *IEEE communications letters*, 7(5):242–244, 2003.

[138] Yaqi Sun, Fang Yang, and Ling Cheng. An overview of OFDM-based visible light communication systems from the perspective of energy efficiency versus spectral efficiency. *IEEE Access*, 6:60824–60833, 2018.

[139] Yuichi Tanaka, Toshihiko Komine, Shinichiro Haruyama, and Masao Nakagawa. Indoor visible communication utilizing plural white LEDs as lighting. In *12th IEEE International Symposium on Personal, Indoor and Mobile Radio Communications. PIMRC 2001. Proceedings (Cat. No. 01TH8598)*, volume 2, pages F–F. IEEE, 2001.

[140] V. Tarokh, H. Jafarkhani, and A.R. Calderbank. Space-time block codes from orthogonal designs. *IEEE Transactions on Information Theory*, 45(5):1456–1467, 1999.

[141] Deyang Teng, Yanxi Zheng, Man Luo, Yiqiao Luo, and Wu Jinyuan. Joint user pairing and subcarrier allocation for NOMA-based hybrid power line and visible light communication systems. In *Journal of Physics: Conference Series*, volume 1693, page 012159. IOP Publishing, 2020.

[142] JT Tengdin. Distribution line carrier communications-an historical perspective. *IEEE transactions on Power Delivery*, 2(2):321–329, 1987.

[143] Mohamed Tlich, Ahmed Zeddam, Fabienne Moulin, and Frederic Gauthier. Indoor power-line communications channel characterization up to 100 MHz—Part I: One-parameter deterministic model. *IEEE Transactions on Power delivery*, 23(3):1392–1401, 2008.

[144] Andrea M Tonello, José Antonio Cortés, and Salvatore D'Alessandro. Optimal time slot design in an OFDM-TDMA system over power-line time-variant channels. In *2009 IEEE International Symposium on Power Line Communications and Its Applications*, pages 41–46. IEEE, 2009.

[145] Andrea M Tonello and Fabio Versolatto. Bottom-up statistical PLC channel modeling—Part I: Random topology model and

efficient transfer function computation. *IEEE Transactions on Power Delivery*, 26(2):891–898, 2011.

[146] Andrea M Tonello, Fabio Versolatto, and Salvatore D'Alessandro. Opportunistic relaying in in-home PLC networks. In *2010 IEEE Global Telecommunications Conference GLOBECOM 2010*, pages 1–5. IEEE, 2010.

[147] Andrea M Tonello, Fabio Versolatto, and Alberto Pittolo. In-home power line communication channel: Statistical characterization. *IEEE Transactions on Communications*, 62(6):2096–2106, 2014.

[148] Andrea M Tonello and Tao Zheng. Bottom-up transfer function generator for broadband PLC statistical channel modeling. In *2009 IEEE International Symposium on Power Line Communications and Its Applications*, pages 7–12. IEEE, 2009.

[149] Mojtaba Vaezi, Zhiguo Ding, and H Vincent Poor. *Multiple access techniques for 5G wireless networks and beyond*, volume 159. Springer, 2019.

[150] DA Vanderwater, I-H Tan, GE Hofler, DC Defevere, and FA Kish. High-brightness algainp light emitting diodes. *Proceedings of the IEEE*, 85(11):1752–1764, 1997.

[151] AJ Vinck. Coded modulation for powerline communications. *Internationa Journal of Electronics and Communications*, 54(1):45–50, 2000.

[152] AJ Han Vinck. Coding for a terrible channel. *Telecommunications and Information Science and Technologies COST*, 2005.

[153] AJ Han Vinck and Hendrik C Ferreira. Permutation trellis codes. In *Proceedings. 2001 IEEE International Symposium on Information Theory (IEEE Cat. No. 01CH37252)*, page 279. IEEE, 2001.

[154] Thomas Q Wang, Cuiwei He, and Jean Armstrong. Performance analysis of aperture-based receivers for MIMO IM/DD visible light communications. *Journal of Lightwave Technology*, 35(9):1513–1523, 2016.

[155] Matthias Wetz, Werner G Teich, and J Lindner. OFDM-MFSK with differentially encoded phases for robust transmission over fast fading channels. In *11th International OFDM-Workshop*. Citeseer, 2006.

[156] Yitong Xu, Zixiong Wang, Peixi Liu, Jian Chen, Shiying Han, Changyuan Yu, and Jinlong Yu. Accuracy analysis and improvement of visible light positioning based on VLC system using orthogonal frequency division multiple access. *Optics Express*, 25(26):32618–32630, 2017.

[157] Gilbert Yammine, Eva Peiker, Werner G Teich, and Jürgen Lindner. Improved performance of coded OFDM-MFSK using combined alphabets and extended mapping. In *2014 8th International Symposium on Turbo Codes and Iterative Information Processing (ISTC)*, pages 17–21. IEEE, 2014.

[158] Liang Yin, Xiping Wu, and Harald Haas. SDMA grouping in coordinated multi-point VLC systems. In *2015 IEEE Summer Topicals Meeting Series (SUM)*, pages 169–170. IEEE, 2015.

[159] Fahad Zafar, Masuduzzaman Bakaul, and Rajendran Parthiban. Laser-diode-based visible light communication: Toward gigabit class communication. *IEEE Communications Magazine*, 55(2):144–151, 2017.

[160] Andrea Zanella, Nicola Bui, Angelo Castellani, Lorenzo Vangelista, and Michele Zorzi. Internet of things for smart cities. *IEEE Internet of Things journal*, 1(1):22–32, 2014.

[161] Sergey V Zhidkov. Analysis and comparison of several simple impulsive noise mitigation schemes for OFDM receivers. *IEEE Transactions on Communications*, 56(1):5–9, 2008.

[162] Wenfei Zhu, Xu Zhu, Enggee Lim, and Yi Huang. State-of-art power line communications channel modelling. *Procedia Computer Science*, 17:563–570, 2013.

[163] Wenfei Zhu, Xu Zhu, Enggee Lim, and Yi Huang. State-of-art power line communications channel modelling. *Procedia Computer Science*, 17:563–570, 2013.

[164] Manfred Zimmermann and Klaus Dostert. An analysis of the broadband noise scenario in powerline networks. In *International Symposium on Powerline Communications and its Applications (ISPLC2000)*, pages 5–7, 2000.

[165] Manfred Zimmermann and Klaus Dostert. A multipath model for the powerline channel. *IEEE Transactions on communications*, 50(4):553–559, 2002.